THE UNIVERSITY OF MICHIGAN

INDUSTRY PROGRAM OF THE COLLEGE OF ENGINEERING

ON THE ANALYSIS OF GAMMA RAY PULSE HEIGHT SPECTRA

Jacob Israel Trombka

A dissertion submitted in partial fulfillment
of the requirements for the degree of
Doctor of Philosophy in The
University of Michigan
Department of Physics
1961

September, 1961

IP-531

Doctoral Committee:

Professor Marcellius L. Wiedenbeck, Chairman
Professor Robert C Bartels
Professor Henry J. Gomberg
Professor William Kerr
Professor John S. King
Associate Professor Charles S. Simons

ACKNOWLEDGEMENT

It is a pleasure to express my gratitude to Dr. M. L. Wiedenbeck for his kind and invaluable helpfulness and supervision throughout this work. I am also indebted to my committee for their continued cooperation, advice and assistance.

I wish to thank Dr. W. F. Miller and W. J. Snow of the Applied Mathematics Division, Argonne National Laboratory, for their cooperation and important work in performing the Monte Carlo calculation of the pulse height distribution for spherical crystals. I am grateful to Mr. R. W. Johnson of the Harshaw Chemical Company for his help in connection with problems in the preparation of spherical NaI(Tl) crystals.

The untiring patience and constant encouragement of my wife have been a genuine contribution to the completion of this research. To my wife, I wish to express my deepest appreciation.

The partial support of this work by the Michigan Memorial-Phoenix Project and the United States Atomic Energy Commission is gratefully acknowledged.

TABLE OF CONTENTS

TABLE OF CONTENTS (CONT'D)

LIST OF TABLES

LIST OF FIGURES

CHAPTER I

INTRODUCTION

In recent years, the scintillation spectrometer has become an important instrument for the detection and energy measurement of gamma rays.(1,2) Other important experimental techniques used for gamma ray spectroscopy are magnetic spectrometry and diffraction and reflection spectroscopy. These latter techniques are used mainly for energy identification and are extremely precise for this measurement. Both of these two methods require very high source strengths with respect to those required for scintillation spectroscopy. This is the first important limitation. Furthermore, magnetic spectrometry and diffraction and reflection spectroscopy measurements can only be performed for point source or parallel beam geometries. Efficiency values are very difficult and sometimes impossible to determine for these two systems. Thus the problem of determining gamma ray intensities is either extremely difficult or impossible. Problems involved in studying the continuous gamma ray energy distribution would also be impossible using magnetic spectrometry and diffraction and reflection spectroscopy. Also the instrumentation required for these two techniques is so difficult and expensive to obtain, that their general use is greatly limited. Scintillation spectroscopy therefore appears the best general method for the investigation of gamma ray spectra. It is the purpose of this work to develop general analytic methods for use in gamma ray spectroscopy and dosimetry using scintillation detectors.

NaI(Tl) crystal scintillators are particularly used for gamma ray spectroscopy because of their comparatively high efficiency in converting the energy of the gamma ray into scintillations. Further, over a large energy

range, there is a linear relationship between the amount of gamma ray energy lost in the crystal, and the intensity of scintillations produced. Thus a flux of gamma rays passing through such a crystal will produce a distribution of scintillation intensities dependent upon the energy lost in the crystal. A multiplier phototube is used to measure the intensity of these scintillations and a voltage pulse whose height is proportional to the scintillation intensity is produced at the phototube output. An analysis of the pulses as a function of pulse height can be made using various types of pulse height analysers. A so-called "pulse height" spectrum is obtained from such a measurement.

For the case of an incident monoenergetic flux and a well-defined source detector geometry, rather simple techniques have been developed to determine the absolute magnitude or intensity of the incident beam from the monoenergetic pulse height spectrum.[2,3] Since a gamma photon may lose its energy to the NaI(Tl) crystal by photoelectric absorption, by Compton scattering, and by pair production, and since there is a further smearing due to mechanics in light collection and in the statistical variation in the gain of the phototube, a monoenergetic gamma flux incident upon a NaI(Tl) crystal produces a distribution of pulse heights. The monoenergetic pulse height spectrum will be characterized by a photo-peak, a Compton continuum, and annihilation escape peaks. The pulse height spectrum due to a polyenergetic gamma flux can be shown as a summation of the pulse height spectra of the various monoenergetic components in the polyenergetic beam.

When the incident gamma flux is polyenergetic and when the source detector geometry cannot be well defined, it becomes extremely difficult to determine the incident gamma energy distribution from a measurement of the

pulse height spectrum. It has been the purpose of this work to develop methods of analyzing such complex pulse height spectra for both those cases wherein the source detector geometry can and cannot be specified.

A method for analyzing complex pulse height spectra for the case of a well defined source detector geometry has been described by Stephenson and Bell,[3] the so-called "peeling off" process. It was believed that a more rigorous analytic technique than this was required. A least squares fitting technique for the analysis of the data was therefore developed. In this the pulse height spectrum due to a polyenergetic distribution is synthesized by using a series of normalized pulse height distributions due to the monoenergetic components in the incident beam. Each of these monoenergetic pulse height distributions is weighted so that their sum is a best fit to the experimentally determined polyenergetic pulse height distribution.* The monoenergetic pulse height spectra used in these calculations can be both theoretically calculated[4] and experimentally determined.

A further experimental difficulty lies in the fact that both the shapes of the monoenergetic pulse height distribution and the crystal efficiencies are dependent on source detector configuration. It was predicted and found that by using spherical rather than cylindrical NaI(Tl) crystals this dependence can be greatly reduced for many cases.

The above analysis has been used both for the measurement of discrete and continuous gamma ray energy distributions. In the case of a distribution continuous in energy, the monoenergetic component corresponds to an energy in region ΔE about E.

---

* This technique has been programmed for the IBM 704 computer. See Appendix 1.

These techniques have been applied to a number of problems; the determination of thermal neutron fluxes, the determination of complex gamma decay schemes, and the determination of the linear absorption coefficients and energy buildup factors from a measurement of the undegraded, and of the degraded gamma pulse height spectra due to the scattering of gamma rays which pass through a scattering media. Experimental results have been obtained, and have been compared with theory.

CHAPTER II

PROPERTIES OF SCINTILLATION DETECTOR SYSTEMS

A. The NaI Crystal

Energy exchange between gamma rays and matter can take place in many ways, but in terms of the scintillation process, there are only three processes of major interest. They are photoelectric absorption, Compton scattering and pair production. Other interaction processes do not impart a significant energy loss to the crystal.[2,5] Since it is the amount of kinetic energy imparted to the secondary electrons by the interacting gamma ray which is of interest in the scintillation process, it is important to investigate the three above mentioned interaction processes in order to ascertain the amount of the total gamma ray energy given up as kinetic energy to secondary electrons in each process.

Photoelectric absorption is considered at first. This is the interaction of a gamma ray with the bound or orbital electrons. All of the energy of the gamma ray is lost in this interaction, but not all of the energy is imparted to secondary electrons as kinetic energy. Some energy is required to overcome the binding energy of the electron in the given shell.[6] Thus the amount of energy available to produce scintillation is equal to the energy of the gamma ray minus the binding energy of the electron. Of course, after the photoelectric absorption, x-rays are produced with energies almost equal to the binding energy. The absorption of these x-rays and their conversion to the kinetic energy of secondary electrons will then reclaim, in a sense, the lost energy.

In the Compton scattering process, the electron may be treated as unbound or free with both conservation of energy and momentum.(7) The gamma ray can be scattered through any angle with a diminution of energy. In terms of the scintillation process, all the energy lost in scattering will be given up to secondary electrons as kinetic energy. Furthermore, the gamma ray may suffer one or a number of Compton scatterings. As the energy is degraded, the probability of photoelectric absorption increases. Thus the gamma ray may lose only part of its energy (only Compton scattering) or its total energy (Compton scattering followed by photoelectric absorption) to the crystal.

In the pair production process, a gamma ray loses its energy in the field of the nucleus to produce an electron positron pair. The energy above that which is required to produce the electron positron pair is imparted as kinetic energy to the electron and positron.(8) This kinetic energy is then available to produce scintillations. The positron annihilates with an electron and two 0.51 Mev gamma rays (most probably) are produced. These gamma rays can either lose all or part of the energy by Compton scattering or photoelectron absorption in the crystal. Thus, there is a possibility that the gamma ray may lose any amount of its energy from the maximum energy down to the maximum minus 1.02 Mev.

By any of the above mentioned processes or combination thereof, the gamma ray loses all or part of its energy to the crystal. Having converted this energy to high energy electrons, the crystal will then experience ionization due to an energy loss per unit path (dE/dx) of the electron in moving through the crystal. This is similar to the ionization of a gas by a charged particle. In the case of the crystal one deals with an insulator in which the band theory is applicable.(9,10)

The allowed values of energy for bound electrons in a perfect NaI crystal belong to intervals of energy, the valence and conduction bands, which are separated by unallowed intervals, the forbidden bands. Passage of a high energy electron through the crystal excites electron-hole formation in the valence band.

The NaI(Tl) crystal is not perfect and because of the presence of thallous ions and lattice defects, there are localized permitted electron levels that lie in the normally forbidden interval between the conduction band and the valence band. Some of the levels are called trapping centers and are due largely to lattice imperfections but are partly due to the presence of impurity ions. There are other allowed levels between the bands called luminescence center levels. The mechanism of light emission (scintillations) is attributed to the existence of these centers. An energy level diagram is shown in Figure 1.(11,12)

It is believed that the luminescence centers consists of pairs of thallous ions. These pairs have some of the properties of ordinary diatomic molecules. The energy E of those electrons within the radius of a pair of thallous ions as a function of the inter-ion separation r is of the type shown in Figure 1. (The luminescence center level.)

The lower curve A is for the electronic ground state and the upper curve B is for an excited electronic state. A and B have shapes that allow the thallous ion to vibrate along r. Some of the vibrational levels are excited at room temperature. By the Frank-Condon principle,(11) changes in electronic energy are represented by vertical lines at the extremes of the ion vibration locus on the energy diagrams, whereas the ions are instantaneously stationary in the classical picture. In the transition of the electron

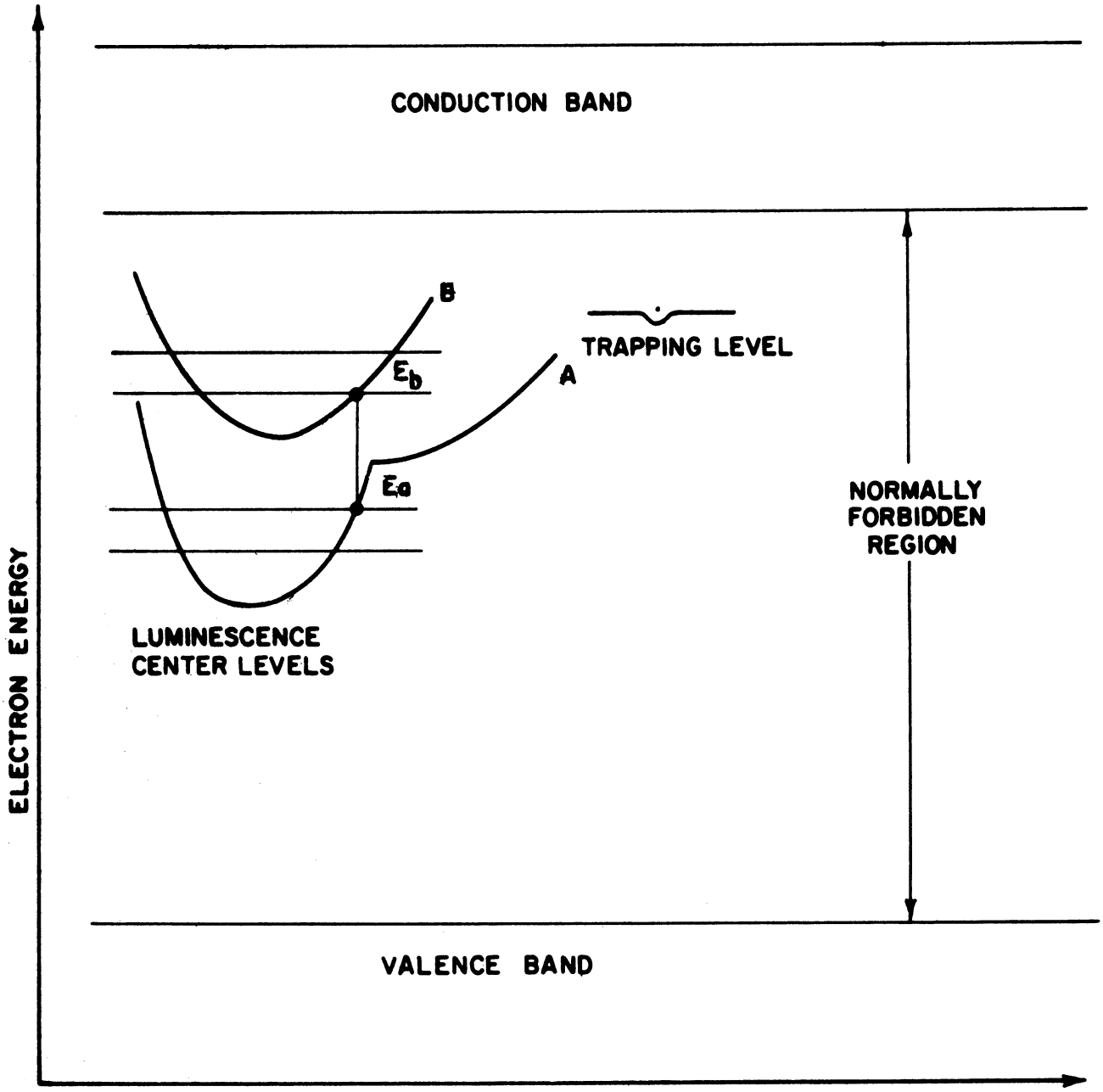

Figure 1. Energy Level Scheme for NaI(Tl) Phosphor.

from E_b to E_a, a photon of energy $E_b - E_a$ is emitted. Since transition may occur at the extremes of these ion vibrations, one obtains photons whose wavelengths lie in another broad band about energies corresponding to 3 ev or 4100 Å.(13)

Electrons excited to the conduction band can fall to the valence band through the trapping levels and the luminescence center levels. Transitions via the luminescence center levels are accompanied by the emission of light. This is the light of interest in the scintillation process. Transition by other levels are radiationless in terms of the scintillation process.

NaI(Tl) has the property that the intensity of scintillation or total light energy produced is proportional to the energy lost by gamma radiation, the fast particle, or particles that produced it. This is the property of NaI(Tl) that makes it useful in gamma-ray spectrometry. With respect to gamma ray interaction, Figure 2 shows the emission spectrum and the absolute conversion efficiency of the crystal ionization excitation into light emission.(14) The total light energy produced E_ℓ, starting with the initial excitation energy of electron, E_e is

$$E_\ell = E_e \int_0^\infty C_{np}(\lambda)d\lambda \qquad (1)$$

where $C_{np}(\lambda)$ is the conversion efficiency as a function of wavelength λ of the photons produced in the scintillation process. $C_{np}(\lambda)$ does not depend upon the initial excitation energy of electron E_e.(12,14) Thus there is a linear relationship between the total light energy E_ℓ produced and the excitation energy of electron E_e.

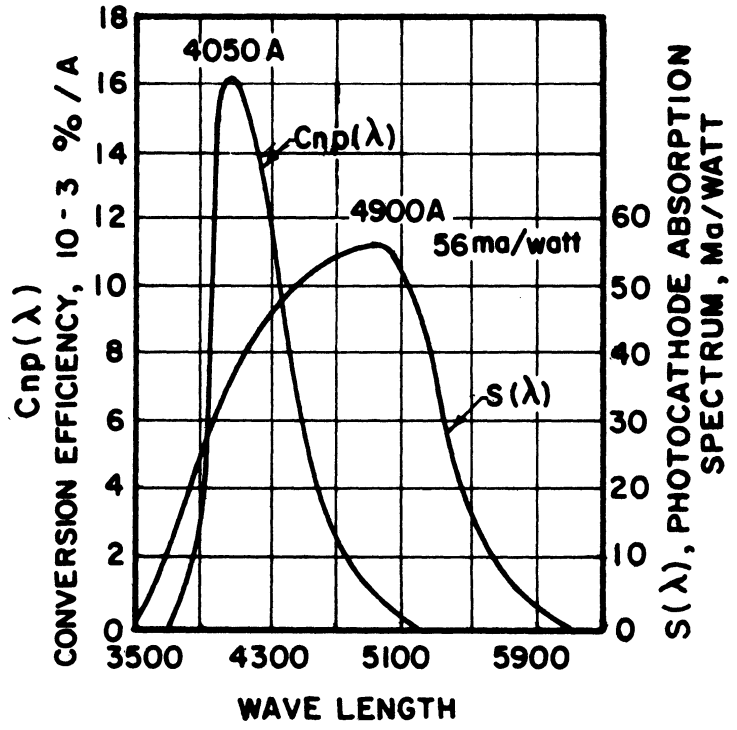

Figure 2. Emission Spectrum, Absolute Conversion Efficiency Spectrum and Photocathode "Absorption" Spectrum for NaI(Tl) Crystal and End Window ($Sb\ Cs_3$) Photocathode Multiplier Phototubes.

Finally, other properties of NaI(Tl)[1] of interest with respect to the design of a detector are the following:

1. Transparency to its own luminescence.
2. High relative light yield (compared to other scintillators).
3. 0.25 μ sec decay constant of scintillation.
4. Very hygroscopic.

B. The Multiplier Phototube

The intensity of the scintillation produced in the NaI(Tl) crystal induced by the absorption and scattering of gamma rays have to be measured accurately. Both DuMont 6292 and RCA 6342A multiplier phototubes were used in this measurement. Light from the scintillating NaI(Tl) crystal passes through the glass envelope and ejects photoelectrons from the photocathode. The photosensitive material in the photocathode of the DuMont 6292 and RCA 6342A multiplier phototube is Cs-Sb. This material is used because of its good photoelectric yield for the wave length of luminescent emission from scintillation crystals. The photocathode absorption spectrum is also shown in Figure 2. The photoelectrons are electrically accelerated to the first dynode, where they eject secondary electrons. The process is cascaded in ten stages so that the charge of electrons ejected from the tenth dynode and collected on the anode is about 6×10^5 times the original charge from the cathode. This is true for the case where the potential difference per stage is 105 volts.[13] The fraction of photon energy which strikes the photocathode surface is $E_\ell(T_p \cdot F_p)$ where T_p is the transparency of the crystal and of the phototube optical seal, and F_p is the nonescape probability.

For a well reflected crystal both T_p and F_p should be nearly unity. A fraction of this energy will be absorbed in the photocathode, giving rise to a number of low energy photoelectrons released inside the phototube. The efficiency of this conversion from photons to electrons depends on the absorption spectrum of $SbCs_3$ and on the electronic stopping power of the photocathode and is measured by the sensitivity factor $S(\lambda)$, shown also in Figure 2.

Now $dn_e/dE = S(\lambda)$ or $dn_e = S(\lambda)\, dE$ but from (1) above,

$$dE = dE_\ell = E_e\, C_{np}(\lambda)\, d\lambda$$

So

$$dn_e = E_e\, C_{np}(\lambda)\, S(\lambda)\, d\lambda \cdot T_p \cdot F_p$$

or the number of photoelectrons ejected is n_e and depends on the product of the spectra of Figure 2.

$$n_e = E_e \int_0^\infty C_{np}(\lambda)\, S(\lambda)\, d\lambda \qquad (2)$$

If F_c is defined as the fraction of such electrons striking the first dynode and if the subsequent phototube multiplication is M, the total charge q produced at the anode, due to a single original gamma ray interaction is

$$q = n_e \cdot e \cdot M \cdot F_c = V_o/C \qquad (3)$$

where e is electronic charge, the charge q is collected on the input capacity C of an amplifier and measured as a voltage pulse. Thus it is seen that the magnitude or height of the pulse is proportional to the initial excitation energy of electron E_e. However because of the statistical

fluctuation in dE/dx, n_e, M, and F_c, a distribution of voltage pulse heights about some mean value V_o will be observed rather than a constant pulse height as is indicated in Equation (3). This point will be further considered later in this Chapter.

C. Construction of the NaI(Tl) Detector

Figure 3 shows the construction of the two scintillation detectors used in this experiment. Most difficulties in the mounting and construction of scintillation detectors can be attributed to two properties of the NaI(Tl) crystals. First of all, NaI is hygroscopic and in the presence of water vapor and due to the release of free iodine, a yellow discoloration occurs. This discoloration interferes with the optical properties of the crystal. Therefore one must take great care to prevent any moisture from contacting the crystal surface. Secondly, NaI(Tl) has a high index of refraction ($\sim$ 1.8) in the wavelength region of its fluorescence. Because of its small critical angle with respect to air, the light generated by the phosphor will be almost totally reflected unless a good optical coupling is made with the phototube glass.

The crystals are handled and polished in a dry box having a relative humidity less than 10%. The exit face should be highly polished to eliminate scratches and other flaws in this surface. The other sides are polished mainly to clean the surface of water and free iodine, and to eliminate any large scratches or flaws which might trap the light. These sides are left so that one has diffusely reflecting surfaces. Specular reflections in the crystal will cause the light to be trapped in the crystal, and thus remove it from measurement by the photomultiplier tube. Further, in order to more

effectively return the light striking the top and lateral surface of the crystal to the exit face, a diffusely reflecting material (α - aluminum oxide) is packed around the crystal. The system is then housed in an aluminum can. (See Figure 3.) In case of the cylindrical crystal, the aluminum housing is made of 0.010" aluminum, and the aluminum housing for the spherical crystal is made of 0.020" aluminum. The only reason that a 0.020" aluminum housing was used for the spherical crystal was that thinner housings were not available in the shape required. It is desirable to use as thin a housing as possible so as to decrease the amount of scattering from the materials surrounding the crystals. This scattering tends to perturb the measurement.

The exit face is optically coupled to the phototube envelope with a material such as Dow-Corning DC-200 Silicone oil with a viscosity of 10^6 centistokes or white ophthomological petrolatum. Care must be taken in making this optical connection (e.g., one should attempt to exclude large bubble formation in the optical connection). The canned crystal is then hermetically sealed to the multiplier phototube using Apiezon Q vacuum wax. A hyperdermic needle is inserted through the Apiezon seal and a vacuum applied. The needle is then withdrawn while pressing on the seal. This technique has been described in more detail by P. R. Bell.(2)

It was necessary to use a lucite light pipe for the spherical crystal in order to seal the exit face to the phototube. An optical seal is therefore necessary between the light pipe and the crystal. It is believed that one of the reasons for the loss in resolution of the spherical crystal can be attributed to difficulties in making proper optical connection between crystal, light pipe, and phototube. It is rather difficult to polish the

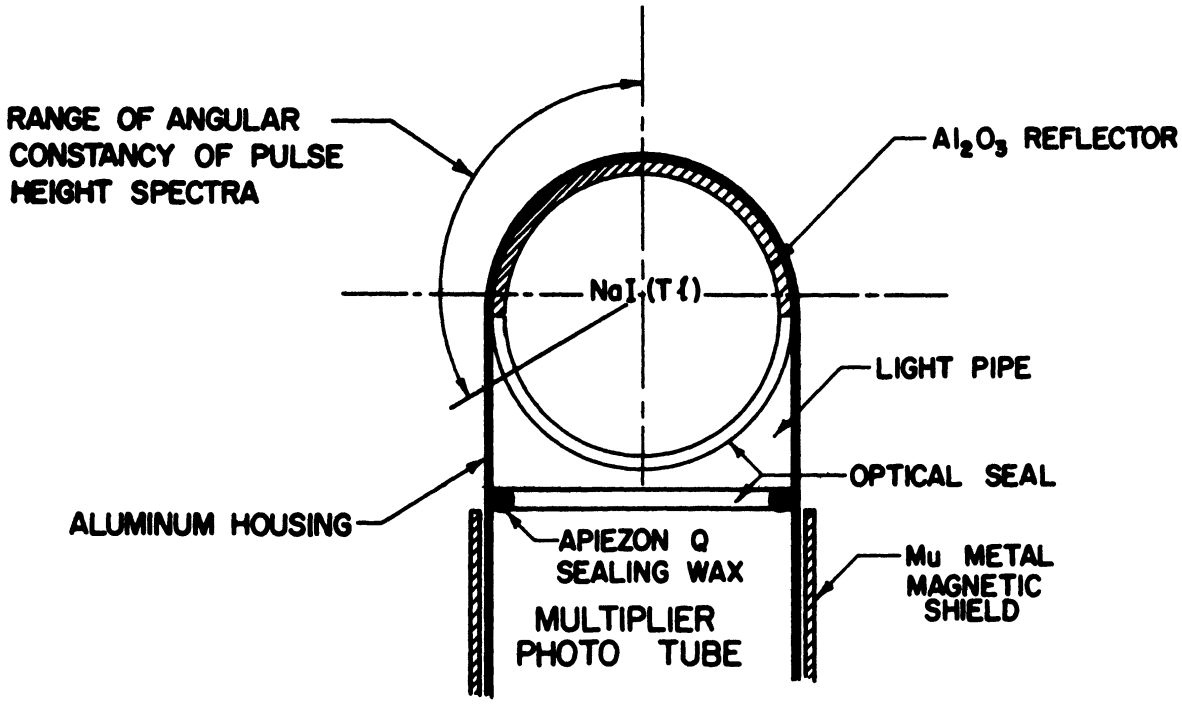

Figure 3a. Spherical Crystal Design.

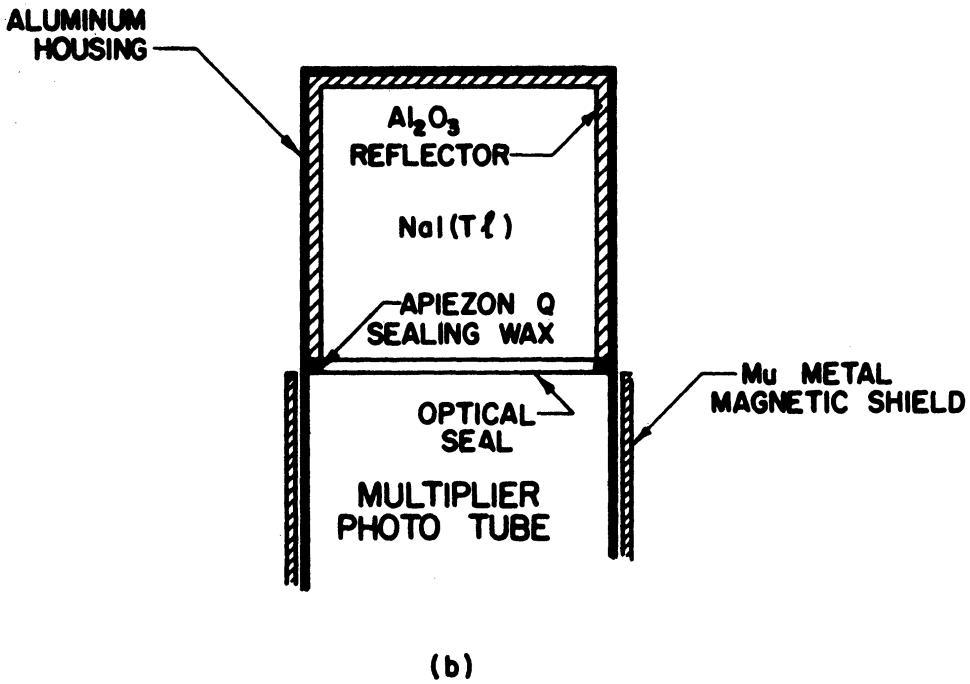

Figure 3b. Cylindrical Crystal Design.

exit face of the sphere without deforming the sphere and it is also rather difficult to eliminate air bubbles between the light pipe and the sphere.

Stray magnetic fields can have quite a large effect on the output current of the phototube. A mu metal magnetic shield is used to reduce the effects of the earth's or other stray magnetic fields. Further, any object at anode potential outside the glass envelope, which touches the glass may produce spurious pulses. This effect can be prevented by either wrapping the phototube with electrical tape or by wrapping the tube with a metal shield which is held at cathode potential.

D. Factors Affecting Resolution

The gamma ray dissipates its energy in the phosphor producing high energy photoelectrons. High energy photoelectrons produced in this way produce pulses with varying magnitudes at the output of a scintillation counter. A number of experimental and theoretical studies[15,16] of the widths of the generated pulse height distributions have been performed. The following processes contribute most significantly to the broadening of the pulse height spectrum.

1. Emission of Photons by the Phosphor

There is a statistical fluctuation in the number of photons per scintillation. Other statistical variations may be attributed to a local variation in luminescent efficiency of the phosphor due possibly to a non-uniform distribution of activity ions, to the fact that successive particles lose different amounts of energy to the phosphor due to interaction, edge, and scattering effects, and also to the luminescence process itself (i.e.,

conversion of absorbed energy to photon energy fluctuates for successive particles).

2. Collection of Emitted Photons by the Photocathode

Successive scintillations never occur at exactly the same position in the crystal, and thus the photon collection efficiency of the photocathode depends on the position where the scintillation is produced. Optical flaws in the crystal and at the various optical seals further smears out the distribution.

3. Emission of Photoelectrons n_e by the Photocathode

There is a statistical fluctuation of photoelectrons per scintillation released from the photocathode. Further, there is a point-to-point variation of photocathode response; also a random emission of thermal electrons by the photocathode which adds to the variation in the pulse height distribution.

4. Collection of Photoelectrons by the First Dynode F_c and Multiplication M by the Successive Stages

The variance due to the multiplication process can be shown to be fundamentally statistical in nature.[17] Further, losses can be attributed to the variations in the fraction of photoelectrons collected by the first dynode, in the collection efficiencies of subsequent dynodes, and in dynode response.

Other processes have also been considered such as the statistical variation in dE/dx, and have been found to be negligible with respect to those mentioned above. For further detail see References 13, 15, and 18. Also it is shown in these references that the effects considered in (1) and (2) above are small compared with those in (3) and (4). Therefore the

theoretical calculation of energy resolution usually considers the statistical fluctuation in (3) and (4).[13,16,17,18] The statistical variation in the number of photoelectrons n_e produced at the photocathode can be considered to be Gaussian.[13,16,17,18] If V_o is the mean value of the pulse height produced at the phototube anode due to the absorption of the gamma ray energy E_o in the phosphor, then the probability P_1 that a pulse of height V_1 is produced at the phototube anode due to the statistical fluctuation in n_e is

$$P_1 = \frac{n_e(V_o)}{n_e(V_1)} = \exp - \frac{(V_1-V_o)^2}{2\sigma_n^2} \qquad (4)$$

where σ_n^2 is the dispersion in the photoelectron production. Here we have only considered the variance in n_e.

Now we consider the effect of the variance in the multiplication M. It is assumed that the distribution due to the statistical fluctuation in M is Gaussian.[16,17] Therefore the probability that the phototube multiplication of $n_e(V_1)$ produces a pulse corresponding to height of V_2 is

$$P_2 = \frac{M(V_2)}{M(V_1)} = \exp - \frac{(V_2-V_1)^2}{2\sigma_m^2}$$

where σ_m^2 is the dispersion due to the statistical variation in the multiplication.

The probability P_3 of obtaining a pulse of height V_2 due to the complete absorption of E_o energy is the product of $P_1 \cdot P_2$ integrated over all V_1

$$P_3 = \int_{-\infty}^{+\infty} \exp\left[\frac{-V_1-V_o)^2}{2\sigma_n^2}\right] \exp\left[\frac{-(V_2-V_1)^2}{2\sigma_m^2}\right] dV_1$$

let $\epsilon = (V_2 - V_o)$ and $x = (V_1 - V_o)$

$$P_3 = \int_{-\infty}^{+\infty} \exp[\frac{-x^2}{2\sigma_n^2}] \exp[\frac{-(\epsilon - x)^2}{2\sigma_m^2}] \, dx$$

$$= \int_{-\infty}^{+\infty} \exp-[(x - \frac{2\sigma_n^2 \epsilon}{2\sigma_n^2 + 2\sigma_m^2})^2 \quad \frac{4\sigma_n^2 \sigma_m^2 \epsilon^2}{(2\sigma_n^2 + 2\sigma_m^2)^2}][\frac{(2\sigma_n^2 + 2\sigma_m^2)}{4\sigma_n^2 \sigma_m^2}] \, dx$$

Let $z = (x - \frac{2\sigma^2 \epsilon}{2\sigma_n^2 + 2\sigma_m^2})$

$$P_3 = \exp[-\epsilon^2/2\sigma_n^2 + 2\sigma_m^2] \int_{-\infty}^{+\infty} \exp[-\frac{2\sigma_n^2 + 2\sigma_m^2}{4\sigma_n^2 \sigma_m^2} z^2] \, dz$$

$$= C\exp[-\epsilon^2/2\sigma_n^2 + 2\sigma_m^2] = C\exp[-\epsilon^2/2\sigma^2] \qquad (6)$$

where σ^2 is the dispersion of the photoelectron rate and subsequent multiplication rate, respectively. C is a constant obtained from the definite integral over z.

Analysis has shown [17,18] that

$$\sigma_n^2 \sim \bar{n}_e = C_1 E_o = C_1' V_o$$

and

$$\sigma_m^2 \sim \bar{n}_e f(M) = C_2 E_o = C_2' V_o$$

where $f(M)$ is a function of the multiplication, and is constant for a fixed M.

$$\sigma^2 = C_3 E_o = C_3' V_o \qquad (7)$$

Experimentally it has been found that relation (7) is true for limited energy ranges.[16]

The Gaussian form given in (6) describes the pulse height distribution generally, although one cannot use relation (7) to determine σ^2 in

general. Over limited energy range, it has been found by this author that the relation

$$\sigma^2 = CE_o^n = C'V_o^n \qquad (8)$$

can be used more generally. n is determined experimentally. This equation will therefore be used later for calculation (see Chapter V).

E. The Multichannel Pulse Height Analyser

The voltage pulse distribution at the output of multiplier phototube due to the scintillation produced in the phosphor must now be measured as a function of the magnitude of the voltage pulse. This can be done using various types of pulse height analysers. A brief outline of the operations of the multichannel analyser used in this experiment is given below. Detail information concerning the exact design can be found in the operating manual.[19]

Figure 4 is a block diagram of the pulse height analyser. The voltage pulses from the multiplier phototube is fed into a linear amplifier. The amplified voltage pulse from the output of the linear amplifier is then fed simultaneously to three different places. The voltage is fed to the stretcher which maintains this voltage as a bias on the discriminator. The voltage signal also starts the address scaler which begins counting pulses from an oscillator. Finally, a ramp-generator is started by this amplified voltage pulse. The ramp generator begins generating a linearly increasing voltage which is fed to the discriminator. When this voltage "ramp" exceeds the bias voltage on the discriminator the discriminator sends a stop signal to the address scaler which turns off the scaler count. The address scaler has counted the number of oscillator pulses proportional to the magnitude of input voltage pulse, and thus to the pulse height. The input pulse height

PULSE HEIGHT ANALYZER BLOCK DIAGRAM

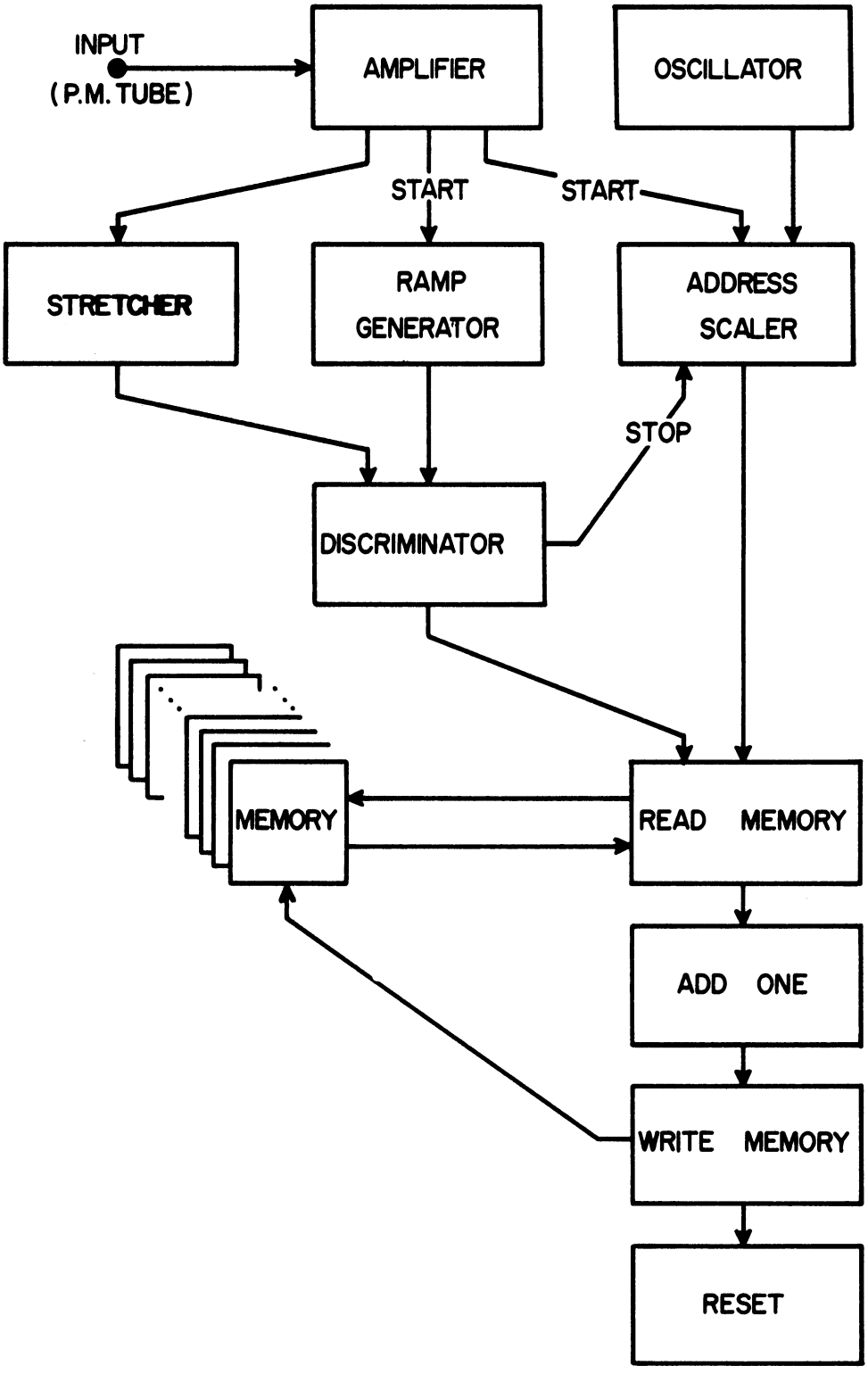

Figure 4. Pulse Height Analyser Block Diagram.

information (data in analogue form) has been transformed into a number (data in digital form). The information is now stored in the address scaler.

The number or "address", stored in the address scaler, corresponds to a position in the memory. This "address" or memory position is then sent to the read memory. Upon a signal from the discriminator, the number stored in the memory at the "address" in the read memory unit is extracted. The number extracted is equal to the sum of all the previous pulses of the same pulse height as the one being presently analyzed. This number is increased by unity in the add one unit, and is then returned to the memory at the appropriate address by the write memory unit. After this step the analyser is reset to accept another pulse.

All the pulses are placed in the same pulse height channel, if they differ in pulse height by a voltage increment less than the voltage change of the ramp in one oscillator cycle. The pulse height interval ΔV is given by

$$\Delta V = \frac{\text{Ramp slope}}{\text{Oscillator frequency}}$$

Thus using this pulse height analyser one obtains the total number of pulses in ΔV about V as a function of V. The spectrum measured in this way is called the pulse height spectrum.

The above discussion only describes part of the analyser operation. The method of data readout, the problems of what happens when one pulse arrives before another has been completely processed, (pulse pile up) and other such problems have not been considered. These problems are handled differently by various types of analysers, and it is believed that such discussion will not add significantly to the discussion of the problems

considered in this paper, although it must be noted that there is a possibility of distorting the shape of the pulse height spectra due to pulse pile up. This problem will limit the source strength that can be used for this measurement. The problem of pulse height distortion due to pile up for the pulse height analyser used in this work is discussed in Reference 19. Care was taken in performing this experiment, not to use sources strengths which would distort the pulse height spectrum due to pulse pile up.

CHAPTER III

PROPERTIES OF PULSE HEIGHT SPECTRA

A. Shapes of Gamma Ray Pulse Height Spectra

The pulse height spectrum obtained when monoenergetic gamma-rays are detected using a scintillation system is never a line, but is of a shape determined by the energy of the gamma ray and the source detector configuration. The shapes of these monoenergetic pulse height spectra are determined by the following factors.

1. The relative magnitude of the photoelectric, Compton, and pair production cross sections.
2. The losses and statistical fluctuation that characterizes the crystal, light collection and photomultiplier system.

The second point was discussed in the previous section, and it was indicated that one could describe this smearing for a given energy E_o (or pulse height position V_o) by

$$y = Am \exp - \frac{|E - E_o|^2}{\alpha^2 E_o^n} \qquad (9)$$

where y is the count rate at energy E or pulse height V, and Am is a constant.

The first case considered is that wherein photoelectric absorption predominates and Compton scattering and pair production can be considered negligible. In this process, as was discussed in the previous section, the kinetic energy imparted to a secondary electron is equal to the energy of the gamma minus the electron binding energy. This binding energy can be reclaimed in terms of the scintillation process by the absorption of the x-rays

produced after photoelectric absorption. There is also the possibility that the x-rays may escape the crystal without being absorbed. The pulse distribution due to photoelectric absorption is characterized by two regions; the region of total absorption (the photopeak) and the region of total absorption minus x-ray escape energy (the escape peak). This smearing plus the Gaussian smearing discussed above yields a pulse height spectrum similar to that shown in Figure 5.[20] The distribution under the photopeak can be described by Equation (9).

When Compton scattering becomes an important energy loss mechanism, another region is observed in the pulse height spectrum, the so-called Compton continuum. In terms of the scintillation process as was discussed in the previous section, all the energy lost in scattering will be given up to the electron as kinetic energy. The gamma ray may lose part of its energy to the crystal. Furthermore, after suffering a Compton collision or a number of Compton collisions it may then suffer a photoelectric absorption losing its remaining energy. Thus there is both a possibility for the gamma ray to lose all of its energy in the crystal, or part of its energy in the crystal and part escaping the crystal at a diminished energy. Because of the multiple scattering events, the shapes of the Compton continua can only be calculated theoretically using Monte Carlo techniques.[4] The shapes of the Compton continua have been theoretically calculated, and experimentally determined. There seems to be agreement between experiment and theory.[4] In Figure 6, the unsmeared Monte Carlo calculation obtained from Reference 4, the smeared theoretical calculation and experimental determination of the pulse height spectrum for a Cs^{137} (.661 Mev) are shown. The experimental measurement was

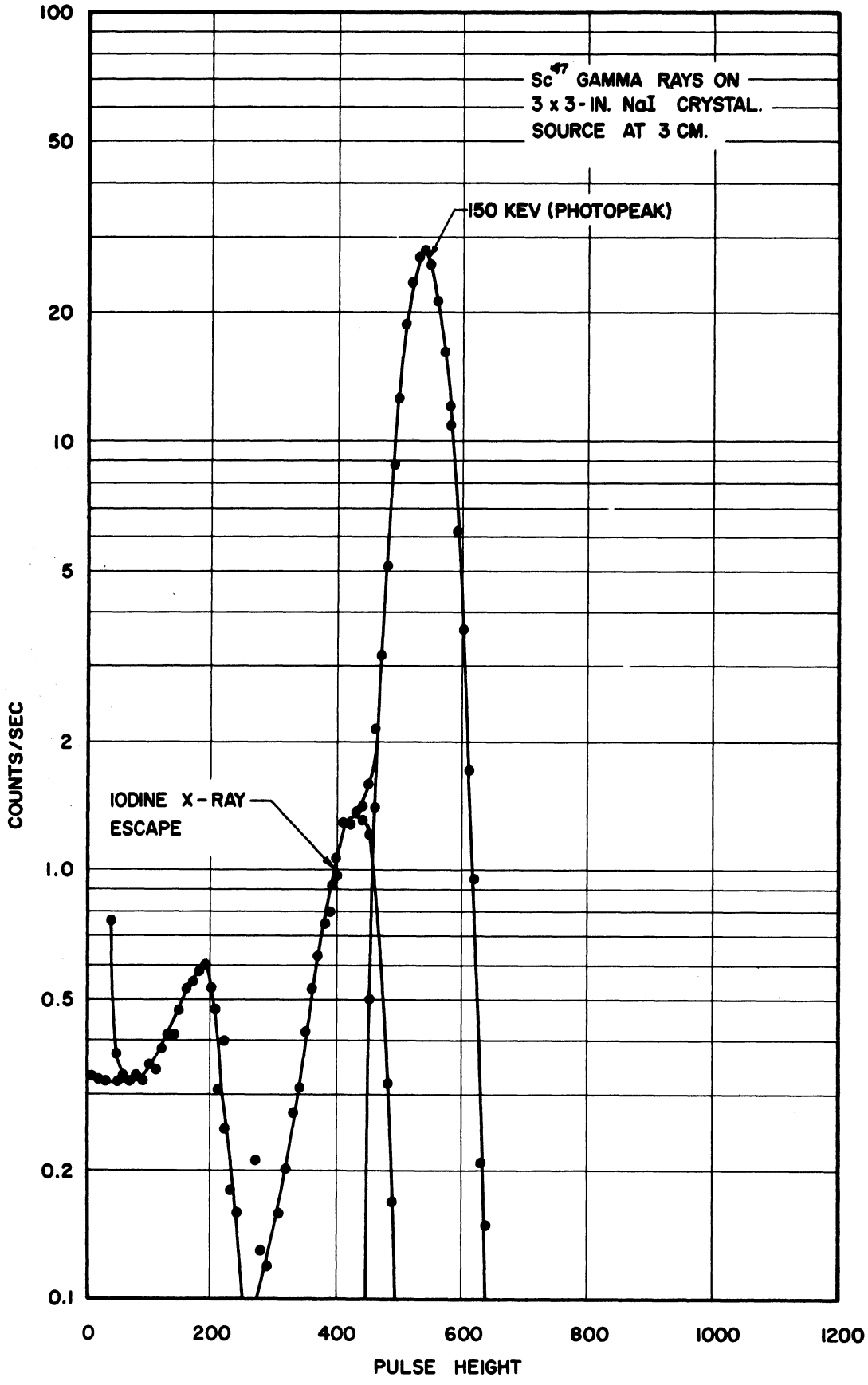

Figure 5. Sc^{47} Gamma Rays on 3" x 3" NaI(Tl) Crystal. Source at 3 cm.

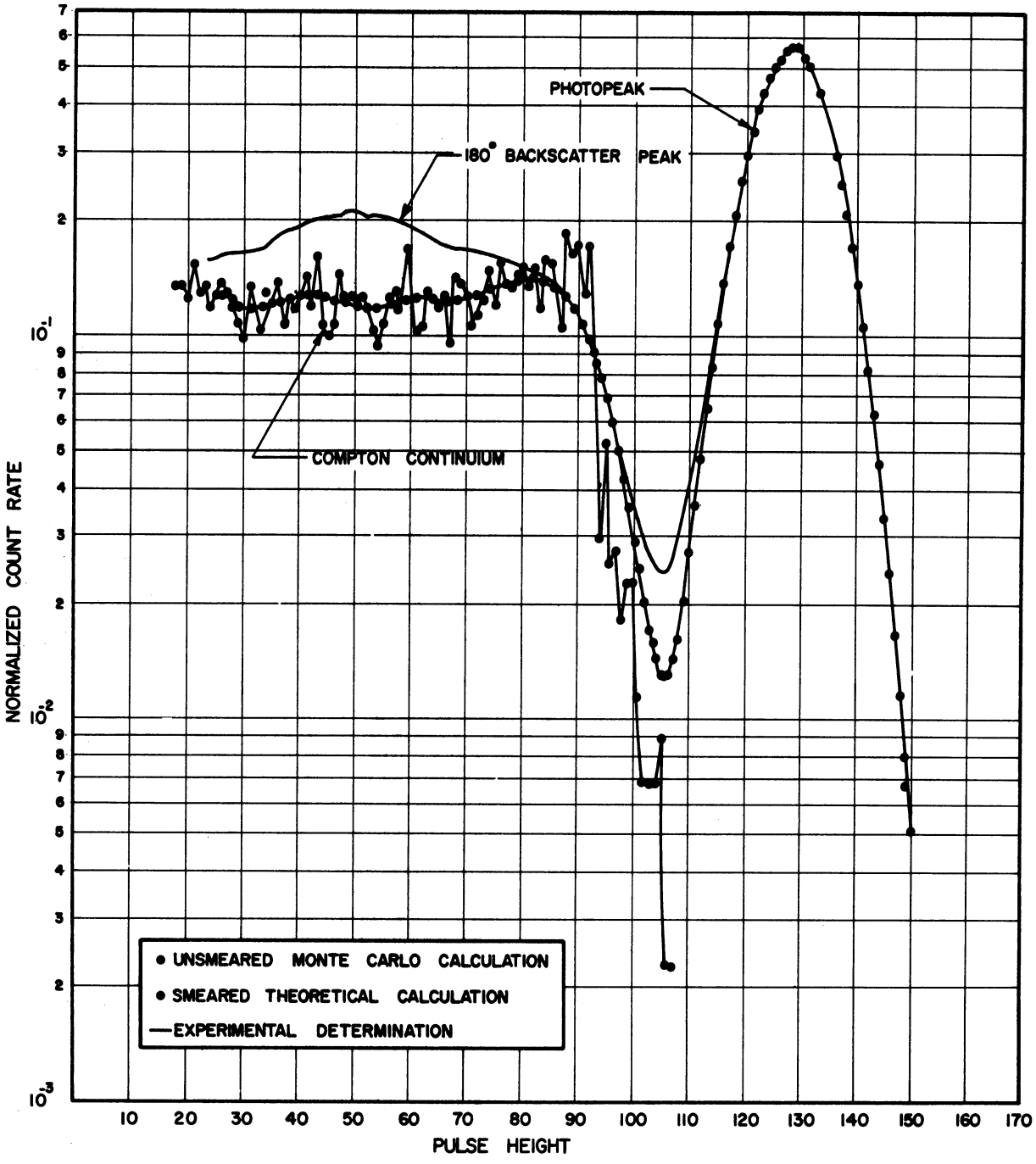

Figure 6. Theoretically Calculated and Experimentally Determined Pulse Height Spectrum for Cs^{137} (0.661 Mev). Parallel Beam Incident upon a 2" Spherical NaI(Tl) Crystal.

made using a 2" spherical crystal. The value α^2 and n in Equation (9) were determined experimentally by studying the shape of the photopeaks for monoenergetic emitters as a function of energy (see Chapter V). The numbers obtained by Monte Carlo calculation[4] were smeared out using Equation (9) and the experimentally determined values of α^2 and n and are shown in Figure 6. The difference between the theoretical and experimentally determined pulse height spectrum can be attributed to the scattering of the gamma rays from surrounding materials external to the crystal. When the amount of material surrounding the crystal is decreased, there is much better agreement between theory and experiment.[4] There is an attempt being made at present to include the effects of the scattering in the surrounding materials (e.g., the materials used for canning, the reflector, and phototube) in the Monte Carlo calculation by the Applied Mathematics Division Argonne National Laboratory. Hopefully with this scattering included in the calculation even better agreement will be obtained.

At energies higher than 2 Mev pair production becomes appreciable. Two false "photopeaks" are then observed. Figure 7 is the pulse height spectrum of Na^{24}. The gamma ray energies emitted by Na^{24} are 2.76 Mev and 1.38 Mev. The three peaks of greatest pulse height are due, in order of increasing pulse height, to

1. Pair production with escape of both annihilation quanta
2. Pair production with the absorption of one annihilation quantum
3. Pair production with absorption of both annihilation quanta, and to total absorption by photoelectric effect or any combination of other effects leading to total absorption.

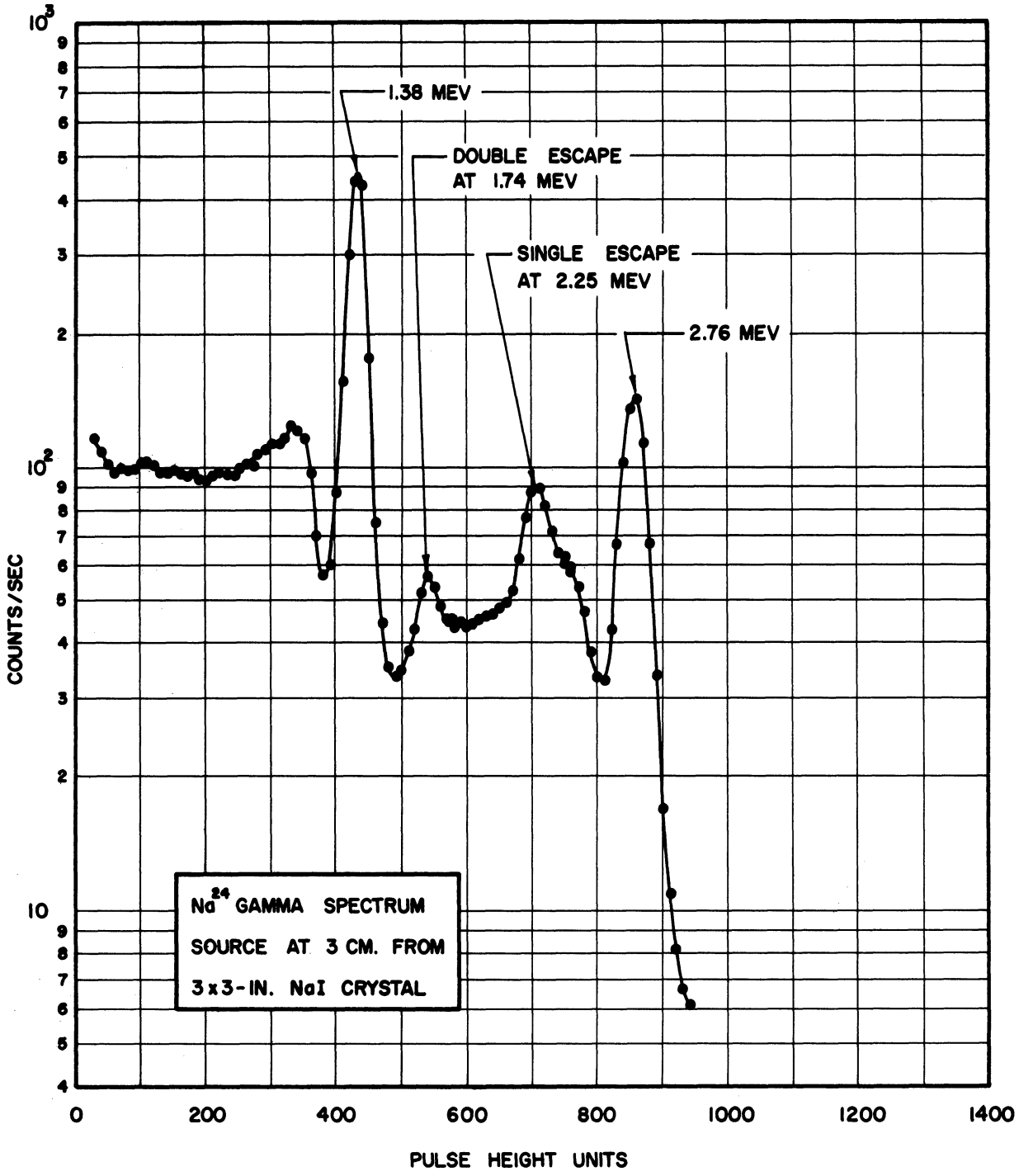

Figure 7. Na^{24} Gamma Spectrum Source at 3 cm from 3" x 3" NaI(Tl) Crystal.

In addition to the photopeak, iodine x-ray escape peak, Compton continuum, and pair escape peaks, there are a number of other regions characteristic of experimentally determined monoenergetic pulse height spectra which are as follows

1. Multiple Compton scattering region. Because of such scattering from materials surrounding the source and crystal which degrades the primary energy, there is a continuous distribution of gamma rays incident upon the crystal with energies less than the maximum energy. This tends to smear out the true Compton continuum due to gamma rays of the undegraded energy scattering in the crystal.
2. Annihilation radiation from the surroundings. Positrons emitted from the source may annihilate in surrounding material. Some of the 0.51 Mev gamma rays produced in such a manner will reach the crystal and a pulse height spectrum characteristic of 0.51 Mev gamma rays will be superimposed on the monoenergetic pulse height spectrum (see Figure 8).
3. Coincidence distribution. If two gamma rays interact with the crystal during a time which is shorter than the decay time of the light produced in the scintillation process, a pulse will appear whose height is proportional to the sum of the energy lost to the crystal by both interacting gamma rays.

Since the interaction time for a single interaction or multiple interactions is shorter than the decay time of the light in the crystal, a single gamma ray interacting with the crystal produces only one pulse, the

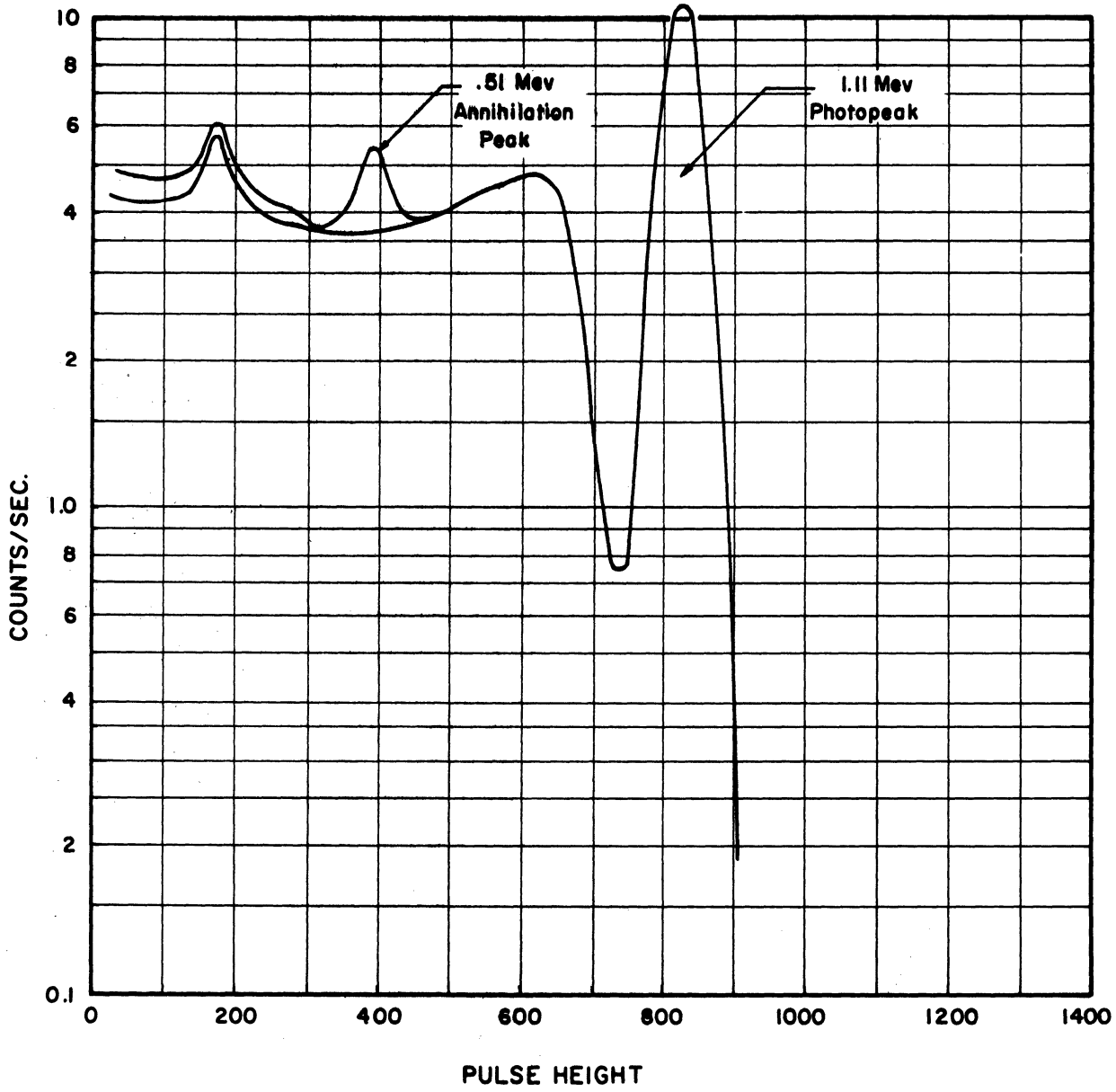

Figure 8. Zn^{65} at 0.24 cm from NaI(Tl) Crystal.

magnitude of the pulse height is effected by the type or number interactions for a given gamma ray. Thus if the above mentioned coincidence effects are negligible, the measured monoenergetic pulse height spectrum can be considered as a distribution of the probability of energy loss as a function of energy for the given gamma ray energy and geometrical configuration. In addition the shape of the monoenergetic pulse height distribution depends on the source detector geometry. By using spherical rather than cylindrical crystals, it will be shown later in this chapter that this geometric dependence can be greatly reduced. This factor is of great importance in certain cases where the source detector geometry cannot be specified. This point will be discussed further later in this Chapter and also in Chapter V.

Again if coincidence losses are negligible, the pulse height distribution due to a polyenergetic gamma flux will be a summation of the pulse spectra due to the various monoenergetic components in the polyenergetic gamma flux. A simple example is shown in Figure 9. The pulse height spectrum due to a source which is a mixture of Cs^{137} (0.661 Mev) and Cr^{51} (0.320 Mev) was measured, Figure 9a. The pulse height spectra of Cs^{137} and Cr^{51} were also measured separately obtaining the pulse height spectra in Figure 9b. The sum of the monoenergetic spectra is also shown in Figure 9b, and is exactly the same as the spectrum obtained in Figure 9a. The source strength of Cs^{137} and Cr^{51} were the same in both measurements.

B. Detection Efficiencies

One pulse appears for every primary collision. The number of pulses produced independent of pulse height is equal to the number of primary collisions. Only the pulse height is affected by the multiple

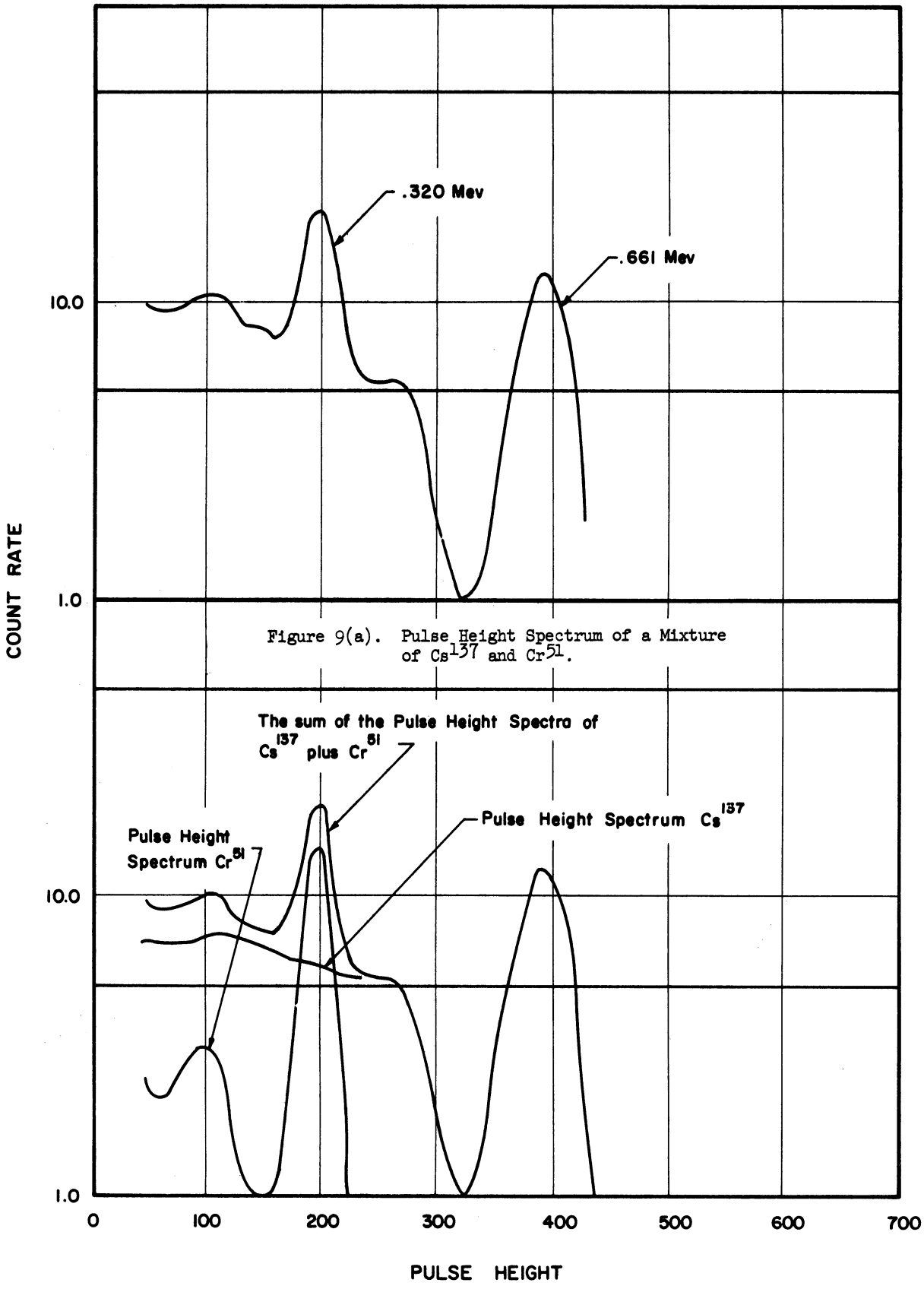

Figure 9(a). Pulse Height Spectrum of a Mixture of Cs^{137} and Cr^{51}.

Figure 9(b). The Pulse Height Spectra of Cs^{137} and Cr^{51}.

collisions. The total area under the pulse height distribution A_T (i.e., total number of interactions independent of pulse height) equals the number of primary interactions which have occurred

For a point source I_o of gamma rays

$$A_T = I_o(\Omega/4\pi)\epsilon_{Ti} \tag{10}$$

where $\Omega = 2\pi(1-\cos\Theta)$ (see Figure 10), and ϵ_{Ti} the crystal detection efficiency.

The nature of the detection efficiencies is now considered. In the following discussion pair production is not included. The analysis of course can be extended to include this process but in this paper, only energies where this effect is either zero or negligible is considered. The cross sections of interest therefore will be those for photoelectric absorption and Compton scattering.

Consider the case of a monoenergetic point source. It is assumed that there is no scattering from surrounding source materials.

If I_o gamma rays per unit time are emitted from the source then $I_o(\Omega/4\pi)$ is the number of gamma rays incident upon the surface of the detector. Further, if any interaction in which a gamma ray produces scintillations in the crystal is considered an absorption interaction, then μ can be defined as the linear absorption coefficient for first interactions due to photoelectric and Compton interactions. With respect to Figure 10, $e^{-\mu\rho}$ is the noninteraction probability along the path ρ through the crystal, and $(1-e^{-\mu\rho})$ is the probability of suffering a first interaction along ρ. Then

$$\epsilon_{Ta} = \int_{\Omega} (1-e^{-\mu\rho})\, d\Omega/4\pi = \text{the total absolute efficiency} \tag{11}$$

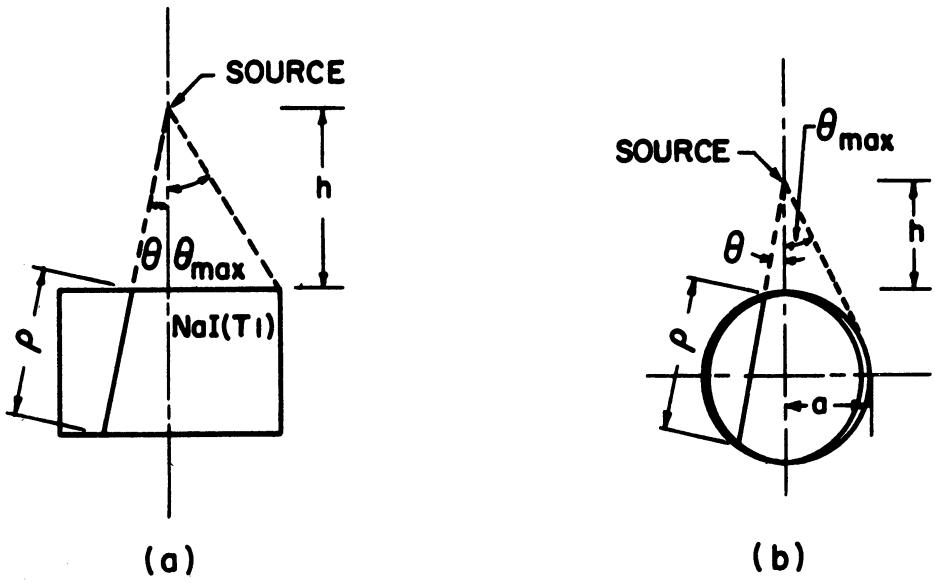

Figure 10. Source Detector Geometry for (a) Cylindrical Crystal and (b) Spherical Crystal.

This is the probability that a gamma ray emitted from the source will interact in the crystal. ρ is the path length in the crystal. The integration is carried out over the solid angle subtended by the source and surface of the crystal.

Then

$$\epsilon_{Ti} = \frac{\epsilon_{TA}}{\int_{\Omega} d\Omega/4\pi} = \text{the total intrinsic efficiency} \qquad (12)$$

Both integrations are carried out over the solid angle described above. ϵ_{Ti} then is the efficiency factor discussed previously in Equation (10). This efficiency factor has been studied as a function of source detector geometry for a number of energies and for two differently shaped crystal detectors, the right cylinder and the sphere. Values of ϵ_{Ta} as a function of source crystal geometry for cylindrical crystals are available in the literature.(21,22,23)

Equation (12) has been studied for spherical crystals. The results are outlined below. See Figure 10b.

$$\epsilon_{Ta} = \int_{\Omega} (1-e^{-\mu\rho})\, d\Omega/4\pi$$

For spherical crystals

$$\epsilon_{Ta} = 1/2\ (1-e^{-2\mu a}) - \int_{o}^{2a} \frac{\mu e^{-\mu\rho}}{4\beta} \sqrt{\rho^2 + 4(\beta^2 - a^2)}\, d\rho \qquad (13)$$

where

$$\beta = h + a$$

and

$$\rho = 2\sqrt{a^2 - \beta^2 \sin^2\theta}$$

h is the height of the source above the crystal surface and a is the radius of the sphere. The fraction of solid angle subtended is

$$\Omega/4\pi = 1/2(1-\cos\theta) = 1/2\left(1 - \frac{\sqrt{\beta^2 + a^2}}{\beta}\right) \tag{14}$$

Let $h = ma$. Then $\beta = a(m + 1)$ and $d = 2a$. Using this substitution in (13) and (14),

$$\epsilon_{Ta} = 1/2\,(1-e^{-\mu d}) - \int_o^d \frac{\mu e^{-\mu\rho}}{2d} \sqrt{\frac{\rho^2}{(m+1)^2} + d^2\left(1 - \frac{1}{(m+1)^2}\right)}\, d\rho \tag{13a}$$

$$\Omega/4\pi = 1/2\left[1 - \sqrt{1 - \frac{1}{(m+1)^2}}\right. \tag{14a}$$

Now let

$$\gamma^2 = \left[1 - \frac{1}{(m+1)^2}\right]$$

then

$$\epsilon_{Ta} = 1/2\left[(1 - e^{-\mu d}) - \mu/d \int_o^d e^{-\mu\rho}\sqrt{\frac{\rho^2}{(m+1)^2} + \gamma^2 d^2}\, d\rho\right] \tag{13b}$$

$$\Omega/4\pi = 1/2\,(1 - \gamma) \tag{14b}$$

Now the intrinsic total efficiency is obtained from (13b) and (14b)

$$\epsilon_{Ti} = \frac{\epsilon_{Ta}}{\frac{\Omega}{4\pi}} = \frac{1}{1-\gamma}\left[1 - e^{-\mu d} - \frac{\mu}{d}\int_o^d e^{-\mu\rho}\sqrt{\frac{\rho^2}{(m+1)^2} + \gamma^2 d^2 d\rho}\right] \tag{15}$$

This can be rewritten as

$$\epsilon_{Ti} = \frac{1}{1-\gamma}\int_o^d \mu e^{-\mu\rho}\left[1 - \sqrt{\gamma^2 + \frac{\rho^2}{d^2(m+1)^2}}\right] d\rho \tag{16}$$

The form of the integral, as $m = 0$ and as $m \to \infty$, (i.e., for the source on top of the crystal and for a parallel beam source) is $m = 0$

$$\epsilon_{Tio} = \int_o^d \mu e^{-\mu\rho}\,[1 - \rho/d]\, d\rho \tag{17}$$

and $m \rightarrow \infty$

$$\epsilon_{Ti\infty} = \int_0^d \mu e^{-\mu\rho} \left[1 - \frac{\rho^2}{d^2}\right] d\rho \qquad (18)$$

Both of these expressions can be integrated and ϵ_{Ti0} and $\epsilon_{Ti\infty}$ can be obtained. For other cases the definite integral cannot be found; therefore consider the following factor in the integral Equation (17)

$$F_m = \frac{1}{1-\gamma}\left[1 - \sqrt{\gamma^2 + \frac{\rho^2}{d^2(m+1)^2}}\right]$$

to a good approximation, it has been found by the author that

$$F_m \simeq a_{0m} + a_{1m}(\rho/d) + a_{2m}(\rho/d)^2 + a_{3m}(\rho/d)^3 + a_{4m}(\rho/d)^2 = \sum_{\ell=0}^{\ell=4} a_{\ell m}(\rho/d) \qquad (19)$$

The value of $a_{\ell m}$ can be found for various values of m and (ρ/d). The results are presented in Table I. Using (19) in (16a) and using the following definition

$$I_0 = (1 - e^{-\mu d}) \qquad I_3 = 3/\mu d \; I_2 - e^{-\mu d}$$
$$I_1 = I_0/\mu d - e^{-\mu d} \qquad I_4 = 4/\mu d \; I_3 - e^{-\mu d}$$
$$I_2 = 2I_1/\mu d - e^{-\mu d}$$

after integration, it is found that

$$\epsilon_{Ti} \simeq \sum_{\ell=0}^{\ell=4} a_{\ell m} I_\ell \qquad (20)$$

With these results ϵ_{Ti} as a function of distance above a 2" spherical NaI(Tl) crystal for a number of energies was calculated. The results are presented in Table II and some of the results are plotted in

TABLE I

THE VALUES OF $a_{\ell m}$ FOR VARIOUS m's AND (ρ/d)'s

ℓ	ρ/d	m = 0	m = 0.05	m = 0.1	m = 0.2	m = 0.5	m = 1.0	m = 2.0	m = ∞
0	0	1	1	1	1	1	1	1	1
1	1/4	-1	0.50310	0.02772	0.025523	0.008280	0.000508	0.000244	0
2	1/2	0	-2.488485	-2.024169	-1.638707	-1.240919	-1.088209	-1.03268	-1
3	3/4	0	2.186250	1.393994	0.748565	0.195392	0.38016	0.006816	0
4	1	0	-0.748075	-0.397547	-0.135381	0.037247	0.049685	0.025621	0

TABLE II

INTRINSIC TOTAL EFFICIENCIES AS A FUNCTION OF
DISTANCE AND ENERGY FOR A 2 " SPHERICAL NaI(Tl) CRYSTAL

Distance in cm above 2 in. Sphere E =	0.130 Mev	0.152 Mev	0.211 Mev	Ti 0.333 Mev	0.566 Mev	1.10 Mev	2.04 Mev
0.0	0.934	0.902	0.804	0.637	0.485	0.372	0.300
0.127	0.984	0.967	0.892	0.727	0.558	0.406	0.351
0.254	0.987	0.971	0.900	0.738	0.571	0.428	0.359
0.508	0.989	0.975	0.909	0.751	0.583	0.448	0.369
1.27	0.990	0.978	0.918	0.764	0.598	0.464	0.379
2.54	0.991	0.979	0.922	0.771	0.604	0.469	0.384
5.08	0.991	0.980	0.924	0.774	0.608	0.470	0.386
	0.991	0.981	0.925	0.777	0.610	0.471	0.388

Figure 11. Theoretical calculations using Monte Carlo techniques have been carried out[4] and the results are also plotted in Figure 11. In Figure 12 a comparison of ϵ_{Ti} as a function of distance for two energies is made between a 2" spherical and a 1-1/2" x 1" right cylindrical crystal. It is seen in both Figures 11 and 12 that ϵ_{Ti} is within 5% of the parallel beam case for a distance of 1.27 cm from the top of a 2" spherical crystal and therefore for all practical purposes is constant from this distance to infinity, i.e., the parallel beam case. Such a constancy does not occur until almost 20 cm from the top of a 1-1/2" x 1" NaI(Tl) right cylindrical crystal. The results for the right cylindrical crystal were obtained for a point source placed on the axis of the cylinder at the various distance above the crystal's face.[21] These results for the right cylindrical crystal are angular dependent whereas of course this is not true for the sphere. The results presented for other sized right cylinders yield similar results.

In terms of the analysis, it is more accurate to study the area under the photopeak only. (See Chapter V) This area can be determined much more precisely than the total area. There are two major reasons for the difficulty in obtaining the total area. First, it is rather difficult to eliminate all scattering effects due to the surrounding materials. These will appear as pulses in the Compton continuum. Secondly, pulse height analyzers cannot detect all pulses down to zero pulse height, for below certain pulse height levels, the equipment noise and the thermal noise of the phototube completely interfere with the detection. Therefore, consider

A_p = the area under the photopeak

ϵ_{pi} = the intrinsic peak efficiency

or, ϵ_{pi} is the fraction of those gamma rays striking the crystal face which are totally absorbed.

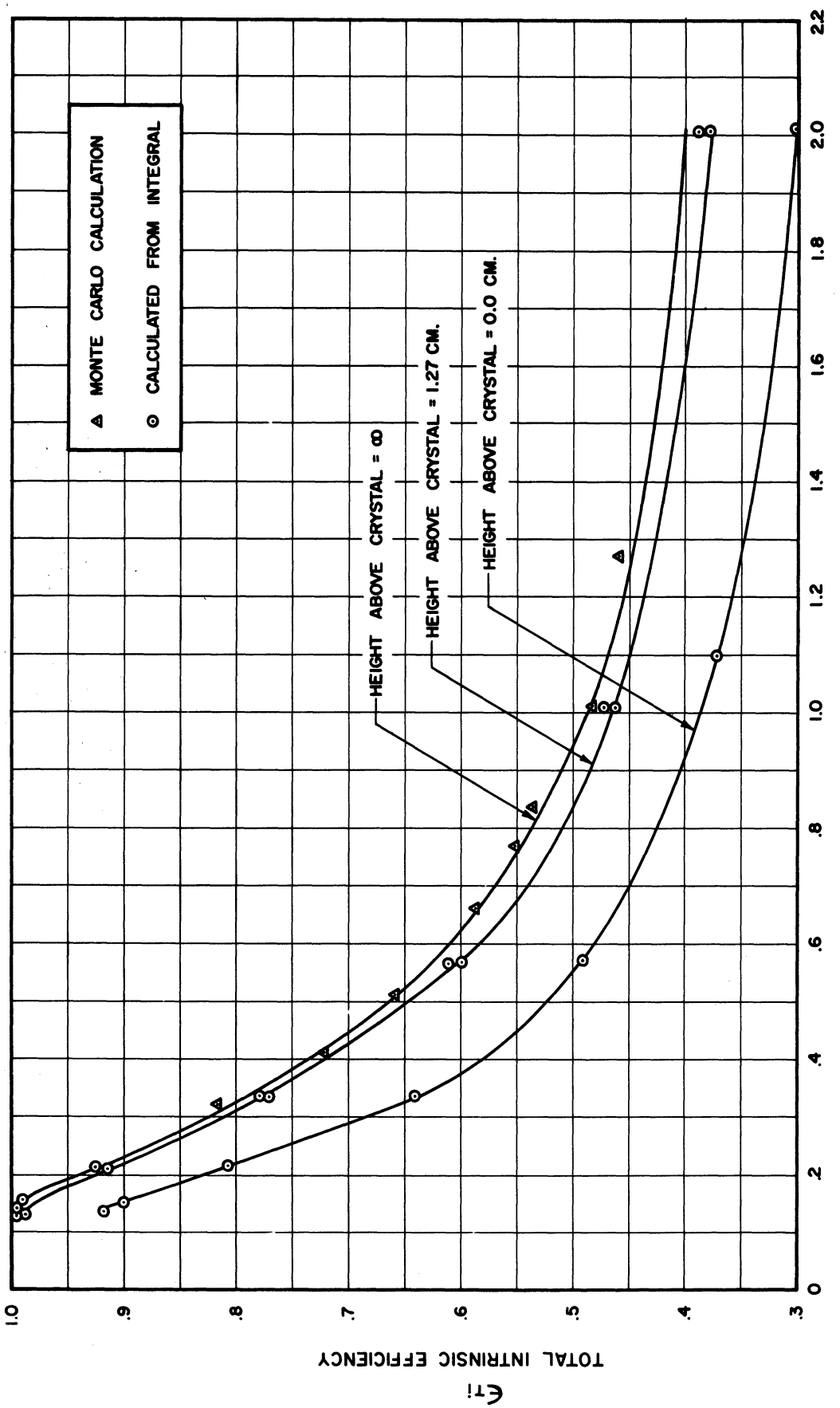

Figure 11. Total Intrinsic Efficiency as a Function of Distance for 2" NaI(Tl) Spherical Crystal.

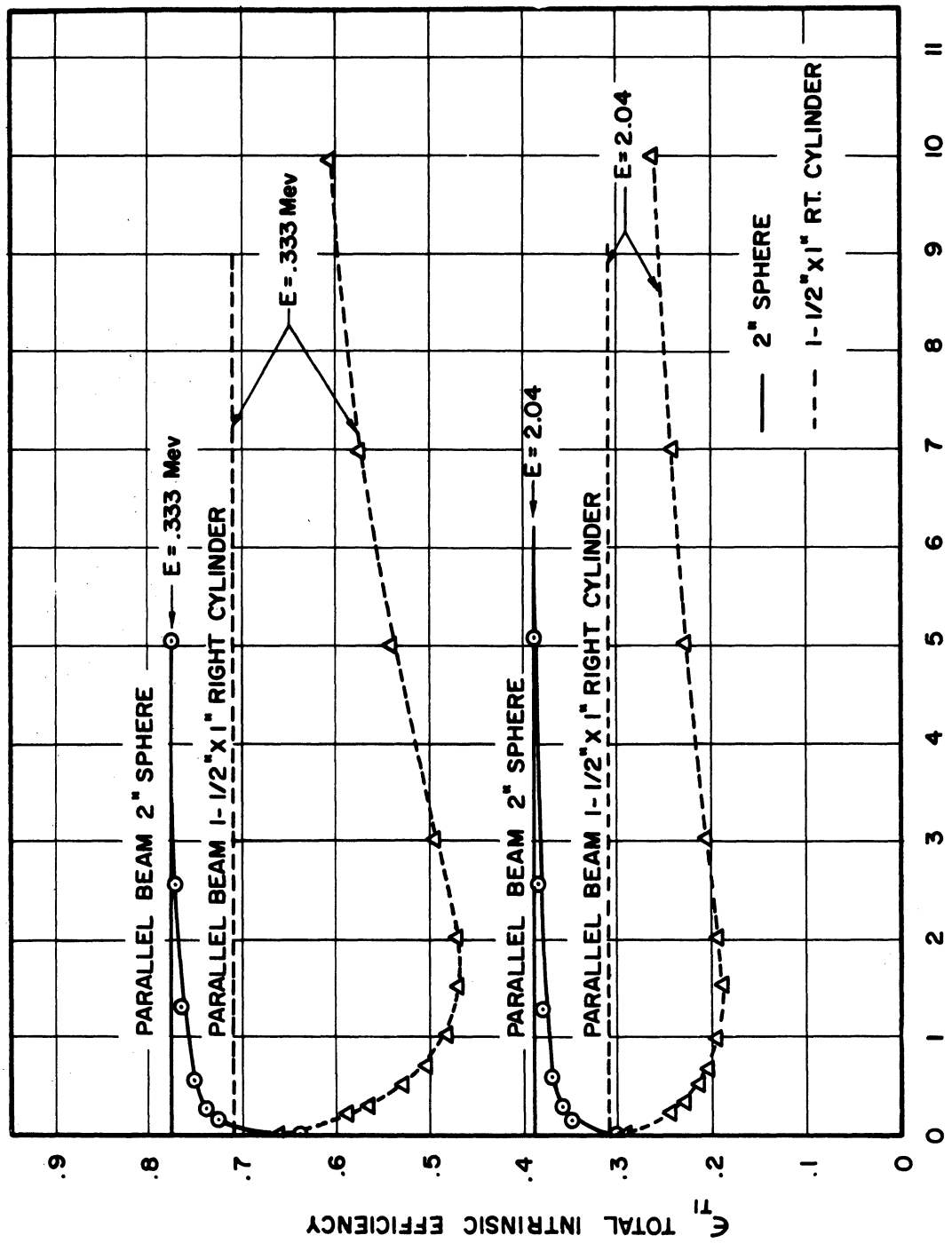

Figure 12. Comparison of ϵ_{Ti} Between 2" Spherical Crystal and 1 1/2" x 1" right Cylindrical Crystal.

If both sides of (10) are divided by A_T/A_p we obtain

$$A_p = I_o \, \Omega/4\pi \quad \epsilon_{pi}$$

where

$$\epsilon_{pi} = A_p/A_T \, \epsilon_{Ti} = P_T \epsilon_{Ti} \tag{21}$$

P_T is the peak to total ratio A_p/A_T .

For right cylindrical crystals the peak to total ratio does not change significantly as a function of distance along the axis of the cylinder.(22)

If the pulse height distribution should not change as a function of distance and angle, then the peak to total value does not change. Experiments described in Chapter V using a 2 " spherical crystal indicate that this holds true for the S_1 spherical crystal. Furthermore for a given distance (in our case 6 cm) the pulse height spectrum did not change as a function of angle as long as the source remained in the angular range indicated in Figure 3a.

Theoretical calculations of the peak to total values have been carried out by the Applied Mathematics Division, Argonne National Laboratory, and the results are presented in Table III.

In Figure 13, the intrinsic peak efficiencies for spherical crystal are plotted. These efficiencies are used in the calculation to be presented in Chapter V.

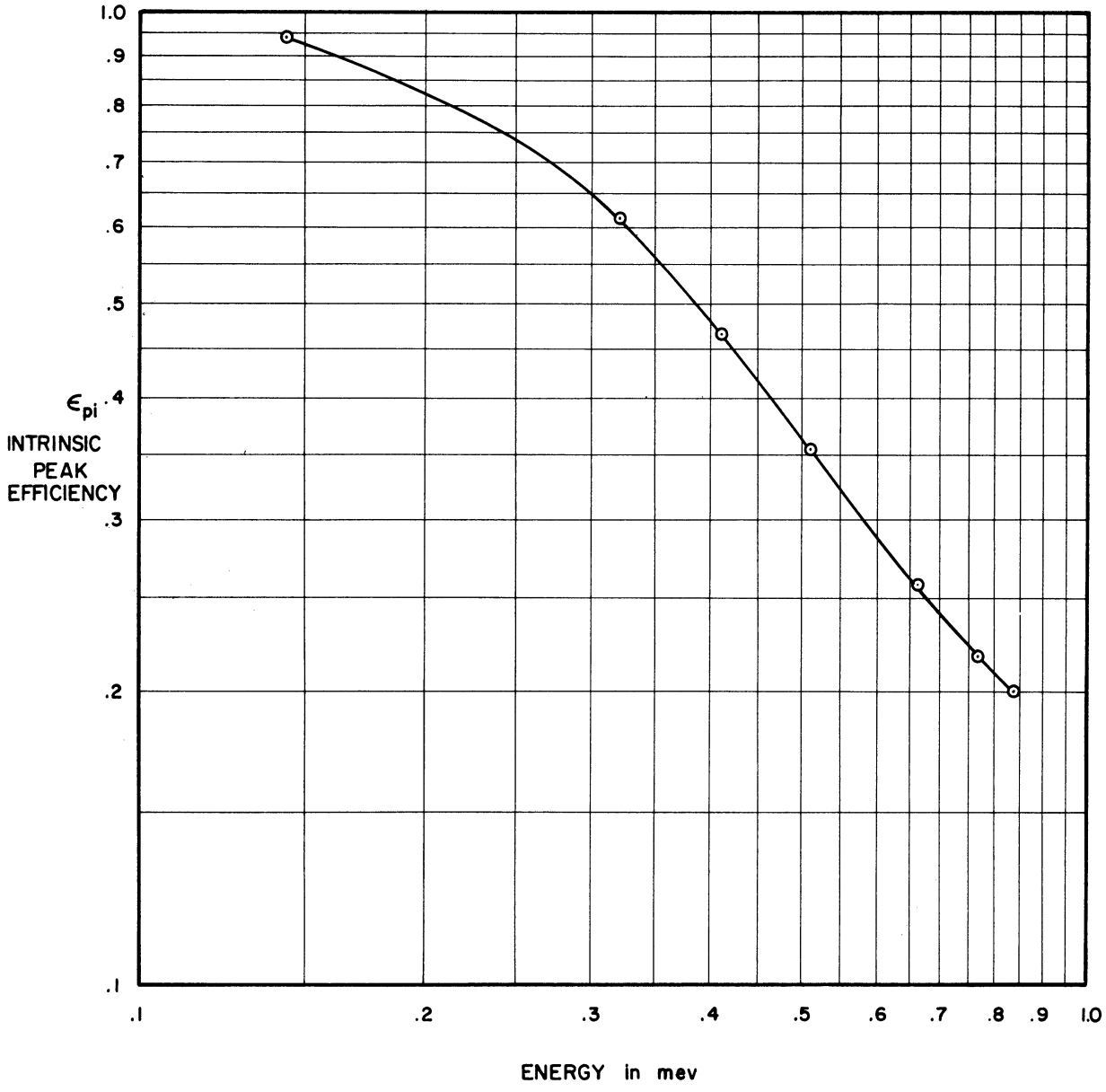

Figure 13. Intrinsic Peak Efficiency ϵ_{pi} as a Function of Energy for a Parallel Beam Incident Upon a 2" Spherical NaI(Tl) Crystal.

TABLE III

PEAK TO TOTAL VALUE FOR 2 " SPHERICAL CRYSTAL INCIDENT UPON THE CRYSTAL PARALLEL BEAM OF GAMMA RAYS

Energy in Mev	Peak to Total (Photofraction)
0.142	0.927
0.320	0.749
0.411	0.645
0.510	0.540
0.661	0.438
0.768	0.395
0.835	0.374
1.114	0.306
1.277	0.284

CHAPTER IV

LEAST SQUARE ANALYSIS OF COMPLEX GAMMA RAY SPECTRA

A. Formulation of the Principal of the Least Square

In the previous chapter, it was pointed out that if a number of gamma rays are incident upon a NaI(Tl) crystal, the pulse height spectrum is made up of a summation of the photopeaks and Compton continua of the various monoenergetic components. The problem now is to find the contribution of each monoenergetic component in the polyenergetic pulse height distribution. It was shown that for a monoenergetic source of energy E_n of gamma rays that

$$I_{on} = \frac{A_{Tn}}{\frac{\Omega}{4\pi}\,\epsilon_{Ti_n}} = \frac{\sum_i X_{in}}{\frac{\Omega}{4\pi}\,\epsilon_{Ti_n}} \tag{10a}$$

where

A_{Tn} is the total area under the pulse height distribution corresponding to energy E_n

I_{on} is the source strength in gamma rays per unit time for energy E_n

X_{in} is the most probable interaction rate at pulse height i due to the interaction of monoenergetic gamma rays of energy E_n

ϵ_{Ti_n} is the total intrinsic efficiency for a gamma ray of energy E_n

The summation is used because the measured pulse height spectrum is a histogram; that is, one measures the total number of pulses in some pulse height interval ΔV_i about V_i.

Further

$$N_n = \sum_{i=1}^{i=n} X_{in} = I_o^n \frac{\Omega}{4\pi} \epsilon T i_n \tag{10b}$$

N_n is the total number of gamma rays per sec emitted from the source which interacts with the crystal. If we have a polyenergetic flux of gamma rays with p monoenergetic components, the total number of gamma rays interacting with the crystal can be expressed as

$$N = \sum_{n=1}^{n=p} N_n = \sum_n \sum_i X_{in} = \sum_i \rho_i / t_i \tag{22}$$

in terms of its monoenergetic components and ρ_i is the total count at pulse height i in the polyenergetic pulse height spectrum for a time t_i.

Further

$$\rho_i = \sum_n B_{in} \tag{22a}$$

where $B_{in} = X_{in} t_i$ or the most probable number of interactions occurring in channel i due to a most probable interaction rate X_{in}.

The problem now is to determine the B_{in} for all p monoenergetic components. Then from (10) the source strength of each component can be determined.

In order to obtain the B_{in}'s, the shape of the pulse height spectra for each of the p energy components in the polyenergetic flux are determined. These pulse height spectra are normalized so that the area under the photopeak is unity. The area under the pulse height spectrum for energy E_n is N_n' where

$$N_n' = \sum_i Y_{in} \tag{23}$$

where

Y_{in} is the most probable normalized interaction rate occurring at pulse height i for the monoenergetic gamma rays of energy E_n

and

$$A_{in} = Y_{in} t_i \tag{23a}$$

Now take the ratio of (22) to (23) and define

$$\beta_n = \frac{N_n}{N_n'} = \frac{\sum X_{in}}{\sum Y_{in}} \tag{24}$$

further

$$X_{in} = \beta_n Y_{in}$$

and now substituting in (22a)

$$\rho_i = \sum_n \beta_n A_{in} \tag{25}$$

Due to the variance in the determination of ρ_i and $\beta_n A_{in}$, $\beta_n A_{in}$ cannot be simply determined from Equation (25). An exact solution cannot be found, therefore the following procedure was used to find the most probable values of $\beta_n A_{in}$.

The error x_i assoicated with the measurement in channel i is

$$x_i = \rho_i - \sum_n \beta_n A_{in}$$

If it is assumed that there are statistical fluctuations in the determination of ρ_i and $\beta_n A_{in}$ and these fluctuations are Gaussian in nature, the probability P_i that there will be an error x_i which lies between x_i and $x_i + dx_i$ associated with the measurement in channel i is

$$P_i = \frac{1}{\sqrt{2\pi}\,\sigma_i} \exp - \frac{x_i^2}{2\sigma_i^2} \tag{26}$$

where σ_i is the mean square deviation associated with the measurement in channel i.

The probability P that there will be m errors x_1, x_2, ... x_m which lie between x_1 and $x_1 + dx_1$, x_2 and $x_2 + dx_2$, ... x_{im} and dx_{im} associated with the measurements in the m channels is the product of m terms like Equation (26), for the measurement in a given channel is independent of the measurement in the other channels. Thus

$$P = \prod_{i=1}^{m} P_i = \left(\exp - \sum_i \frac{x_i^2}{2\sigma_i^2}\right)\left(\prod \frac{dx_i}{\sqrt{2\pi}\ \sigma_i}\right) \qquad (27)$$

The differentials dx_i are arbitrary and the σ_i's are fixed. The validity of this statement is considered in detail in Reference 24.

The criteria for obtaining the most probable values of $\beta_n A_{in}$ is that P be a maximum[24] (i.e., that there is greatest certainty).

$$M = \sum_i \frac{x_i^2}{2\sigma_i^2} = \sum_i \frac{(\rho_i - \sum_n \beta_n A_{in})^2}{2\sigma_i^2} = \sum_i \omega_i \left(\rho_i - \sum_i \beta_n A_{in}\right) \rightarrow \text{Min.} \qquad (28)$$

(since σ_i is fixed and ∂x_i is arbitrary). ω_i is the statistical weight and is equal to $1/2\sigma_i^2$. In the simplest case $\omega_i \sim 1/\rho_i$, if the counting time in each channel is constant and if it is assumed that there is no variance in A_{in}. This then is the formulation of the Principle of the Least Square. If the variation in ρ_i and $\beta_n A_{in}$ is systematic and non-random in nature, then the application of this principle may lead to erroneous results in terms of the inference of the gamma ray spectrum from the pulse height spectrum. For certain cases, error calculations can also be carried out (see Section C).

B. Method of Obtaining Minimum for Least Squares Fit

1. Incident Gamma Flux Discrete in Energy (Energy Distribution Known and Intensities Required)

A number of algorithms can be used to obtain the minimum required in Equation (28). The method of solution used depends on how much is known about the incident flux. The simplest case is considered first. In this case the gamma ray energy distribution is known, and it is desired to determine the intensity.

ρ_i is measured, and since the energy distribution is known, the monoenergetic components A_{in} are known. The minimum is therefore obtained by taking the partial derivative with respect β_k for each of the p monoenergetic components. Each derivative is then set equal to zero. Thus

$$\frac{\partial M}{\partial \beta_k} = -2 \sum_i \omega_i \left(\rho_i - \sum_n \beta_i A_{in}\right) A_{ik} = 0 \qquad (29)$$

for $k = 1, 2, \ldots, p$. There are thus p linear equations to be solved for the β's. Relation (29) can be expressed in matrix notation, as follows:(25)

$$\tilde{A}\omega\rho - (\tilde{A}\omega A)\beta = 0 \qquad (30)$$

where β is a vector of the β_k's.

A is a p by n matrix of the pulse height spectra

n is the maximum pulse height

$\tilde{A}$ is the transpose of A , and

ω is a diagonal matrix of the ω_i's .

Solving for β, it is found that

$$\beta = (\tilde{A}\omega A)^{-1}\tilde{A}\omega\rho \qquad (31)$$

Once the β's are known from (31) the B_{in} can be obtained from (24). The area under the photopeak for each monoenergetic component can then be determined. This number divided by the intrinsic peak efficiency will be equal to the number of gamma rays of energy E_n incident upon the crystal. The calculation described in Equation (31) has been programmed for the IBM 704 computer (see Appendix I for the FORTRAN listing of the program), and can handle up to twenty monoenergetic pulse height spectra and up to one hundred values for each pulse height spectrum.

The pulse height spectra required for this analysis is obtained experimentally and theoretically (see Chapter V).

2. Discrete Incident Energy Spectrum (Both the Energy Distribution and Intensity of the Incident Beam Unknown)

The difficulty in the application of the technique lies in the method of obtaining the minimum. The minimization should be made with respect to both β_n and A_{in}. A_{in} is a function of both pulse height and energy while β_n is only a function of energy. Since the pulse height spectra (A_{in}) is not known analytically as a function of pulse height and energy, it is extremely difficult to attempt to minimize Equation (28) with respect to the A_{in} (i.e., numerical methods would introduce large errors in the calculation). Therefore, the following method was used.

The energy spectrum under consideration is divided into discrete increments. A monoenergetic pulse height distribution corresponding to each increment is included. The energy components or increments will be chosen depending on the photopeaks observed in the measured distribution, and in those regions where the photopeaks are not obvious, the energy region

is divided up depending upon the energy resolution of the system. The method of choosing these increments is considered later in this chapter, and in Chapter V. Now ideally one can use relation (31) to obtain the values β_n for the various energy components. If a given energy component m is not present, β_m should be zero or the statistical variance in β_m should be greater than β_m itself. The presence of these zeros in the inverse transformation leads to the possibility of obtaining negative solutions which in turn leads to oscillating components in the solution of Equation (31). This problem is treated in detail in a work by W. R. Burrus.[26] In this paper it is pointed out that the source of error in unscrambling scintillation data by the incremental technique [i.e., simple inversion of Equation (25)] can be attributed to an error amplification when the basic equations are solved exactly. As is stated in this paper, this amplification is caused by an attempt of the exact solution to restore rapidly fluctuating components in the original gamma ray spectrum which have been attenuated below the statistical error level by the instrumental response. A first attempt to smooth out this fluctuation was made by this author using the least squares technique described above. A further smoothing can be obtained by requiring not only that Equation (28) lead to a minimum but that the solution for the β's be positive or zero.

Before outlining the method of solution for this case, an example is presented to help clarify the discussion. The method described above [Equation (31)] and the method to be discussed below is applied to a simple problem.

A measurement is made with a three channel pulse height analyser. The following data is obtained

Channel i	Counts
1	3
2	2
3	3

It is known that the measured spectrum is some linear combination of the following functions.

	Normalized Count		
Channel i	Ai_1	Ai_2	Ai_3
1	1	1	1
2	1	1	0
3	1	0	0

The following matrices are formed according to previous definitions

$$A = \begin{pmatrix} 1 & 1 & 1 \\ 1 & 1 & 0 \\ 1 & 0 & 0 \end{pmatrix} \tag{32}$$

$$\tilde{A} = \begin{pmatrix} 1 & 1 & 1 \\ 1 & 1 & 0 \\ 1 & 0 & 0 \end{pmatrix} \tag{33}$$

$$\omega = \begin{pmatrix} 1/3 & 0 & 0 \\ 0 & 1/2 & 0 \\ 0 & 0 & 1/3 \end{pmatrix} \tag{34}$$

$$\rho = \begin{pmatrix} 3 \\ 2 \\ 3 \end{pmatrix}$$

Then

$$(\tilde{A}\omega A) = \begin{pmatrix} 7/6 & 5/6 & 1/3 \\ 5/6 & 5/6 & 1/3 \\ 1/3 & 1/3 & 1/3 \end{pmatrix} \tag{35}$$

$$(\tilde{A}\omega A)^{-1} = \begin{pmatrix} 3 & -3 & 0 \\ -3 & 5 & -2 \\ 0 & -2 & 5 \end{pmatrix} \tag{36}$$

$$(\tilde{A}\omega A)^{-1}\tilde{A}\omega = \begin{pmatrix} 0 & 0 & 1 \\ 0 & 1 & -1 \\ 1 & -1 & 0 \end{pmatrix} \tag{37}$$

The β's or intensities of each component vector can be determir from Equation (31).

$$\beta = (\tilde{A}\omega A)^{-1}\tilde{A}\omega\rho$$

$$= \begin{pmatrix} 0 & 0 & 1 \\ 0 & 1 & -1 \\ 1 & -1 & 0 \end{pmatrix} \begin{pmatrix} 3 \\ 2 \\ 3 \end{pmatrix} = \begin{pmatrix} 3 \\ -1 \\ 1 \end{pmatrix} \tag{38}$$

That is the sum of the vecotrs (1, 1, 1), (1, 1, 0) and (1, 0, 0) which yields the best fit to the experimental data using the least square criteria is $3(1, 1, 1) - 1(1, 1, 0) + (1, 0, 0) = (3, 2, 3)$. The residual is zero.

Now if it is known that the intensities must be positive, the least square fit must be made so as to require Equation (28) to be a minimum with the constraint $\beta_1 \geq 0$, $\beta_2 \geq 0$, and $\beta_3 \geq 0$. One could proceed by eliminating the negative element and then reevaluating Equation (31). That is, the following matrices are now formed

$$A = \begin{pmatrix} 1 & 1 \\ 1 & 0 \\ 1 & 0 \end{pmatrix} \tag{39}$$

$$\tilde{A} = \begin{pmatrix} 1 & 1 & 1 \\ 1 & 0 & 0 \end{pmatrix} \tag{40}$$

and ρ remains the same.

Then

$$(\tilde{A}\omega A) = \begin{pmatrix} 7/6 & 1/3 \\ 1/3 & 1/3 \end{pmatrix} \tag{41}$$

$$(\tilde{A}\omega A)^{-1} = \begin{pmatrix} 6/5 & -6/5 \\ -6/5 & 21/5 \end{pmatrix} \tag{42}$$

$$(\tilde{A}\omega A)^{-1}\tilde{A}\omega = \begin{pmatrix} 0 & 3/5 & 2/5 \\ 1 & -3/5 & -2/5 \end{pmatrix} \tag{43}$$

Using these matrices, β is found to be

$$\beta = (\tilde{A}\omega A)^{-1}\tilde{A}\omega\rho = \begin{pmatrix} 0 & 3/5 & 2/5 \\ 1 & -3/5 & -2/5 \end{pmatrix} \begin{pmatrix} 3 \\ 2 \\ 3 \end{pmatrix} = \begin{pmatrix} 12/5 \\ 3/5 \end{pmatrix} \tag{44}$$

These results indicate that the best fit requiring a positive definite solution is

$$2.4(1, 1, 1) + 0(1, 1, 0) + .6(1, 0, 0) = (3, 2.4, 2.4)$$

The method just completed is rather simple but one must be careful in the method of eliminating the negative components. A method for minimizing quadratics subject to various constraints is described by Beale.[27] The following is an application to the above problem, and is a simplification of the work found in Reference 27. The simplification is possible since when applying the technique to pulse height analysis, the only constraint required is that of a positive solution for the β's when minimizing the quadratic.

In this method one forms the quadratic given in Equation (28). For the conditions in the problem discussed above, Equation (28) can be written as

$$\begin{aligned} M = 8 &- 6\beta_1 - 4\beta_2 - 2\beta_3 \\ &+ \frac{7}{6}\beta_1^2 + \frac{5}{6}\beta_2^2 + \frac{\beta_3^2}{3} \\ &+ \frac{5}{3}\beta_1\beta_2 + \frac{2}{3}\beta_1\beta_3 + \frac{2}{3}\beta_2\beta_3 \end{aligned} \qquad (45)$$

M is to be minimized and also the constraint

and $\beta_1 \geq 0$, $\beta_2 \geq 0$, $\beta_3 \geq 0$ is to be applied.

A geometric solution of the problem can be considered with reference to Figure 14. The method of solution proceeds in the following manner. Start at point 0 (Figure 14), that is, assume the solution $\beta_1 = \beta_2 = \beta_3 = 0$. Keeping $\beta_2 = \beta_3 = 0$, increase β_1 in a positive direction. As β_1 increases along this direction M will decrease until we reach point A. Point A is

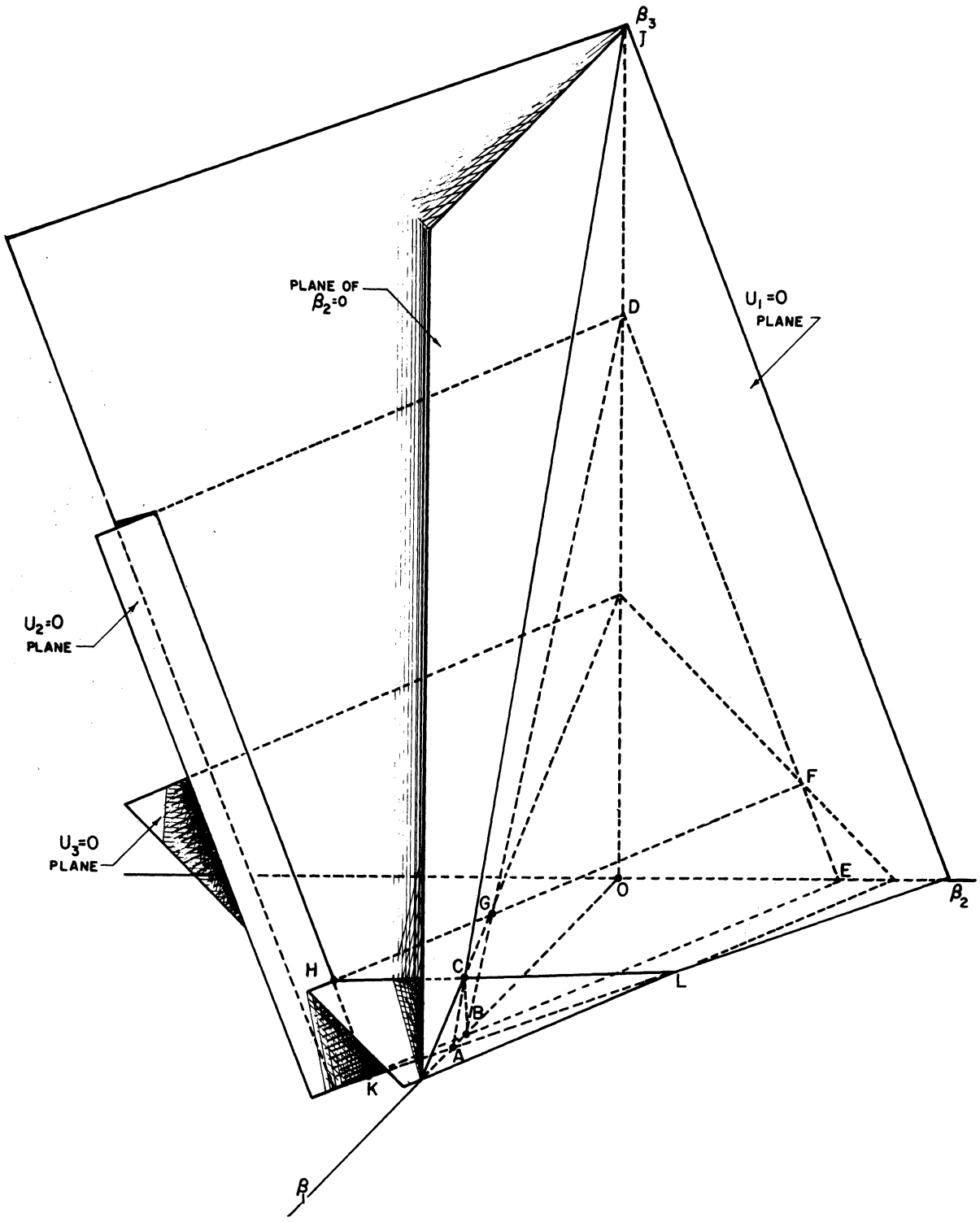

Figure 14. Geometric Solution of Least Square Fitting Problem.

determined by taking the derivative of M with respect to β_1 and setting the derivative equal to zero with $\beta_2 = \beta_3 = 0$.

$$\frac{\partial M}{\partial \beta_1} = -6 + \frac{7}{3}\beta_1 + \frac{5}{3}\beta_2 + \frac{2}{3}\beta_3 = 2u_1 \tag{46}$$

Then for

$$u_1 = \beta_2 = \beta_3 = 0, \quad \beta_1 = 18/7$$

The coordinates of A are $(18/7, 0, 0)$. The plane $u_1 = 0$ in the space described by β_1, β_2, and β_3 contain all points β_1 for which M is a minimum given any values of β_2 and β_3.

Continuing the solution, it is found that increasing β_1 any further will only increase M. A change of basis is now made. Using (46), β_1 is found in terms of u_1, β_2, and β_3.

$$\beta_1 = \frac{6}{7}\left(u_1 + 3 - \frac{5}{6}\beta_2 - \frac{1}{3}\beta_3\right) \tag{46a}$$

This substitution is now made in (44) and

$$M = \frac{2}{7} + \frac{2}{7}\beta_2 - \frac{2}{7}\beta_3 + \frac{6}{7}u_1^2 + \frac{5}{21}\beta_2^2 + \frac{5}{21}\beta_3^2 + \frac{4}{21}\beta_2\beta_3 \tag{45a}$$

Now keeping $u_1 = \beta_3 = 0$, one changes β_2 attempting to decrease M; that is β_2 is increased or decreased by moving along the line of intersection of the $u_1 = 0$ plane and $\beta_3 = 0$ plane. This intersection is along the line $\overline{AKL}$ indicated in Figure 14. The problem is how to determine which direction to move along $\overline{AKL}$ so that M decreases. This can be done by taking the derivative of M (45a) with respect to β_2

$$\frac{\partial M}{\partial \beta_2} = \frac{2}{7} + \frac{10}{21}\beta_2 + \frac{4}{21}\beta_3 + \frac{10}{7}\ u_1 \qquad (47)$$

at

$$\frac{\partial M}{\partial \beta_2} = \beta_3 = u_1 = 0,\ \beta_2 = -\frac{3}{5}$$

That is β_2 must go negative to decrease M. This cannot be allowed because of the constraints, therefore β_2 must be made zero. In this case

$$\beta_2 = u_2' \qquad (48)$$

and again substitution is made in (45a) and (46a). The plane $u_2' = 0$ is the plane of all values of β_2 given any β_1, β_3 for which M is a minimum within the constraints of the problem. Of course because of (48) this means $\beta_2 = 0$ for all values of β_1, β_3.

Starting again at point A, an attempt is made to minimize M by increasing β_3 from zero. β_2 is increased along line $\overline{ACJ}$, the intersection of the $u_1 = 0$ and $u_2' = 0$ planes. This insures that β_1 and β_2 will have values which will yield a minimum value of M within the constraint $\beta_1 \geq 0$, $\beta_2 \geq 0$ for any value of β_3. Using (45a) and (48) and taking the partial derivative of M with respect to β_3, the direction of increase or decrease of β_3 and also the value of β_3 can be determined so as to minimize M.

$$\frac{\partial M}{\partial \beta_3} = -\frac{2}{7} + \frac{10}{21}\beta_3 + \frac{4}{21}u_2 + \frac{4}{7}u_1 = 2\ u_3 \qquad (49)$$

for $u_3 = u_2' = u_1 = 0$, $\beta_3 = 3/5$

This value of β_3 along with the value $\beta_2 = u_1 = 0$ can be substituted in

(46a) to determine the value of

$$\beta_1 = \frac{6}{7}\left[3 - \frac{1}{3}\left(\frac{3}{5}\right)\right] = \frac{12}{5}$$

This is point C on Figure 6 and corresponds to the intersections of the $u_1 = 0$, $u_2' = 0$, and $u_3 = 0$ planes. Thus the values of β_1, β_2, and β_3 required to minimize(45) within the constraints that $\beta_1 \geq 0$, $\beta_2 \geq 0$, and $\beta_3 \geq 0$ are in order 12/5, 0, and 3/5. This is the same result as that obtained in Equation (44). If the solution is continued ignoring the constraints, the absolute minimum (3, -1, 1) is obtained. This is the point H, the intersection of the $u_1 = 0$, $u_2 = 0$, and $u_3 = 0$ planes. The solution will be independent of the path taken to reach the solution.

The method applied to a case where there are n values of β_n to be determined, can be outlined as follows:

1. Using Equation (28) form the quadratic $M = M(\beta_1, \beta_2, \ldots, \beta_n)$
2. Take the partial derivative of M with respect to β_1, and let $2u_1 = \frac{\partial M}{\partial \beta_1}$
3. Let $u_1 = \beta_2 = \beta_3 = \ldots = \beta_n = 0$ and solve for β_1. If $\beta_1 > 0$ then solve for β_1 in terms of $u_1, \beta_2, \ldots, \beta_n$. Substitute this value of β_1 into the equation for M. Now $M = M(u_1, \beta_2, \ldots, \beta_n)$. In this first time around the β_1 chosen will always be positive.
4. Now using the quadratic M found in step 3, the partial derivative of M is taken with respect to β_2. Let $2u_2 = \frac{\partial M}{\partial \beta_2}$.
5. Let $u_1 = u_2 = \beta_3 = \ldots = \beta_n = 0$ and solve for β_2. If $\beta_2 > 0$, then solve for β_2 in terms of $u_1, u_2, \beta_3, \ldots, \beta_n$ and substitute this value in the equation for M step 3. If

$\beta_2 > 0$, then one lets $\beta_2 = u_2'$ and substitute this value of β_2 into M step 3.

6. The above procedure is continued for all β's. At each step the values for all the β's considered up to that point are determined. If any of these β's are negative one makes the change of variable $\beta_k = u_k'$. Further if a previous change of variable was made introducing a $u_j = \frac{\partial M}{\partial \beta_j}$, u_j must be eliminated from the function M using the relations $u_j = \beta_j$ and $u_j = \frac{\partial M}{\partial \beta_j}$ before continuing the iterative process.
7. The n values of β are found after the last iteration by letting all the u's and u''s equal to zero.

This solution is equivalent to the following matrix approach. Assume the measured distribution is made up of only two components (e.g., the A_{i1}'s and A_{i2}'s). One can use least square fitting to obtain the β_1 and β_2 from Equation (31). It has been assumed the $\beta_3 = \beta_4 = \ldots = \beta_n = 0$. If $\beta_1 > 0$ and $\beta_2 > 0$ then one adds a third component (e.g., A_{i3}'s) and solves (31) for β_1, β_2, and β_3. If any of these β's are negative, one sets that given β_j equal to zero by eliminating the A_{ij} components from the matrix calculation involved in (31). In this way, one of the n components are added at a time, the β's determined for each addition and if any one of the β's determined is negative, that β is set equal to zero and its corresponding component eliminated from the matrix A before adding another one of the n components to A. The solution for the β's after all n components have been added in the manner prescribed above, will give the values for the β's for which M is a minimum and $\beta_1 \geq 0$, $\beta_2 \geq 0$, ..., $\beta_n \geq 0$.

In this way the energy distribution and intensity of the energies can be determined for the case where the incident flux is known to have a discrete energy spectrum but the distribution is unknown. This final method is similar to the "peeling off" method[3] except that after each addition of a monoenergetic component, the intensity distribution for all energy components present is reevaluated, and also the fit is made using least squares fitting. This technique could therefore be described as a "dynamic least squares peeling off" process.

The number of monenergetic pulse height spectra used in performing the above will depend upon the energy resolution of the system. If the energy distribution of the incident flux in some region is such that the energy separation between the various energy components is less than some fraction of the half widths of the photopeaks in this region, it may be only possible to determine the total number of gamma rays in this region without being able to uniquely determine the energy distribution in this region. The half width of the photopeak is a measure of the energy resolution of system. The problem of energy resolution and the effects on the analysis will be discussed further in the next section and Chapter V.

3. Continuous Incident Energy Spectra.

The measured pulse height spectrum $\rho(V)$ due to a continuous energy distribution of gamma rays $\beta(E_m)$ can be written analytically in the following manner.

$$\rho(V) = \int_{E_n = 0}^{E_n = E_{max}} \rho(E_n)\, A(V, E_n)\, dE_n \qquad (50)$$

where $A(V,E_n)$ is the smearing out function of the detection system. For a given energy E_n, the smearing out function $A(V,E_n)$ is characterized by the monoenergetic pulse spectrum as a function of pulse height V. $A(V,E_n)$ is not only a function of energy, but is also a function of source detector geometry. In Chapter 3, it was pointed out that the monoenergetic pulse height spectrum could be described by the sum of a Gaussian (the photopeak), a Compton continuum, and the various escape peaks (i.e., x-rays and annihilation). Other effects due to scattering from the surrounding materials are also needed to describe this function in the actual experimental situation. It is impossible to describe $A(V,E_n)$ analytically. Therefore this function is either measured experimentally using monoenergetic gamma ray emitters or calculated theoretically using Monte Carlo calculations[4], but in both cases one obtains only an array of numbers describing the pulse height spectrum, and still no analytic form is available.

The information desired is $\beta(E_n)$ Equation (50), and since $A(V,E_n)$ is not known analytically, it is impossible to perform an inverse transformation to obtain $\beta(E_n)$. In fact even if $A(V,E_n)$ were known it may be extremely difficult, even impossible, to perform the transform exactly. Therefore, it is impossible to perform an inverse transformation to obtain $\beta(E_n)$. Therefore, it is necessary to see whether or not some approximate method can be used to obtain $\beta(E_n)$.

The following technique for obtaining $\beta(E_n)$ is based on a theorem in sampling theory (see References 26 and 28) and upon the

fact that there is a finite energy resolution of the detection system. If a distribution has no oscillatory components with a frequency components greater than f_{max}, then the Shannon Sampling Theorem asserts that samples at discrete points not further apart than $\frac{1}{2f_{max}}$ describes the original function exactly, and in fact the original function may be reconstructed from the samples.[28] If this theorem is applicable, Equation (50) can be written as

$$\rho i = \sum' \beta_n A_{in} \tag{51}$$

where ρi is the measurement of the distribution $\rho(V)$ in channel i, β_n is the total number of gamma rays in energy group ΔE_n about E_n, and A_{in} is the value of the n^{th} sampling component (monoenergetic spectrum component) in channel i.

The sampling functions $A(V,E_n)$ (monoenergetic pulse height spectra) are written as arrays of numbers A_{in}. The shapes of these distributions were discussed in Chapter III. Considering only the energies where pair production is negligible, these spectra can be described by a Compton continuum and the photopeak. The Compton continuum is a more slowly varying function than is the photopeak. For all practical purposes the photopeak can be described as a Gaussian, Equation (9)

$$y(x) = \exp - \frac{x^2}{2\sigma_m^2} \tag{9a}$$

where $x = (V - V_m)$ in pulse height units and V_m is the pulse height corresponding to E_n and A_m in Equation (9) is unity. It is assumed

that y(x) is equal to zero, for those values of pulse height where $y(x) \leq 10^{-3}$ (Equation 9a). This assumption does not affect the analysis significantly, since these values y(x) will be lost in the noise (background) of the system.

The frequency of oscillation of the photopeak is determined in the following manner. Keeping in mind the above assumptions and further assuming that the Gaussian (Equation 52) can be closely approximated by a $\cos^2 kx$ distribution. (i.e., the amplitude of the higher frequency is negligible in terms of the analysis.) The comparison is shown in Figure 15. The value of k is chosen so that for x = 0 and for $x = \sqrt{2}\sigma_m$ (i.e., the e^{-1} point on the Gaussian) the amplitudes are equal. k is found to be equal to $\frac{\pi}{4.864\sigma_m}$. The frequency fm can be found in the following manner

$$\cos^2 kx = \tfrac{1}{2}(1 + \cos^2 kx) \tag{52}$$

The frequency is therefore

$$f = \frac{2k}{\pi} = \frac{2}{4.864\sigma_m} = \frac{1}{2.432\sigma_m} \tag{53}$$

The photopeak is assumed to contain the oscillatory component with the maximum frequency. This frequency is given by Equation (53). From the considerations briefly outlined above, and under the assumption also made above, it is believed that Equation (51) can be used for the analysis of continuous spectra. A more complete discussion of the application of Shannon's sampling theorem to such problems can be found in Reference 26 and 28.

Now from Equation (8) Chapter II, $\sigma_m = C\, E_m^{n/2}$ where E_m is the energy of the m^{th} energy component. For a given detector then,

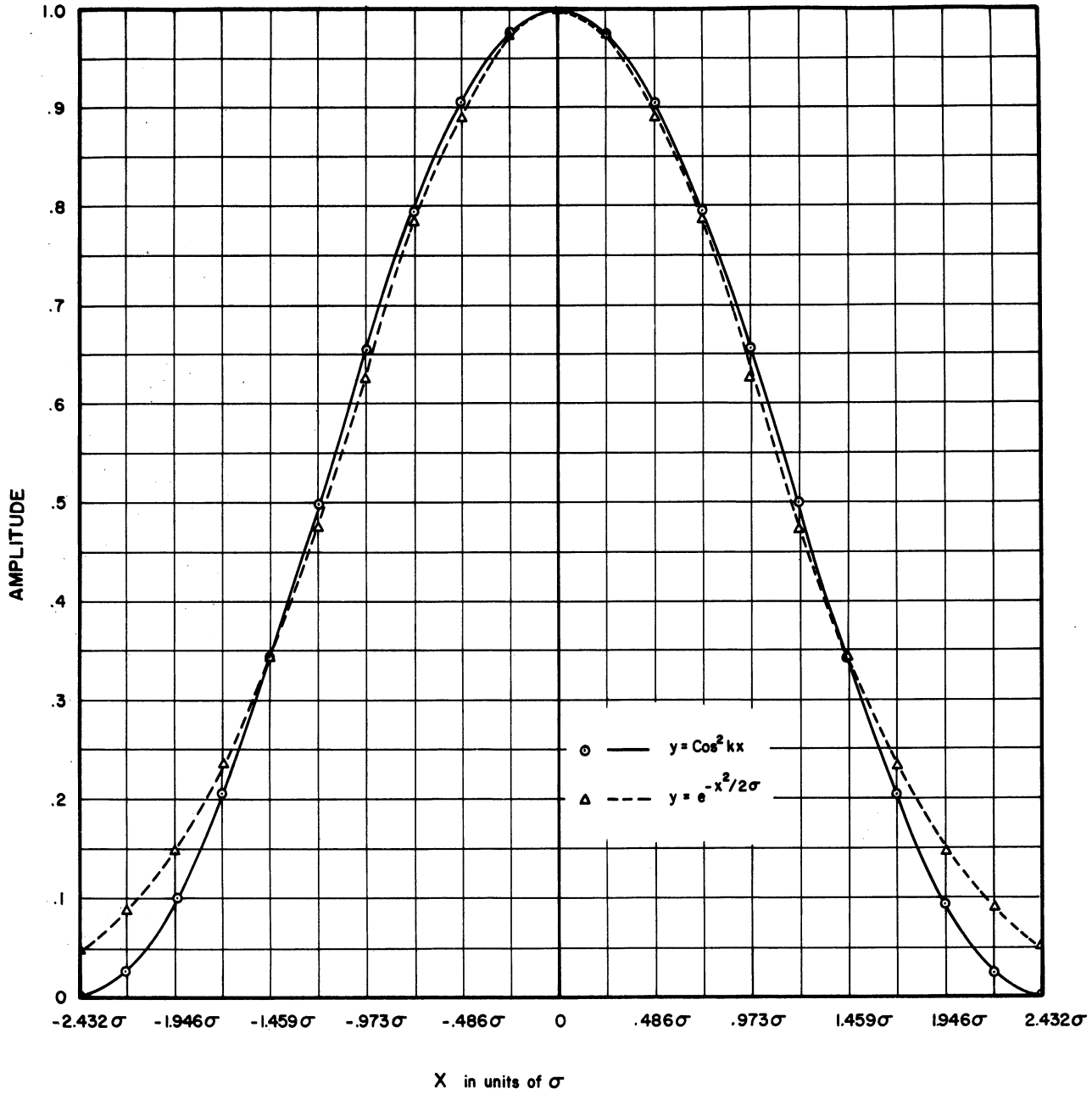

Figure 15. Comparison of Gaussian Distribution with $\cos^2 kx$ Distribution. Fitted at x = 0 and x = $\sqrt{2}\sigma$.

σ_m as a function of energy can be determined. Equation (53) can also be written in terms of the full width at half maximum $W_{\frac{1}{2}}$[1]. This width, also called the resolution width, is of importance in the definition of the resolution of the system[16]. It can be shown that

$$\sigma_m = \frac{W_{m\frac{1}{2}}}{2.354} \tag{54}$$

or using this definition then

$$f = \frac{1}{1.03\ W_{\frac{1}{2}}} \tag{53a}.$$

for all practical purposes the frequency is inversely proportional to the full width of the photopeak corresponding to the energy E_m. The criteria for the maximum separation (M.S.) between the sampling components used in Equation (51) then can be found to be

$$\text{M. S.} = \frac{1}{2\ f_{max}} \simeq \frac{1}{2} W_{m\frac{1}{2}} \tag{51a}$$

That is, the sampling components should be chosen so that their separation in energy be no greater than the half width at half maximum of their photopeaks.

The energy separation is energy dependent, thus the separation will increase for higher energies (see Equations 8 and 54). Once the components are determined, the β_m's in Equation (51) can be determined using the least square fitting techniques described above Equation (31).

A similar calculation for determining the number of samples p_i of the pulse height spectrum required to describe the pulse height distribution has been carried out in detail by Burrus[26]. These calculations indicate that one must make at least two measurements per resolu-

tion width to describe the pulse height spectrum exactly. Thus the gain, the high voltage and the pulse height increments ΔV must be adjusted to fulfill this requirement when performing the experiment.

C. Error Calculation

Once the β's in Equation (31) have been determined, it is possible to determine mean square deviation in β. If it is assumed that the A_{ij}'s (i.e., the pulse height spectra) are known without error, this calculation is rather simple. Then due to the variation in the measurement in ρ_i, there will be a corresponding mean square deviation in the determination of the β_λ's.[25] Using Equation (29), and (31)

$$\beta_\lambda = \sum_i \sum_\nu C_{i\lambda}^{-1} A_{i\nu} \omega_i \rho_i \tag{31a}$$

where the following definitions are used, the matrix $C \cong (\tilde{A}\, \omega\, A)$ is a symmetric matrix and the elements $C_{\nu r}$ of C are given by

$$C_{\nu\gamma} = \sum_i \omega_i A_{i\nu} A_{i\gamma} \tag{55}$$

C^{-1} is the inverse of matrix of C. The elements of C^{-1} are written as $C_{\lambda\gamma}^{-1}$. Thus

$$CC^{-1} = I$$

where I is the identity matrix with elements $I_{\nu\lambda}$ and

$$I_{\nu\lambda} = \sum_\gamma C_{\nu\gamma} C_{\gamma\lambda}^{-1} \tag{56}$$

remembering that both C and C^{-1} are symmetric matrices.

Further

$$I_{\nu\lambda} = 1 \qquad \text{if } \nu = \lambda$$
$$I_{\nu\lambda} = 0 \qquad \text{if } \nu \neq \lambda \tag{57}$$

From Equation (31) it is seen that β_λ is a linear homogeneous function of the counts, under the assumption that there is no error in the A_{ij}. Thus the mean square deviation $\sigma^2(\beta_i)$ corresponding to the variation in ρ_i can be written as

$$\sigma^2(\beta_i) = \sum_i \sum_\nu \sum_\gamma C_{\nu\lambda}^{-1} C_{\gamma\lambda}^{-1} A_{i\nu} A_{i\gamma} \omega_i^2 \sigma^2(\rho_i)$$

where

$$\omega_i = \frac{1}{2\sigma_i^2(\rho_i)}$$

Then

$$\sigma^2(\beta_i) = \tfrac{1}{2} \sum_i \sum_\nu \sum_\gamma C_{\nu\lambda}^{-1} C_{\gamma\lambda}^{-1} A_{i\nu} A_{i\gamma} \omega_i$$

or

$$= \tfrac{1}{2} \sum_\nu \sum_\gamma C_{\nu\lambda}^{-1} C_{\gamma\lambda}^{-1} \sum_i \omega_i A_{i\nu} A_{i\gamma}$$

then from Equation (55)

$$\sigma^2(\beta_i) = \tfrac{1}{2} \sum_\nu \sum_\gamma C_{\nu\lambda}^{-1} C_{\gamma\lambda}^{-1} C_{\nu\gamma}$$

or

$$\sigma^2(\beta_i) = \tfrac{1}{2} \sum_\nu C_{\nu\lambda}^{-1} \sum_\gamma C_{\nu\lambda} C_{\gamma\lambda}^{-1}$$

and from Equation (56) and (57)

$$\sigma^2(\beta_i) = \tfrac{1}{2} C_{\lambda\lambda}^{-1} \tag{58}$$

that is $\sigma^2(\beta_i)$ can be found from the diagonal elements of the C^{-1} matrix. The mean square deviation $\sigma^2(\rho_i)$ in the simplest case where one assumes that background is negligible is

$$\sigma_i^2 = \rho_i \tag{59}$$

Depending on the experimental situation, the corresponding σ_i's can be determined and used in the above situation. The probable error can then be determined from the mean square deviation. The above considerations are only true if it is assumed that the A_{ij}'s are known without error. The effects associated with the variation in A_{ij} has not been investigated in this work.

CHAPTER V

EXPERIMENTAL PROCEDURES AND RESULTS, AND CONCLUSIONS

A. Detector Analyser System

A schematic diagram of The Detector Analyser system used to measure the pulse height spectra is shown in Figure 16.

The design and construction of the scintillation detector was considered in Chapter II (see Figure 3).

The voltage divider and associated regulated high voltage supply, supplies the potential difference across the various dynodes in the multiplier phototube. The design of the voltage divider can be found in Reference 20. A well regulated high voltage supply must be used in these measurements for small changes in the voltage will be reflected as larger changes in the gain of the multiplier phototube.

The output of the anode of the multiplier phototube is fed into the linear amplifier and multichannel analyser. The operation of this unit was outlined in Chapter II. A 256 channel pulse height analyser was used. An electric typewriter was used for the information readout.

B. Measurement and Interpolation of Monoenergetic Pulse Height Spectrum

In the last chapter, analytic methods for inferring the incident gamma spectrum from a measurement of the pulse height spectrum were discussed. From this discussion, it can be seen that a knowledge of the characteristic pulse height spectra due to monoenergetic gamma ray emitters as a function energy is of basic importance in the analysis. These functions cannot be written in a closed analytic form as is indicated in Chapter III, therefore

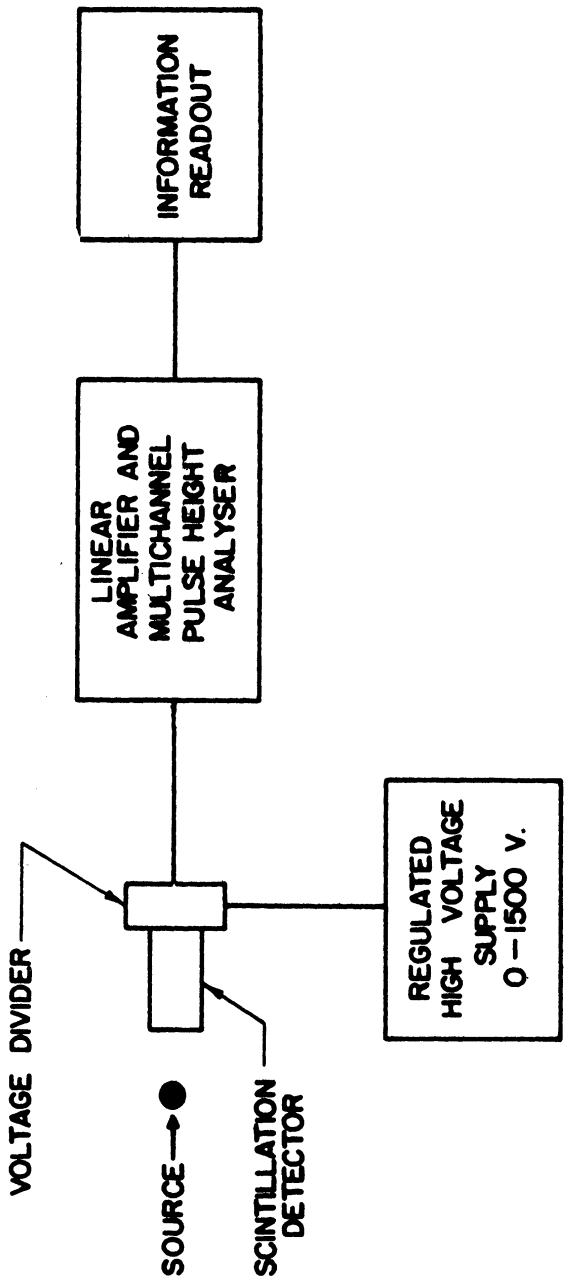

Figure 16. Schematic Diagram of Detector-Analyser System.

it is necessary to either determine these functions theoretically using Monte Carlo techniques,[4] or determine these functions experimentally. Since the Monte Carlo calculations have become available only recently, and further since these calculations do not include the effects of scattering from the crystal containment materials, see Figure 6, it was found necessary to determine these functions experimentally.

The pulse height spectra of the following emitters were measured; Co^{57} (0.14 Mev), Cr^{51} (0.32 Mev), Au^{198} (0.411 Mev), Na^{22} (0.51 Mev), Cs^{137} (0.662 Mev), Nb^{95} (0.768 Mev), Mn^{54} (0.842 Mev) and Zn^{65} (1.11 Mev). The spectra of Na^{22} and Zn^{65} are perturbed by the presence of 1.3 Mev gamma ray in the case of Na^{22} and a 0.51 Mev gamma due to the emission of a positron in Zn^{65}. The amounts of perturbation of the monoenergetic pulse height spectra for 0.51 Mev and 1.11 Mev due to the presence of these other energies is small, but an attempt was made to remove their effect by using the available theoretical calculated shape functions for these energies.

The variation of the photopeak as a function of energy was first considered. In Chapter II, it was argued that the photopeak should be Gaussian in nature, and that for this Gaussian, σ varies as a function of energy in the following manner, $\sigma^2 = \alpha^2 E^n$. σ was experimentally measured from the photopeak of each of the monoenergetic emitters, and σ^2 was plotted as a function of E on log-log paper. This measurement was carried out for both a 2" x 2" cylindrical and a 2" spherical crystal. The measurements with the cylindrical crystal were made at 10.0 cm from the top of the crystal, and the measurements with the spherical crystal were made at 3", 6", and 12" from the spherical crystal. For the 6" distance measurements

were taken at 0°, 45°, 90°, and 135° (see Figure 3a). The pulse height spectra did not change for these distances and did not change as a function of angle as long as the measurements stayed within the region shown in Figure 3a.

From the log-log plots Figure 17 and Figure 18 both α^2 and n were obtained. A comparison between the calculated photopeaks using Equation (9) and the experimentally determined values of α^2 and n, and the experimentally measured photopeaks for 2" x 2" cylindrical is shown in Figure 19. The calculated photopeak shapes are in good agreement with the experimentally determined photopeak shapes. It is therefore believed that Equation (9) can be used to describe the photopeak over the energy range considered. A similar study was carried out for the 2" spherical crystal and similar agreement was obtained.

The Compton continuum as a function of energy cannot be written in an analytic form. It was therefore necessary to interpolate its shape from the measured spectra.

The shape of the Compton continues for those energies which were used in the later sections of this paper, and for which there were no monoenergetic emitters available, were obtained in the following manner. The ratios of the height of the photopeak to the heights of a number of maxima and minima in the Compton continuum (e.g., the ratio of the height of the photopeak to the height of the maximum of the Compton continuum at the pulse height corresponding to 180° Compton scattering of the primary gamma ray in the crystal. A consideration of the number-energy spectrum of Compton electrons produced by primary photon, see References 2, 4, 5, and 17, indicates why such a maximum should be observed.) were recorded as a

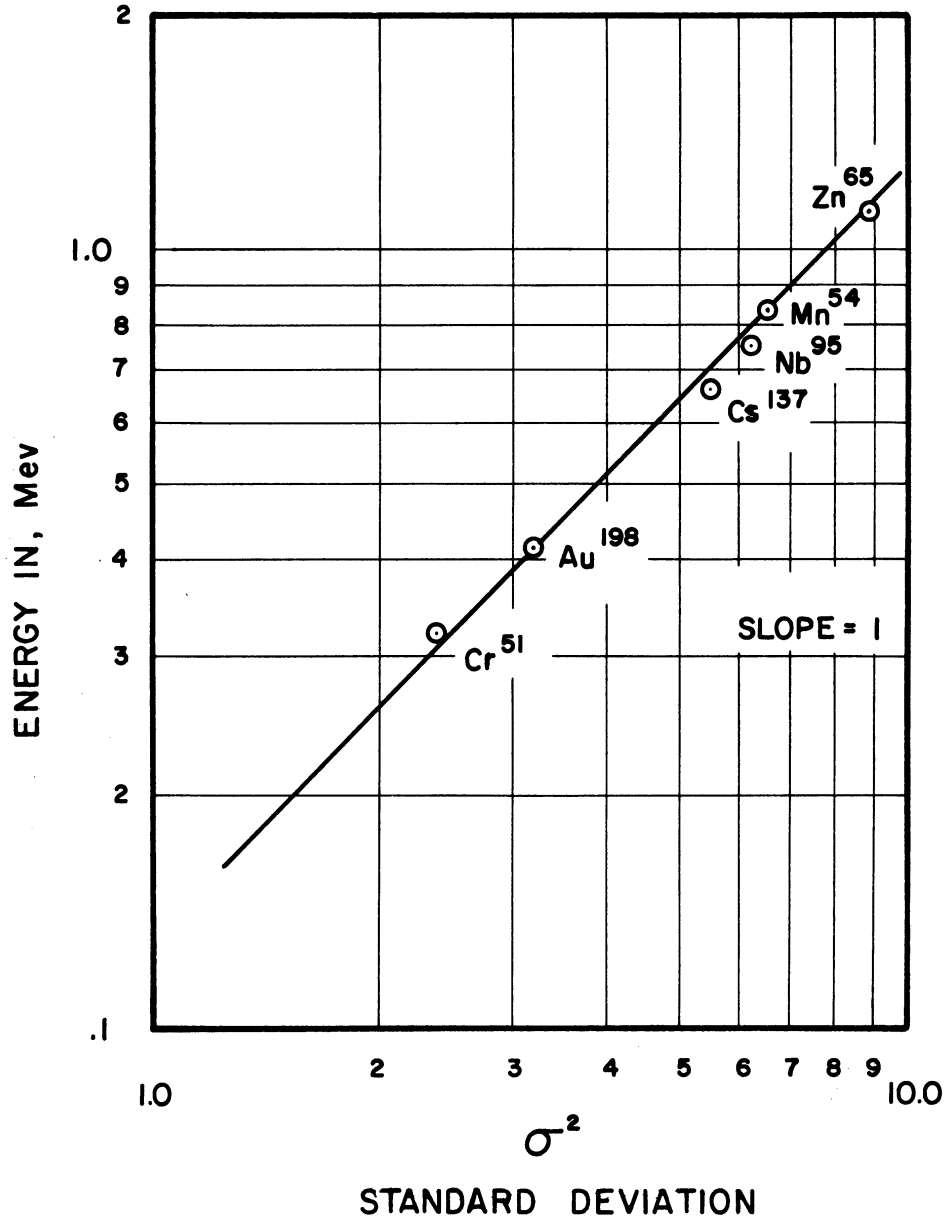

Figure 17. σ^2 as a Function of Energy for a 2" x 2" NaI(Tl) Cylindrical Crystal 9.3 cm from the Top of the Crystal.

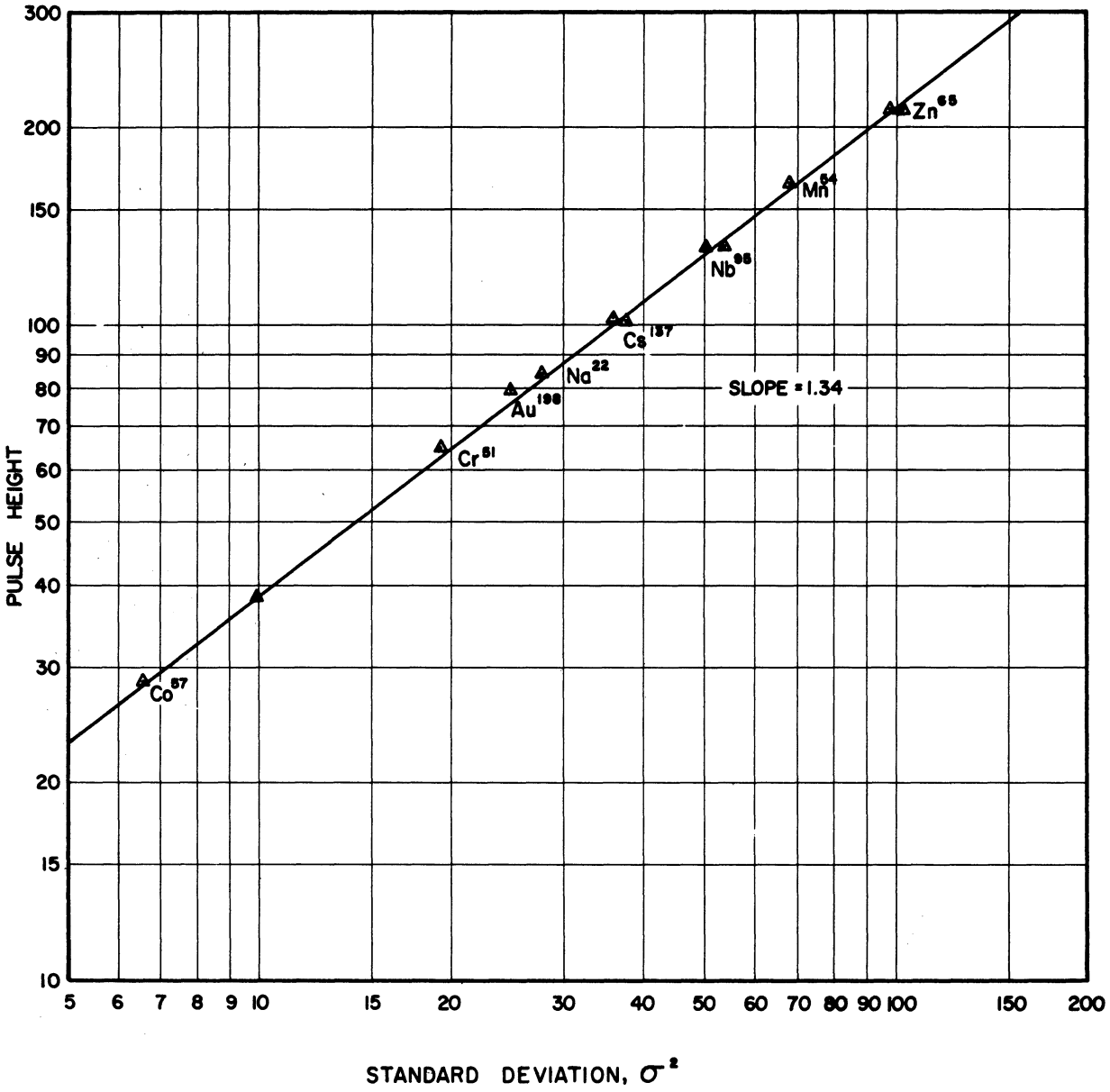

Figure 18. σ^2 as a function of Pulse Height for a 2" Spherical NaI(Tl) Crystal.

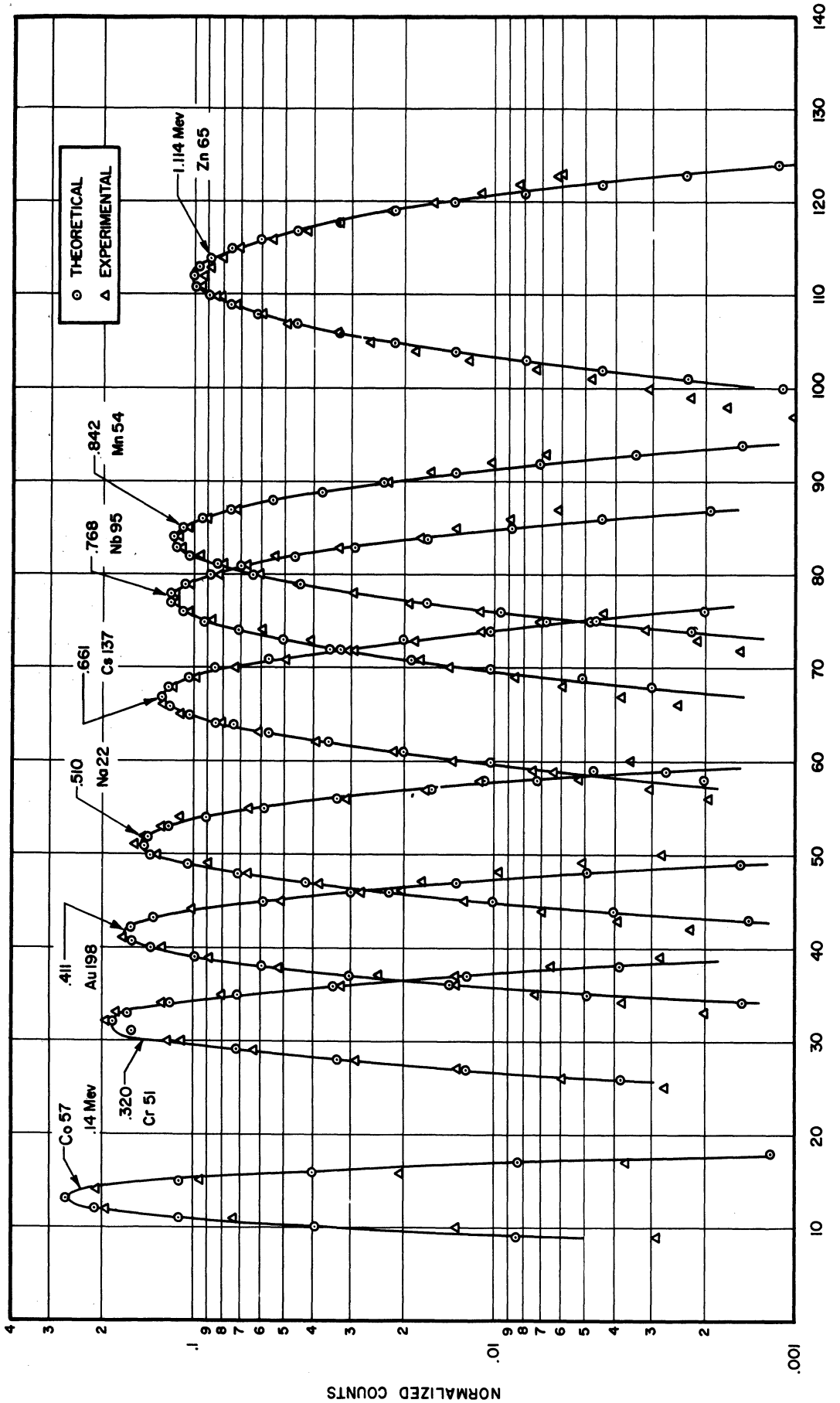

Figure 19. Comparison of Theoretical and Experimentally Measured Photopeaks for a 2" x 2" in NaI(Tl) Crystal.

function of energy. The locations on the pulse height scale of these maxima and minima as a function of energy were also determined. The measured monoenergetic pulse height were then normalized so that the area under their photopeaks were unity. The photopeaks were subtracted from the measured pulse height spectra leaving the Compton continua. The Compton continua obtained in this manner are shown in Figure 20 in dark lines. Next using the information concerning the relative heights of the maxima and minima of the Compton continua compared to their photopeaks, and the locations of these maxima and minima as a function of energy as guides, the desired Compton continua were interpolated from the measured Compton continua. These interpolated Compton continua are shown in Figure 20 in light lines. The calculated photopeak was then added to the interpolated Compton continuum to obtain the adjusted pulse height spectrum. These final adjusted pulse height spectra as a function of energy for a point emitter at 10.0 cm from the top of a 2" x 2" NaI(Tl) cylindrical crystal are shown in Figure 21. A similar analysis was carried out for the 2" spherical crystal, the final results are shown in Figure 22. Both sets of pulse height spectra have been normalized so that the area under the photopeak is unity. Also the pulse height spectra for the spherical was found to be relatively independent of source detector geometry.

In this manner, the monoenergetic pulse height needed for the analysis in the following sections have been constructed. These spectra include the effects of the scattering from the surrounding media.

Parenthetically it should be noted in Figure 17 and Figure 18 that the σ for the spherical crystal is greater than the σ for the cylindrical crystal. The ability to resolve two gamma rays close in energy

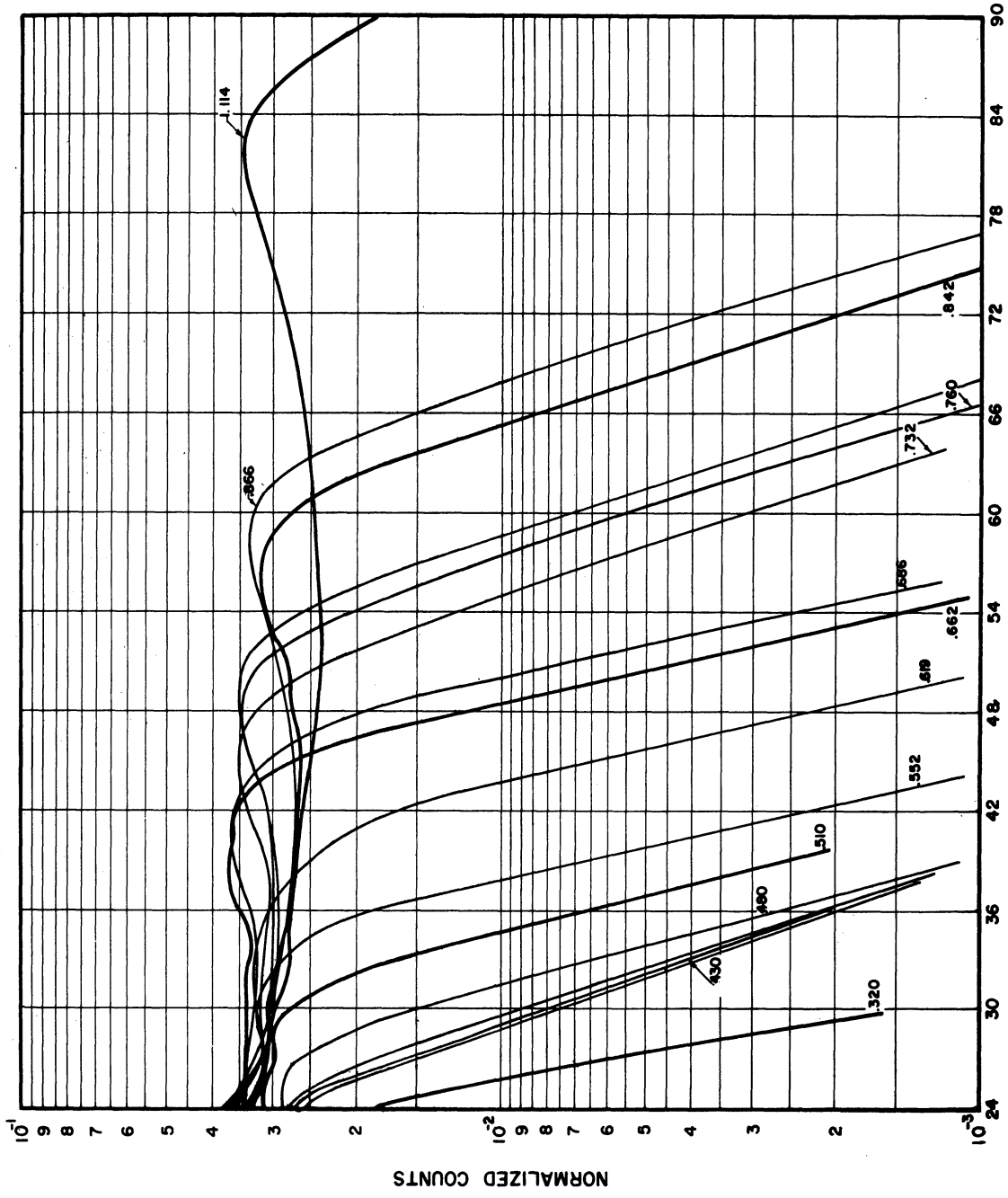

Figure 20. Experimentally Measured and Interpolated Compton Continua for a 2" x 2" NaI(Tl) Crystal.

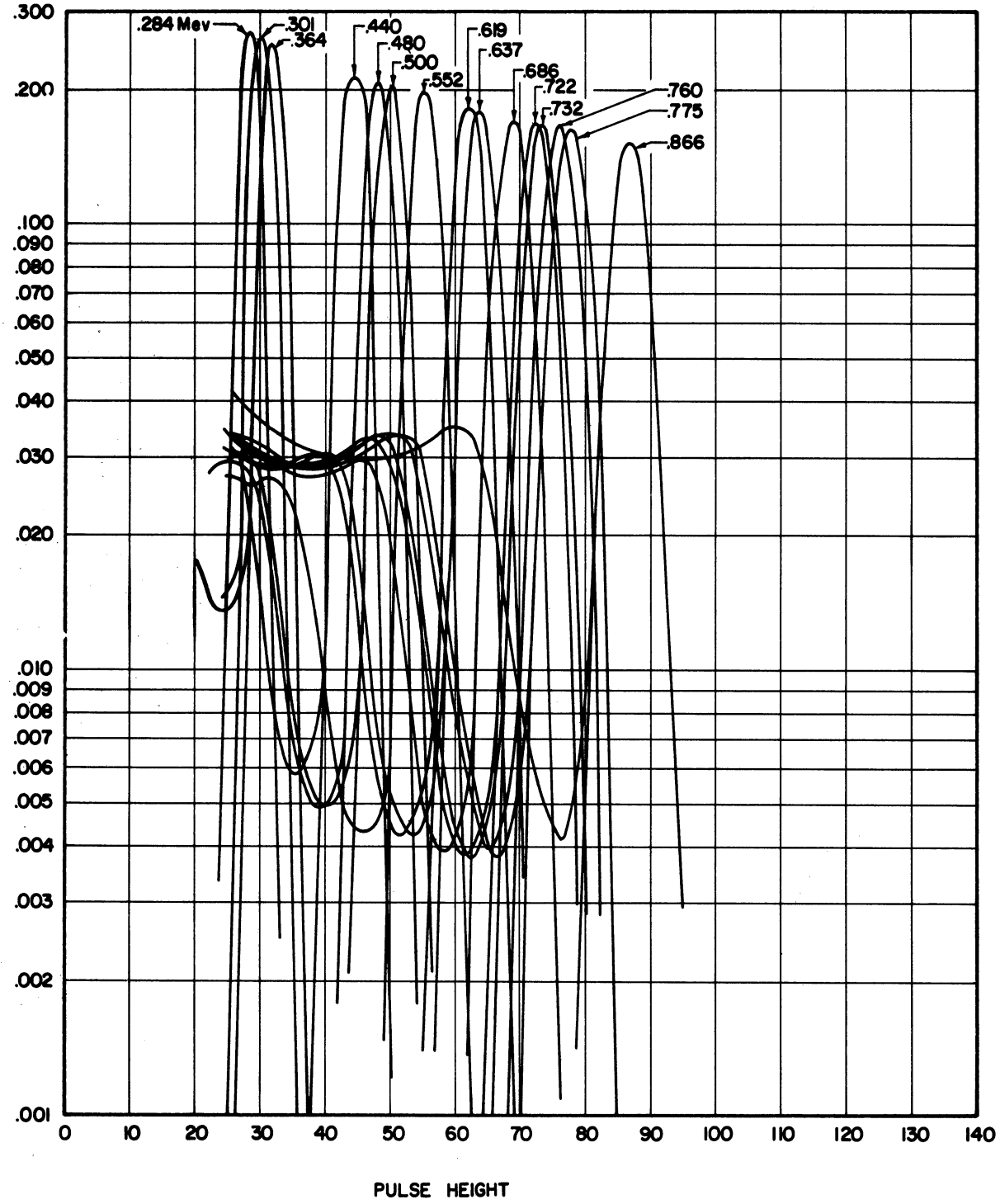

Figure 21. Final Normalized Pulse Height Spectra as a Function of Energy for a 2" x 2" NaI(Tl) Crystal.

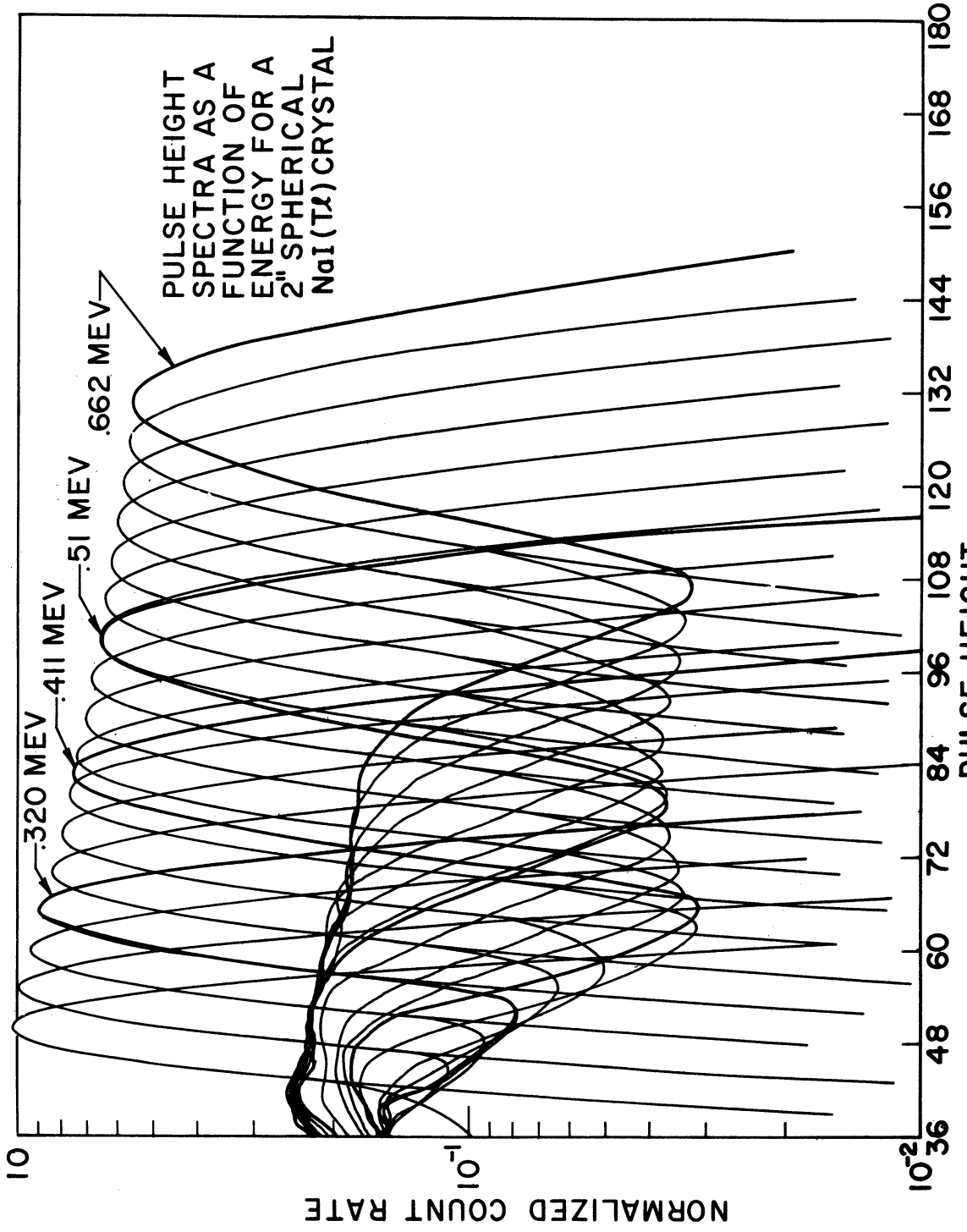

Figure 22. Pulse Height Spectra as a Function of Energy for a 2" Spherical NaI(Tl) Crystal.

depends on these widths as was discussed in Chapter IV. The smaller is σ the better is the energy resolution.[16] Attempts were made to improve the resolution of the spherical crystal detector, but because of the problems mentioned in Chapter II no better resolution was able to be obtained. Thus the spherical crystal was only used in cases where good resolution was not necessary (e.g., see Section E, Chapter V).

C. Experimental Measurements of Spherical Crystal Efficiencies

Both experimental and theoretical determinations of the efficiencies for cylindrical crystals have been carried out,[2,3,4,15,21,22,23] but only theoretical calculations carried out by the author in Chapter III and Monte Carlo calculations carried out by Miller and Snow[4] are available for spherical crystals. In the calculations carried out in Chapter III, only the total efficiencies are available, and the peak to total values or the photofractions required for the determination of the peak efficiencies [Equation (21)] are available in ANL 6318[4] for the case of a parallel beam incident upon a spherical crystal. In ANL 5902[23] photofractions as a function of source detector geometry, (i.e., for point, disc, and line sources,) are calculated and are found to be relatively independent of the source detector geometry. (i.e., for a given energy this value does not vary by more than $\pm 6\%$ as a function of source detector geometry) This seems to indicate that the photofraction may be somewhat independent of the source detector geometry. The constancy of the shape of the monoenergetic pulse height spectra for 2" spherical crystals as a function of source detector geometry was discussed in the preceding section. This seems to indicate that the photofraction may be independent of source detector geometry for

spherical crystals. The following experiment was carried out to investigate this constancy.

The pulse height spectra of the monoenergetic emitter enumerated in the preceding section were measured at 5 cm and 10 cm above a 2" spherical NaI(Tl) crystal. The sources were point sources. Then using relation (21)

$$A_{p5n} = I_n \quad \epsilon_{pi5n} \quad \Omega 5/4\pi \tag{21a}$$

$$A_{p10n} = I_n \quad \epsilon_{pi10n} \quad \Omega 10/4\pi \tag{21b}$$

where A_{p5n} and A_{p10n} are the areas under the photopeaks for the n-th emitter at a distance of 5 cm and at a distance of 10 cm respectively above the NaI(Tl) spherical crystal. $\Omega 5/4\pi$ and $\Omega 10/4\pi$ are the fraction of solid angle subtended by detector with a point source at 5 cm and at 10 cm from the top of the NaI(Tl) spherical crystal. ϵ_{pi5n} and ϵ_{pi10n} are the intrinsic peak efficiencies for n-th emitter with the source at 5 cm and 10 cm from the top of the NaI(Tl) crystal, and I_n is the source strength in gammas per second of the n-th emitter.

If it is assumed that the ϵ_{pi}'s are independent of the source detector configuration then

$$\epsilon_{pi5n} = \epsilon_{pi10n}$$

and

$$A_{pi5n}/A_{pi10n} = \Omega 5/\Omega 10 \tag{61}$$

The results of this measurement are plotted in Figure 23. The ratio of A_{pi5n}/A_{pi10n} are plotted as a function of energy and the ratio $\Omega 5/\Omega 10$

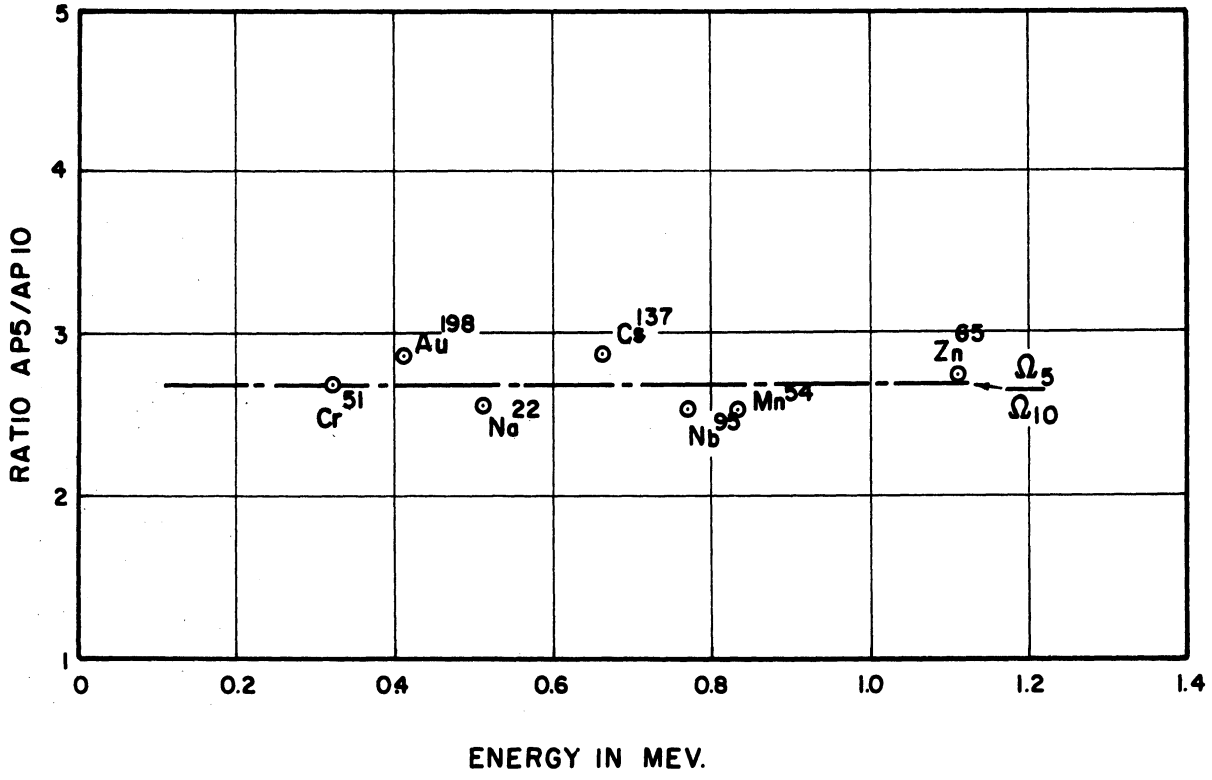

Figure 23. The Ratio of the Areas Under the Photopeaks of the Pulse Height Spectra for Point Sources at 5 cm and 10 cm from the Top of a 2" Spherical NaI(Tl) Crystal as a Function of Energy.

is indicated by the broken line. The constancy asserted in the relation holds within ±7% over the energy range investigated. A more direct measurement of the intrinsic peak efficiencies was obtained in the following manner. The pulse height spectra of the various monoenergetic emitters were measured, using a 2" x 2" right cylindrical NaI(Tl) crystal. The solid angle was kept constant (i.e., the sources were kept 9.3 cm from the top of the crystal). The intrinsic peak efficiencies ϵ_{picn} for 2" x 2" are well known as a function of source detector geometry.[4,15,21,22,23]

The area under the photopeak A_{pcn} for each of the pulse height spectra can be determined and then for the cylinder

$$A_{pcn} = I_n(\Omega c/4\pi)\ \epsilon_{picn} \tag{21c}$$

ϵ_{picn} was determined for the case of a point source 9.3 cm from the top of the crystal. Taking the ratio of (21c) with (21a) and (21b)

$$\frac{\epsilon_{pi5n}}{\epsilon_{picn}} = \frac{A_{p5n}}{A_{pcn}}\frac{\Omega_c}{\Omega_5} \tag{62}$$

$$\frac{\epsilon_{pin10}}{\epsilon_{picn}} = \frac{A_{pn10}}{A_{pcn}}\frac{\Omega_c}{\Omega_{10}} \tag{63}$$

The results are plotted in Figure 24. The broken line shows the results for the ratio of $\epsilon_{pi\infty}/\epsilon_{pic\ 9.3}$, the theoretical intrinsic peak efficiency for a parallel beam incident upon a 2" spherical crystal,[4] to $\epsilon_{pic\ 9.3\ cm}$. In this case the deviation is no more than ± 7% from the parallel beam case. Thus these results and the theoretical calculations carried out in Chapter III, it is believed that the intrinsic peak efficiency is relatively independent of the solid angle as long as there is no source closer than one half the diameter of the crystal.

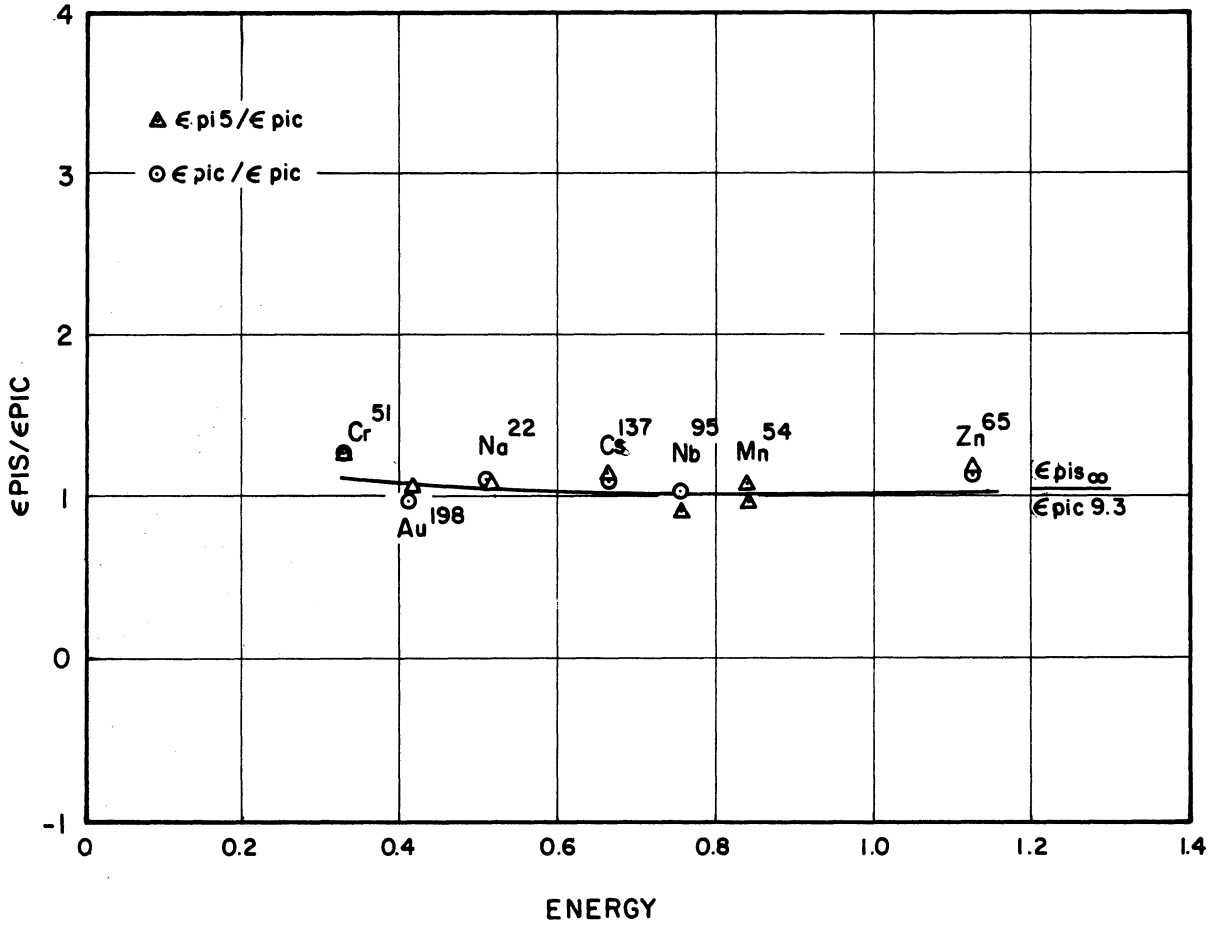

Figure 24. The Ratio of the Intrinsic Peak Efficiency of a 2" Spherical Crystal to the Intrinsic Peak Efficiency of a 2" x 2" Right Cylindrical Crystal as a Function of Energy.

D. The Experimental Determination of Discrete Spectra

1. Monoenergetic Emitters

The simplest case to consider is that of a monoenergetic emitter. The energy of an unknown emitter is determined by measuring the pulse height spectrum of a sample of known energy, and determining the point on the pulse height scale corresponding to the position of the midpoint of the photopeak. This pulse height will correspond to the energy of the emitter as discussed in Chapter II. The series of monoenergetic emitters described in Section A above can be used to calibrate the pulse height scale in terms of energy. Using these emitters, the energy of an unknown monoenergetic emitter can be determined from this calibration.

The source strength can also be determined from an analysis of the monoenergetic pulse height spectrum. The "absolute" determination of the thermal neutron flux using activation analysis is a problem wherein this technique can be easily applied. This application is a digression from problems in gamma ray spectroscopy considered up to this point. However, it is believed that the detailed description of the methods for absolute determinations of source intensity to be described below will indicate how to calculate the relative intensities needed in gamma ray spectroscopy. Furthermore the detailed descriptions of the application to neutron flux determination is included because such a description has not appeared previously in the literature. This method has been used for determining the thermal neutron flux in the core of the Ford Nuclear Reactor and has been found to be extremely useful.

The following experiment was performed. Two gold foils, a bare foil and a cadmium covered foil, were irradiated in the center of the core

of the Ford Nuclear Reactor. The pulse height spectra for these two foils were measured using a 2" x 2" NaI(Tl) right cylindrical crystal. Figures 25 and 26 are the measured pulse height spectra. From relation (21), the source strength in gamma per second I_γ can be determined in the following manner.

$$I_\gamma = \frac{A_p}{\epsilon_{pi} \frac{\Omega}{4\pi}} = \frac{A_p}{\epsilon_{pA}} \tag{21d}$$

where $\epsilon_{pA} = \epsilon_{pi} \frac{\Omega}{4\pi}$ and is the total peak efficiency. The area under the photopeak can be determined in two different ways. First analytically the photopeak is assumed to be described by a Gaussian from Equation (9) Chapter II

$$A_p = \int_{-\infty}^{+\infty} A_{max} \exp - \frac{|E - E_o|^2}{2\sigma^2} \, dE$$

$$= \sqrt{2\pi}\, \sigma A_{max} = \frac{\pi}{L_n 2} \frac{C_{Rm}}{\Delta E} W_{1/2} \tag{64}$$

where A_{max} is the count rate of the maximum of the Gaussian. In terms of the measured pulse height spectrum $A_{max} = C_{Rm}/\Delta E$ where C_{Rm} is the maximum count rate in the measured pulse height spectrum and ΔE is the channel width.

$$\sigma^2 = \frac{W_{1/2}^2}{2Ln2}$$

and $W_{1/2}$ is the half width at half maximum.

Secondly, A_p can be determined numerically in the following manner. The pulse height spectrum is plotted on three cylce semi-log paper. The measured pulse height spectrum is really a histogram; that is, each point corresponds to the total integrated number events in an increment ΔE about E. Then A_p is just the sum of the count rates at each ΔE

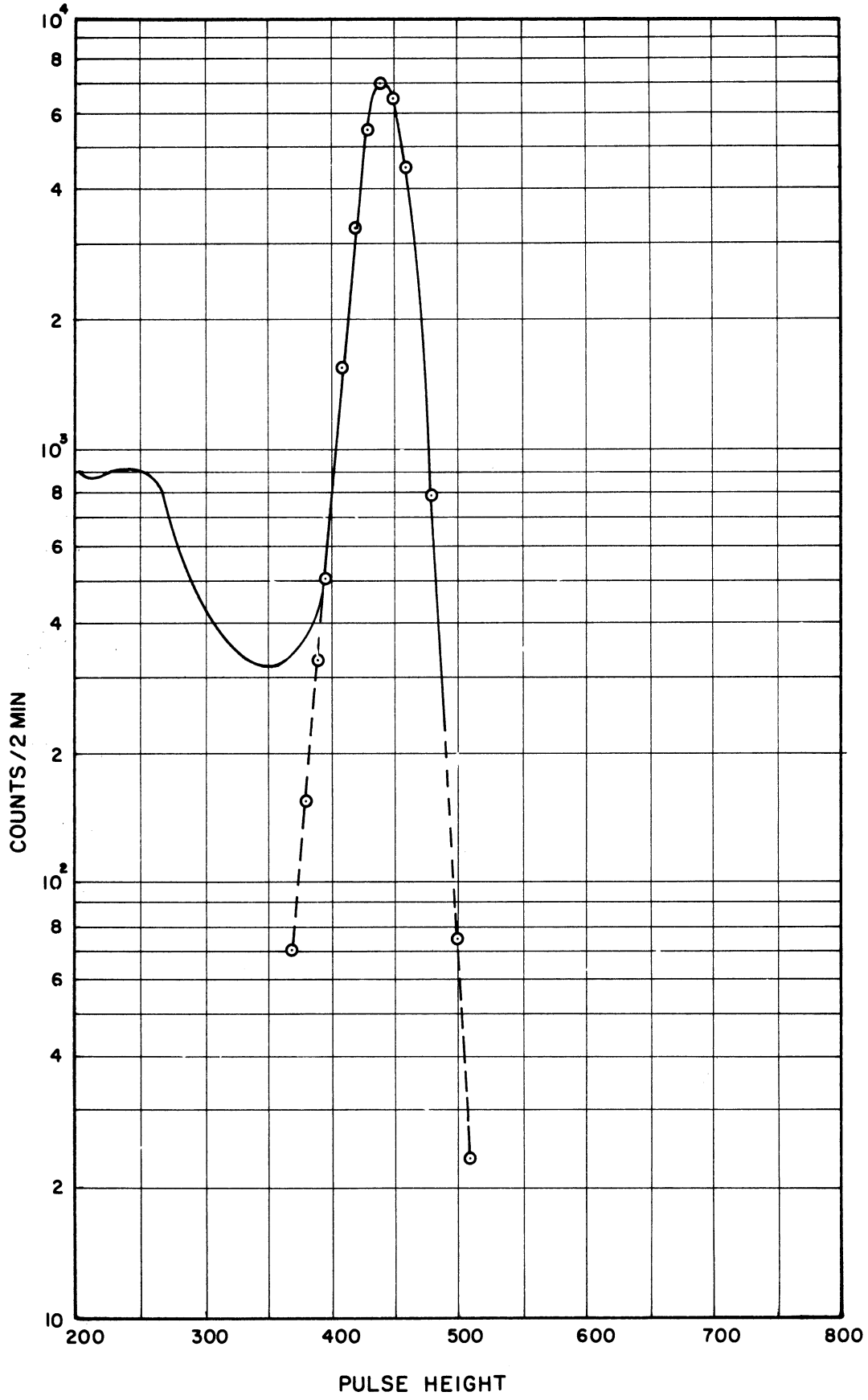

Figure 25. Measured Pulse Height Spectrum Au^{198}. Bare Foil 10.0 cm from 2" x 2" NaI(Tl) Right Cylindrical Crystal.

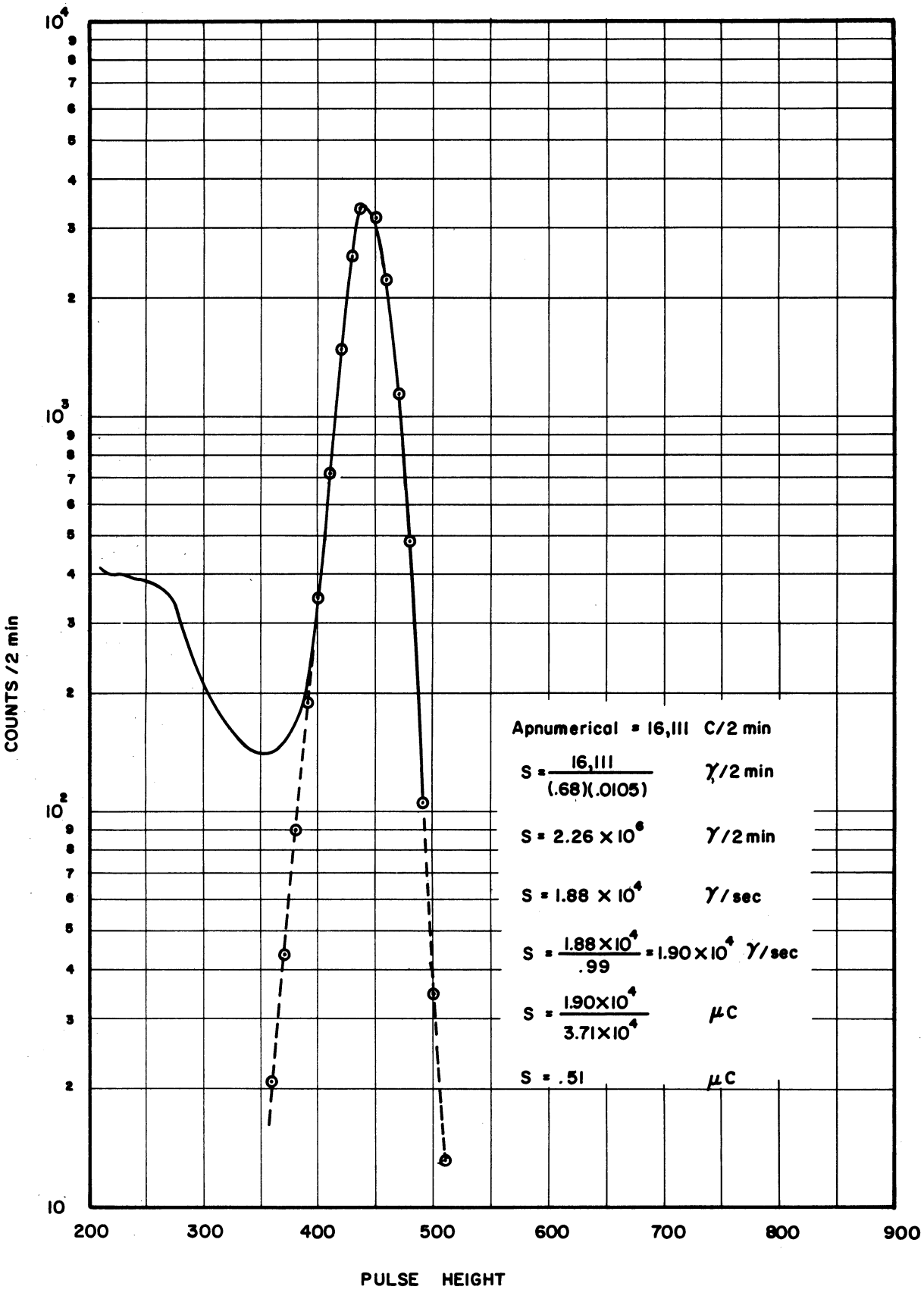

Figure 26. Measured Pulse Height Spectrum Au^{198}. Cadmium covered Foil 10.0 cm from the top of a 2" x 2" NaI(Tl) Right Cylindrical Crystal.

increment about the photopeak. On the left side of the photopeak there is interference by the Compton continuum, therefore it is necessary to extrapolate the photopeak under the Compton continuum (see Figures 25 and 26). The sum of the points over three decades will give A_p. The contribution of the area below three decades will add about 1% to the area under the curve, and therefore this amount is ignored. Using Equation (21d), I_γ can be determined. The value for ϵ_{pA} was found in References 21 and 22. For a 0.411 Mev gamma ray emitter (Au^{198}) $\epsilon_{pA} = 0.714 \times 10^{-2}$. The following is the irradiation data for the foils

Foil	Weight, M	Irradiation, t_e	Time of Removal of Foil from Reactor to the time of beginning the count, t_w
Bare	0.098 gms	4 minutes	78.5 hours
Cadmium Covered	0.098 gms	5 minutes	78.5 hours

The activities of the bare and cadmium covered foils were determined using the techniques described above. The results are in gamma rays/sec. but this within less than 1% is the same as the disintegration note (see the decay scheme of Au^{198}).

Foil	A in dis/sec	A/M in dis/sec/100 mg
Bare	3.85×10^4 d/s	3.93×10^4 d/s/100 mg
Cadmium Covered	1.88×10^4 d/s	1.92×10^4 d/s/100 mg

The following steps are used to calculate the sub-cadmium flux

a. Calculate Saturated Activity, A_S

$$A_S = \frac{A}{(1-e^{-\lambda t_e})e^{-\lambda t_w}}$$

where t_e is the exposure time

t_w is the waiting time

and

λ decay constant for gold = 0.313×10^{-5} sec^{-1}

1) Bare Foil Calculation

$$A_{sB} = \frac{A_B}{(1-e^{-\lambda t_e})e^{-\lambda t_w}}$$

since t_e = 240 sec.

$$(1-e^{-\lambda t_e}) = \lambda t_e$$

$$= (0.313 \times 10^{-5}\ sec^{-1})(2.40\ sec \times 10^2)$$

$$= 0.751 \times 10^{-3}$$

$$t_w = 78.5\ hrs = 2.826 \times 10^5\ sec$$

$$e^{-\lambda t_w} = 0.41$$

Thus

$$A_{sB} = 1.27 \times 10^8\ d/s/100\ mg$$

2) Cd Covered Foil Calculation

Since t_e = 300 sec

$$\lambda t_e = 0.919 \times 10^{-3}$$

Since the waiting time is the same

$$e^{-\lambda t_w} = 0.41$$

Thus

$$A_{scd/M} = 0.509 \times 10^8\ d/s/100\ mg$$

b. Flux Calculation

The sub-cadmium neutron flux ϕ_{scd} is

$$A_{sB} - A_{scd} = V \Sigma_{aT} \phi_{scd}$$

where V is the volume of the foil and Σ_{aT} is the average thermal absorption macroscopic cross section for $Au^{197} = \frac{N_o \rho}{A} \sigma_{AT}$

Since in the above calculation, the saturated activity has been calculated per unit weight, the above relation can be written as

$$\frac{A_{sB} - A_{scd}}{M} = \frac{V}{M} \frac{N_o \rho}{A} \sigma_{AT} \phi_{scd}$$

$$= \frac{N_o \sigma_{aT}}{A} \sigma_{AT} \phi_{scd}$$

where A is the atomic wt. = 197 for gold.

Now

$$\sigma_{AT} = \sigma_a \frac{\sqrt{\pi}}{2} = \frac{\sigma_a}{1.12}$$

where σ_a is the most probable value of the microscopic absorption cross section of gold = 96 barns

$$\sigma_{AT} = 96/1.12 \text{ barns} = 85.7 \text{ barns}$$

It may be necessary to correct for the hardening of the Maxwell-Boltzmann distribution. In the case of the FNR this correction is

$$\sigma_{AT}(.03) = 85.7 \sqrt{.025/.03} \text{ barns}$$

$$= 78.8 \text{ barns}$$

Now the flux can be calculated

$$\phi_{scd} = \frac{A_{sB} - A_{scd}}{M} \frac{A}{N_o \sigma_{AT}}$$

$$\frac{A_{sB} - A_{scd}}{M} = 0.761 \times 10^9 \text{ d/s/gm}$$

In order to have the correct units, one must have M in grams

$$\phi_{scd} = 3.14 \times 10^9 \text{ neut/cm}^2 \text{ sec}$$

The technique has been checked using standard foils calibrated at the Argonne National Laboratory, and the results have agreed to within $\pm 6\%$.

2. Polyenergetic Spectra

The first case considered was that of an emitter whose energies distribution was known but the problem was to determine the relative intensities of these energy components. The emitter chosen was I^{131}. The gamma ray energies in the spectrum of I^{131} were 0.722 Mev, 0.637 Mev, 0.364 Mev and 0.284 Mev. Another gamma ray which is a possible contaminant was also noticed at 0.5 Mev. The measured pulse height spectrum is shown in Figure 27. A point source of I^{131} was placed 10 cm from the top of a 2" x 2" NaI(Tl) crystal. The shapes of the monoenergetic pulse height spectra were determined in section A, Figure 21. These spectra were normalized so that the area under the photopeak is unity. (The curves were normalized in this manner so that the β's obtained would equal the area under the photopeak.) Thus it is only necessary to divide by the peak efficiency to determine the intensity as is done in the case described in the preceding sections. A least squares fit was made using Equation (31). The results are shown in tabular form in Table IV and graphically in Figure 27. Results for two experimentally decay for I^{131} determined by other investigators[29,30] are also presented to show the close agreement with the results obtained using the least squares fitting technique.

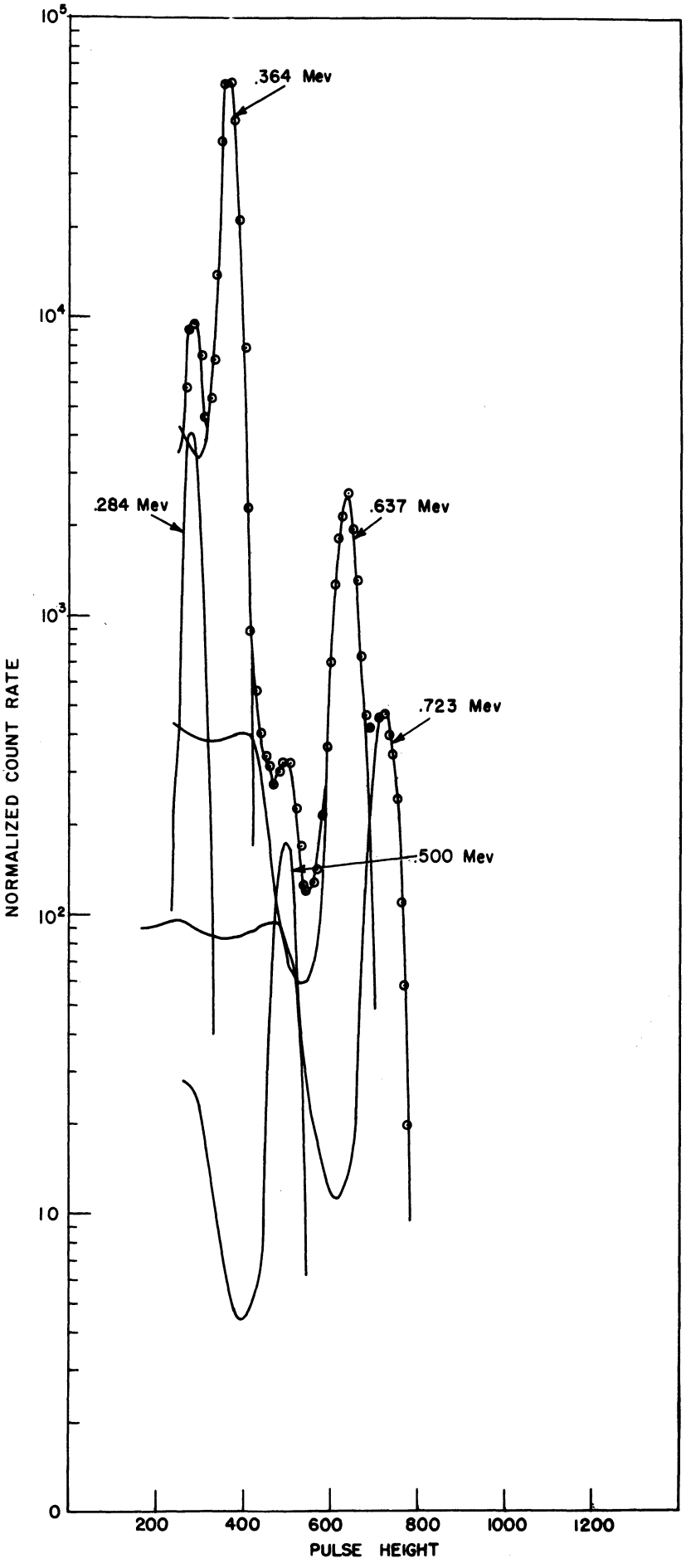

Figure 27. I^{131} Pulse Height Spectrum; 2" x 2" in NaI(Tl) Crystal Source 10 cm from the Top of the Crystal. The Amount of Each Monoenergetic Component Obtained Using the Least Square Felting Technique is Also Indicated.

TABLE IV

I^{131} GAMMA RAY SPECTRA

Energy	Least Mean Square	Other Experimental Results[29,30]	
0.284 Mev	5.2 ± 14%	6.0	4.2
0.364 Mev	100 ± 9%	100	100
0.500 Mev*	0.5 ± 20%		
0.637 Mev	10.2 ± 12%	10	7.2
0.722 Mev	2.4 ± 14%	3	2.4

* Possible contaminant

The errors were determined by the method described in Chapter IV. It was also assumed that the intrinsic efficiencies are known to within ±5%. This assumed error was determined by comparing theoretical and experimental results obtained for the efficiencies of 2" x 2" NaI(Tl) crystals.[2,21,22,23]

The next problem was to determine the energies and intensities of the singlet spectrum of W^{187}. The measured pulse height spectrum is shown in Figure 28. Certain energies are easily identified from the resolved photopeaks. In Table V, the various energies that were assumed present are tabulated. Also four iterations using the least square fitting technique described in Chapter IV are presented in Table V.

The negative β is obtained for the 0.440 Mev gamma. In terms of the decay scheme of W^{187} it is found from other experimental and theoretical calculations that its intensity relative to the other gamma rays present is almost zero,[31] and thus is lost in the background.

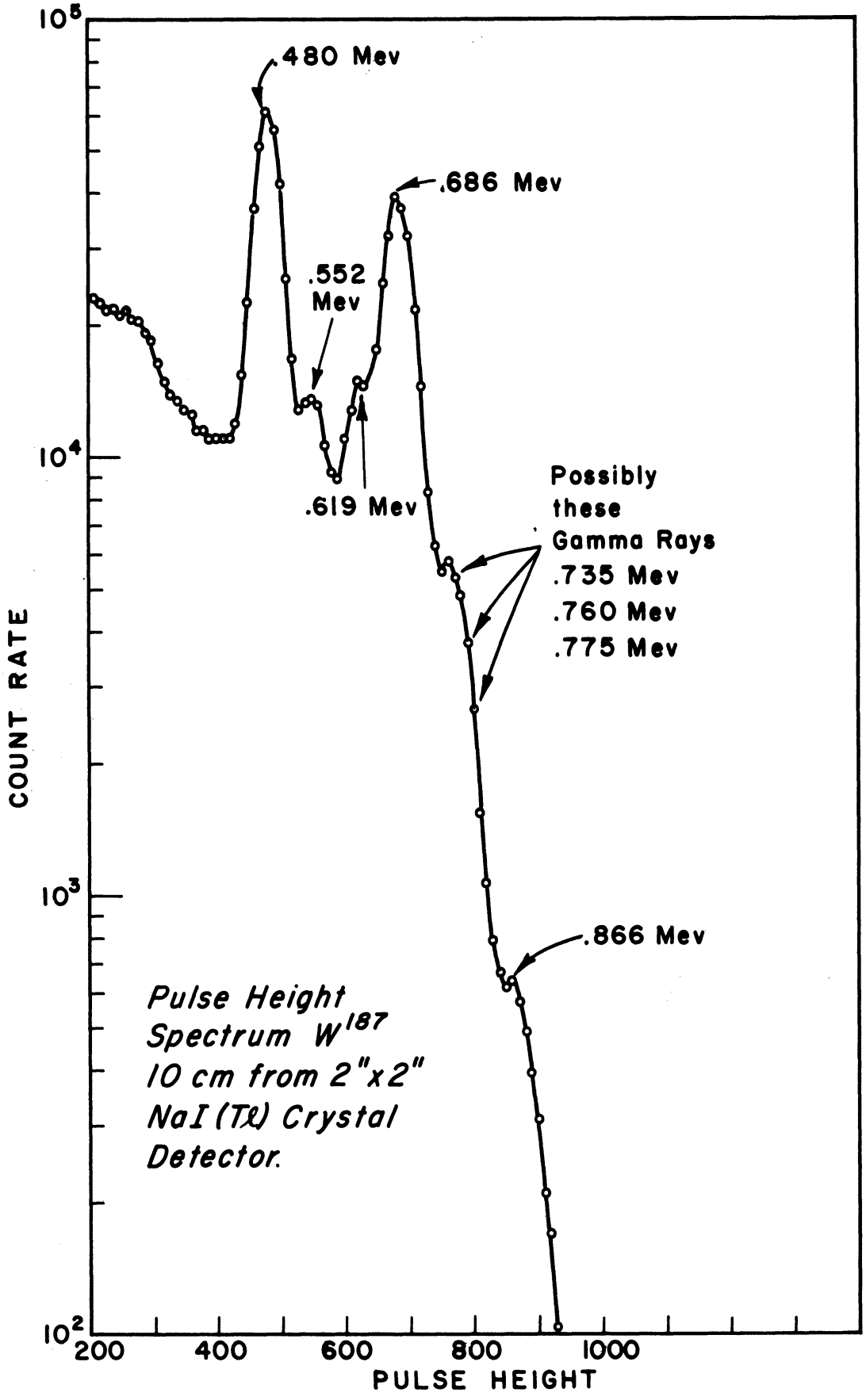

Figure 28. Pulse Height Spectrum W^{187} 10 cm from 2" x 2" NaI(Tl) Crystal Detector.

TABLE V

RESULTS OF LEAST SQUARE
ANALYSIS OF W^{187} SPECTRUM

Energy	for Data 731	for Data 741	for Data 733	for Data 743
0.866	0.464 ± .008	0.462 ± .008	0.438 ± .007	0.437 ± .007
0.775	1.93 ± .06	1.94 ± .06	2.95 ± .02	2.94 ± .04
0.760	1.72 ± .09	1.69 ± .09		
0.735	0.0245 ± .0615	0.0383 ± .0615	1.11 ± .03	1.11 ± .03
0.686	22.7 ± .06	22.5 ± .06	21.8 ± .05	21.7 ± .05
0.619	7.36 ± .03	7.33 ± .03	7.42 ± .03	7.40 ± .03
0.552	6.02 ± .03	6.02 ± .03	6.17 ± .03	6.18 ± .03
0.480	25.9 ± .06	25.6 ± .06	26.1 ± .06	26.0 ± .06
0.440	-0.601 ± .035		-0.223 ± .036	
0.301	0.112 ± .032	0.136 ± .032	0.115 ± .032	0.123 ± .032
0.256	0.867 ± .040	0.850 ± .040	0.806 ± .040	0.799 ± .040

An interesting result to be noted is that a variation in the choice of energy components in one region does not seem to affect the values of β in the other energy regions. Further, an important result is obtained in the region of the 0.730 - 0.866 Mev region. In this region the energies cannot be resolved as separate (i.e., there is loss of resolution due to the smearing out of the information by the detector), but the results obtained show that the number of gamma rays in this region remain constant although the distribution in the region changes depending upon the components chosen to represent the region. These

results seem to hold for other cases investigated. Thus it seems that when one cannot resolve the energy spectrum in a given region, because of the finite resolution of the detection system, only the total number of gamma rays in the region can be determined, but the exact energy distribution in that region cannot be determined. The ability to resolve two energies as separate can be related to the width of the photopeak at half maximum. This problem has been considered theoretically by Burrus.[26] There seems to be a minimum separation in the choice of monoenergetic components to be used in a given region depending on the width at half maximum of the photopeak. This choice will also depend greatly how well numerically (i.e., to how many significant figures) the monoenergetic pulse height spectra are known, for the least squares analysis depends on differences in these numerical values.

The results obtained in this calculation for W^{187} agree well with other experimental and theoretical calculations. The results of this calculation are discussed further in a paper by R.G. Arns and M.L. Wiedenbeck.[31] In this paper the decay scheme of W^{187} is discussed in detail.

E. The Experimental Determination of The Continuous Spectrum

The analytic method was described in the previous Chapter therefore a particular problem will be described to illustrate the method.

The problem under consideration will be that of determining the degraded gamma energy spectrum due to the scattering of gamma rays while passing through some medium. The measurements are made outside the scattering medium. In particular, the scattering of 0.662 Mev (Cs^{137}) gamma rays that pass through steel slabs was measured.

An attempt was made to simulate semi-infinite slab geometry with a plane parallel monoenergetic beam of gamma rays incident upon the front surface; so that the experimental results could be compared with theoretical results. The parallel beam was obtained by placing a point source at a large distance from a finite steel slab. The next problem is to determine how large a slab is required to simulate a semi-infinite slab. The illuminance E (i.e., the luminous or gamma flux incident per unit area) at an axial point produced by a circular disk is determined assuming that the source obeys Lambert's Law.(32) The exit surface of the slab is assumed to be the source of radiation. It is found that the illuminance E obeys the following relation.(32)

$$E = \pi B \sin^2 \alpha \tag{65}$$

where B is a constant and α is shown in the Figure 29.

Now relation (65) can be rewritten in the following manner

$$E = \pi B \left[\frac{1}{1 + \left(\frac{b}{a}\right)^2}\right] \tag{65a}$$

In the limit of the semi-infinite slab $a \to \infty$ and $E = \pi B$. If it is assumed that a point detector is used and if the detector is three inches from the circular source disk of radius 1-1/2 feet, then the illuminance at P due to such a disk will be

$$E = 0.97\ \pi B$$

Thus if the source disk were extended to inifinity the illuminance would only be increased by 3%. Thus the results measured with this disk should

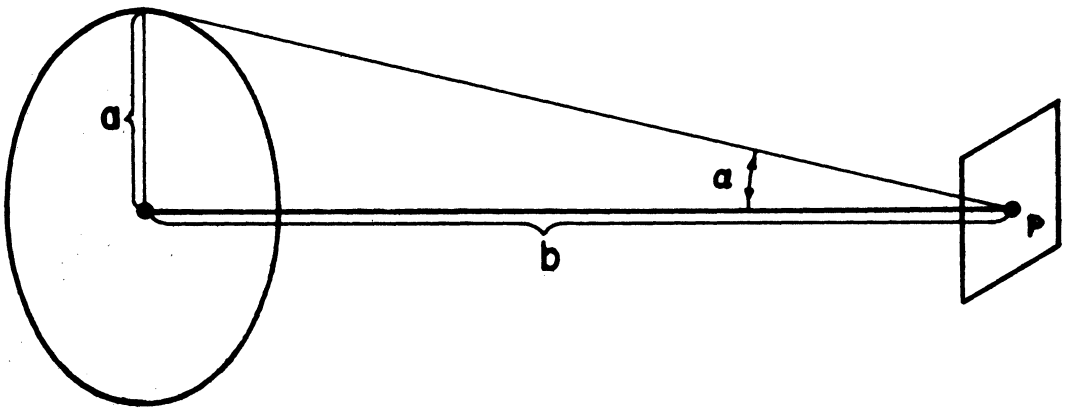

Figure 29. Illuminance at an Axial Point P by a Circular Disk.

not differ from the results obtained with a semi-infinite slab. In actual practice a 2" spherical crystal was used and placed a distance such that the center of the crystal was three inches away from the center of a 3 foot square slab of steel. For all practical purposes the sphere can be assumed to be a point.

Another problem now arises and that is that the source detector geometry cannot be defined since the source of gamma rays in the degraded spectrum is derived from the scattering of the primary beam by the media. The scattering will not only degrade the primary energy, but also the direction of propagation of the scattered gamma ray will be different than that of the primary beam. Therefore it is necessary to use a detector whose response is independent of the source distribution. As is shown in the previous Chapters, a spherical crystal can be used for this measurement as long as there are no sources closer than one half the diameter of the crystal, and as long as there is no source behind the detector. Thus placing the spherical detector outside the scattering medium (the iron slabs) and at a distance such that the center of the 2" spherical crystal is three inches from the surface of the slab, fulfills the above requirements. In this way the measurement in a semi-infinite slab geometry is simulated.

Figure 30 shows the measured pulse height spectra for 0", 1/2", 3/4", 1", 1-1/4", 1-1/2" thickness of steel slabs with a parallel beam source of 0.662 Mev gamma ray. The assumption that the continuous spectrum can be written as a sum of monoenergetic spectra discussed in Chapter IV is used. Since the so-called "dynamic least square peeling off" process has not as yet been programmed for computer computation, the following

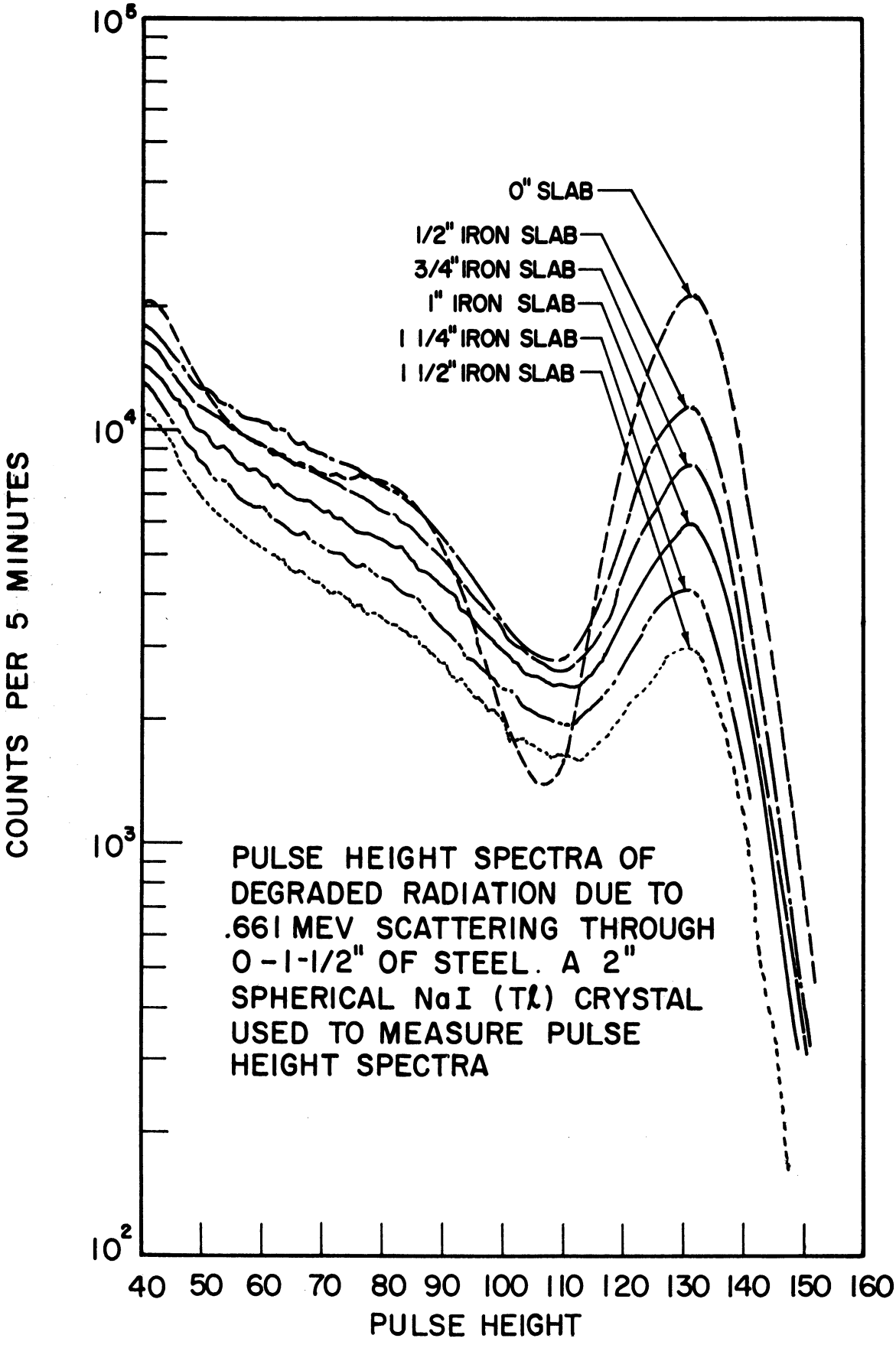

Figure 30. Pulse Height Spectra of Degraded Radiation Due to .661 Mev Gamma Rays Scattering Through 0"-1$\frac{1}{2}$" of Steel. A 2" Spherical NaI(Tl) Crystal Used to Measure Pulse Height Spectra.

iterative process was used. The energy region from 0.18 Mev to 0.66 Mev was divided into twenty equal increments. Pulse height spectra corresponding to the energy at the middle of each energy region were determined and are shown in Figure 22. The choice was made such that the monoenergetic components at the lower energy region increments were not separated in energy by more than 0.7 times the widths of their photopeaks at half maximum. The half widths vary in the manner given in Equation (8). Thus at higher energies the energy separation will correspond to increments which will be less than 0.7 times the width of the photopeaks at half maximum. Experimentally it seems that as long as one keeps the energy separation in the choice of monoenergetic less than the total width of the photopeaks at half maximum, rather than the half width at half maximum, derived theoretically in Chapter IV, that one can describe the continuous distribution. This result was determined by decreasing the number of monoenergetic components used to describe a given energy region, and for each choice of monoenergetic components calculating the number of photons in this region using least squares analysis. This number remained relatively constant, and the distribution described remained consistent until the energy separation was greater than the width at half maximum of photopeaks.

Once the monoenergetic components were chosen for the analysis of the pulse height spectra (Figure 30) a least squares analysis of the data was carried out, and the β's or intensity of each monoenergetic component was determined. Oscillatory solutions were obtained at the higher energy region where there are four or five energy components per photopeak half width. These oscillations can be attributed to the fact that the information in the energy increments is below the statistical noise or background level. That is, the more monoenergetic components are included the

smaller the ΔE increment, and thus the fewer events occurring in that increment. Correspondingly, there will be a greater statistical uncertainty in the number of events in that increment. Five iterations were made eliminating the highest energy component containing a negative solution for each iteration. The elimination of a given energy component in a region does not imply that this component is necessarily zero, it may imply that the energy increment ΔE corresponding to this increment is too small to infer statistically significant information. The elimination of an energy component in a sense increases the width of the ΔE regions corresponding to the energy regions one step lower and higher in energy from that energy component removed.

The fifth iteration yielded positive solutions for all components, for all thicknesses of slabs considered and it was found that the separation in energy of the monoenergetic spectrawas no greater than 0.7 times the half width of the corresponding photopeak throughout the energy region analysed. The results of the least square analysis yields the area under the photopeaks of each component because of the method of normalization of the monoenergetic pulse height distribution. This number divided by the intrinsic peak efficiency corresponding to that energy gives the total number of photons in that energy region. The final results are indicated in Table VI. The results have been further normalized so that the total incident gamma intensity for each slab thickness is 100 gamma rays/sec.

The analysis of the pulse height spectra could not be extended to energy region below that indicated in Table VI because of the scatter from the surrounding media (i.e., both the materials surrounding the crystal

in the detector, reflection from the walls, floors and ceilings, and the material supporting the iron slabs). This scattering greatly affects the shape of the monoenergetic pulse height spectra in this low energy region and is a function of source detector geometry. These scattering effects must be greatly diminished in order to analyze this region.

Because of the presence of the scattering and because of the uncertainty in the knowledge of the monoenergetic spectrum, no attempt was made to calculate the error involved in the results. The validity of the results were investigated in the following manner. The linear absorption coefficient for 0.662 Mev gamma rays and the energy buildup factor as a function of thickness of steel were determined from the results in Table VI and compared with theory.

The linear absorption coefficient was determined by plotting the number of photons in the region of 0.662 Mev as a function of slab thickness. The photons in this region should correspond to the undegraded gamma rays (i.e., those gamma rays which have suffered no interaction when passing through the scattering media). Any interaction should either totally remove the gamma ray by complete absorption or by scattering out of the given energy group. The results are plotted on a semi-log plot, and the results should lie on a straight line on such a plot since the removal is exponential in nature. The slope of this line is the removal cross section. The results are plotted in Figure 31. The removal cross section μ measured in this way is $\mu = 0.525$ cm^{-1}. Theoretical results for the mass absorption coefficients μ/ρ for 0.66 Mev gamma rays are available in the literature.(33) $\mu/\rho = 0.073$ cm^2/gm for 0.66 Mev gamma rays. The density

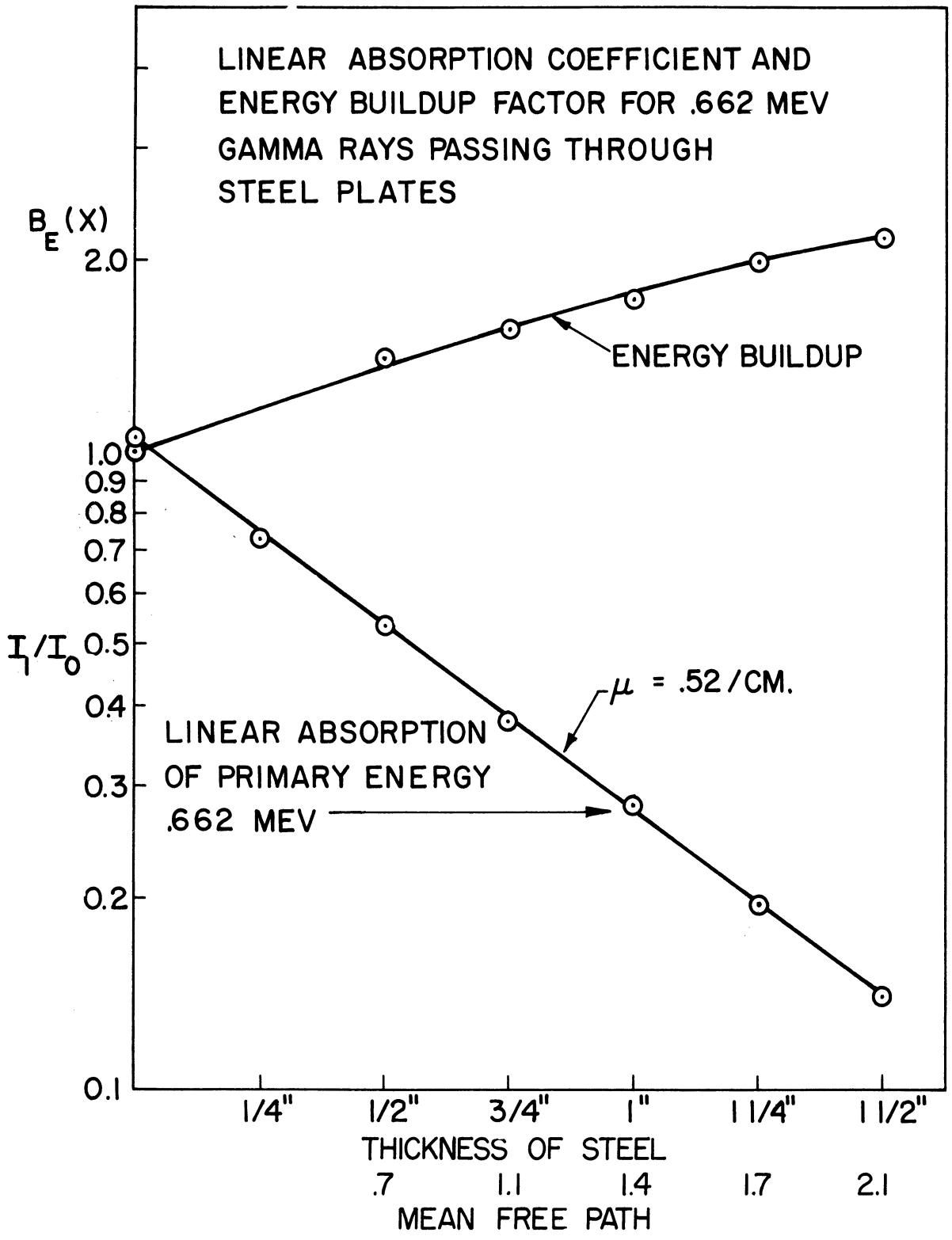

Figure 31. Linear Absorption Coefficients and Energy Buildup Factors for .662 Mev Gamma Rays Passing Through Steel Slabs.

TABLE VI

FINAL LEAST SQUARE FITTING RESULTS FOR THE DEGRADED PULSE HEIGHT SPECTRA NORMALIZED TO AN INCIDENT GAMMA INTENSITY OF 100 GAMMA'S/SEC

E Mev	PH	E_o	1/2"	3/4"	1"	1-1/4"	1-1/2"
0.58	115	0	0.424	0.384	0.339	0.357	0.305
0.53	105	0	0.338	0.425	0.418	0.323	0.270
0.48	95	0	0.438	0.473	0.435	0.386	0.338
0.42	82.5	0	0.383	0.403	0.393	0.347	0.300
0.38	75	0	0.532	0.508	0.442	0.412	0.306
0.35	70	0	0.458	0.458	0.441	0.384	0.358
0.33	65	0	0.362	0.380	0.358	0.298	0.232
0.30	60	0	0.480	0.462	0.396	0.378	0.316
0.28	55	0	0.344	0.374	0.360	0.306	0.272
0.25	50	0	0.344	0.386	0.362	0.344	0.306
0.23	45	0	0.148	0.240	0.326	0.316	0.314
0.20	40		0.0	0.0	0.492	0.548	0.562

of the steel used was 7.6 gm/cm^3. Thus $\mu = 0.555\ cm^{-1}$. The results obtained experimentally is 6% lower than the theoretical value. This difference can be partially attributed to the inclusion of the coherent scattering cross section in the theoretical results and to the forward Compton scattered gamma rays. Since the detector does not subtend a zero solid angle with respect to the scattered beam, coherently scattered gamma rays and small angle forward Compton scattered gamma rays, whose energy is

slightly changed from the primary energy, will be detected as photons in the 0.66 Mev region. This effect has been noted by other experimenters.(3)

Next the energy buildup factor $B_E(x)$ was calculated as a function of shield thickness in terms of lengths measured in mean free paths. The energy buildup factor is defined as follows.(34)

$$B_E(x) = \frac{\int_0^{E_o} I_x(E,E_o)\, dE}{I_{xo}(E_o)} \qquad (66)$$

where $I_x(E,E_o)\, dE$ is the differential energy flux measured due to the scattered and unscattered flux of gamma rays with incident energy E_o, measured at the exit surface of the scattering media of thickness x. $I_{xo}(E_o)$ is the energy flux due to the unscattered flux of gamma rays measured at the exit surface of the scattering media of thickness x.

The integral can be easily evaluated from Table VI in the following manner. The total number of gamma rays in a region ΔE about the average energy E are tabulated in this table. Thus multiplying the average energy by the total number of photons in the ΔE about E and summing over all E will yield the value of the integral in Equation (66). Monte Carlo calculations carried out by the Oak Ridge National Laboratory indicate that the integration from 0 to 0.17 Mev adds only about 6% to the integral.(35) Therefore this region can be excluded without affecting the results significantly. $I_{xo}(E_o)$ is found simply by multiplying 0.66 by the number in this energy group. $B_E(x)$ can then be found. The results for $B_E(x)$ were compared with theoretical calculations carried out by Peebles using a multiple scattering technique.(36) In the energy region from 0.5 Mev to 1.0 Mev the shape of the energy buildup agree well.

Further, $B_E(x)$ calculated by multiple scattering techniques at two mean free paths is 2.0 which agrees well with the results obtained experimentally.

F. Conclusions and Proposed Further Experimentation

The use of least square techniques in the analysis of the gamma ray pulse height spectrum allows one to infer information concerning the energy distribution and intensities of the gamma ray flux which produced that pulse height spectrum. This least squares technique has been programmed for the IBM 704 computer. Experimental results for both discrete and continuous energy distribution seem to agree well with theoretical calculations. A more general method of solution the so-called "dynamic least squares analysis" is proposed. Because this method has not been programmed for computer use, the technique has been used only in a limited way. One of the major limitations in programming of this latter method for the IBM 704 computer, available at The University of Michigan, is the lack of sufficient fast memory capacity. Further, the use of the least squares fitting analysis also allows one to obtain some measure of the statistical variance in the measurement. It is believed that further work is required to include the effect of the error in the shape function of the monoenergetic pulse height spectra on the analysis.

It has also been shown theoretically and experimentally that in certain cases when the source detector geometry cannot be well defined, that the use of spherical crystals allows one to make the measurement and perform the analysis. The geometric limitation is that there be no sources of radiation behind the detector nor any sources closer to the spherical detector than one-half the diameter of the sphere.

One of the great limitations in the use of this scintillation method can be attributed to the lack of precise knowledge concerning the shapes of the monoenergetic pulse height spectra. It is believed that it would be rather fruitful to experimentally study this problem, compare the results with the theoretical calculations[4], and develop a more precise method for obtaining these pulse height functions.

Another problem which must be considered carefully when performing these experiments is that of the perturbation of the pulse height spectra by the scattering from the surroundings. For fixed source geometry, this may not be too great a problem. Although the scattering will greatly distort the analysis at low energies, the effect is rather constant for fixed geometry. The problem is of utmost importance in the analysis of spectra in geometries which cannot be well defined since this effect can be geometrically dependent. Care must be taken to decrease the effects of scattering from the surrounding walls, floors, ceilings, equipment containing the experiment, and from the materials making up the detector itself (i.e., the canning material, light pipes, photomultiplier, voltage divider, and preamplifiers).

APPENDIX

FORTRAN STATEMENT OF LEAST SQUARE ANALYSIS[37]

```
C
C      THIS PROGRAM CALCULATES A VECTOR BETA, EQUAL TO THE MATRIX
C      PRODUCT OF THE INVERSE OF THE PRODUCT (ATRAN*OMEGA*ALPHA) AND
C      THE PRODUCT (ATRAN*OMEGA*RHO).  ALPHA IS AN ARRAY HAVING KMAX
C      COLUMNS AND JMAX ROWS AND IS READ IN AS DATA.  ATRAN IS THE
C      TRANSPOSE OF ALPHA.  RHO IS A COLUMN MATRIX HAVING JMAX ROWS AND
C      IS ALSO READ IN AS DATA.  OMEGA IS A DIAGONAL MATRIX HAVING
C      DIMENSIONS JMAX BY JMAX, AND MAY BE READ IN AS DATA, SET EQUAL
C      TO THE UNIT MATRIX, OR CALCULATED FROM RHO.  IN THE LATTER CASE
C      THE DIAGONAL ELEMENTS ARE THE RECIPROCALS OF THE CORRESPONDING
C      ROW ELEMENTS OF RHO.  INTERMEDIATE PRODUCT ARRAYS IN THE CALCULA-
C      TION ARE AS FOLLOWS.
C          ATROM  = ATRAN*OMEGA
C          ATROMR = ATROM*RHO
C          ATROMA = ATROM*ALPHA
C          UNVERT = INVERSE OF ATROMA
C      OTHER ARRAYS USED IN THE INVERSION CALCULATION ARE AUX,C, AND UNIT.
C      ANY OF THESE ARRAYS CAN BE PRINTED OUT IF DESIRED BY SETTING THE
C      APPROPRIATE CONTROL CONSTANT TO 1, SEE BELOW.
C
C      THE SAME ALPHA ARRAY CAN BE USED FOR CALCULATION WITH SEVERAL
C      SETS OF RHO AND OMEGA VALUES BY PROPERLY SETTING A CONTROL
C      CONSTANT.  SEE BELOW.
C
C
C      INPUT TO THE PROGRAM CONSISTS OF THE FOLLOWING.
C
C      READ STATEMENT 2.
C      A)ONE CARD CONTAINING.
C          1.  IDALPH.     AN IDENTIFYING NUMBER FOR THE ALPHA ARRAY
C                          CONSISTING OF NO MORE THAN 5 DECIMAL DIGITS.
C          2.  JMAX.       THE NUMBER OF ROWS IN ARRAY ALPHA, NO MORE THAN
C                          ONE HUNDRED.
C          3   KMAX.       THE NUMBER OF COLUMNS IN ARRAY ALPHA, NO MORE
C                          THAN TWENTY.
C      B)ANY NUMBER OF CARDS CONTAINING THE JMAX*KMAX ELEMENTS OF ALPHA,
C        SEVEN PER CARD.  DATA IS ENTERED AS A LINEAR STRING, FIRST BY
C        ROW, THEN BY COLUMN.
C
C      READ STATEMENT 5.
C      A)ONE CARD CONTAINING.
C          1.  IDRHO.      AN IDENTIFYING NUMBER FOR THE RHO ARRAY
C                          CONSISTING OF NO MORE THAN 5 DECIMAL DIGITS.
C          2.  NOMEG1.     *SET EQUAL TO 1 IF OMEGA IS TO BE READ IN AS
C                          DATA USING INPUT STATEMENT 418.
C                          *SET EQUAL TO ZERO IF OMEGA IS TO BE CALCULATED
C                          FROM THE RHO ARRAY.
C                          *SET EQUAL TO 2 IF OMEGA IS TO BE THE UNIT MATRIX.
C          3.  NSYM.       SET EQUAL TO 1 WHEN ATROMA IS KNOWN TO BE A
C                          SYMMETRIC SYSTEM.  IF SYMMETRIC, THE NUMBER OF
C                          CALCULATIONS INVOLVED IN THE INVERSION PROCESS
C                          IS CONSIDERABLY SMALLER (ABOUT HALF) THAN
C                          REQUIRED IF NON-SYMMETRIC.
C          4.  NSWTCH.     SET EQUAL TO 1 IF A NEW ALPHA SET IS TO BE READ
C                          IN BEFORE THE NEXT (NOT THE CURRENT) RHO DATA
C                          SET.  IF NOT EQUAL TO 1 THE PROGRAM WILL EXPECT
```

	TO KEEP THE SAME ALPHA ARRAY FOR THE NEXT SET OF RHOS.
5. NDUMP.	SET EQUAL TO 1 IF A DUMP OF CORE IS DESIRED AFTER THE COMPUTATION FOR THE CURRENT RHO SET HAS BEEN COMPLETED.
6. NOMEG2.	SET EQUAL TO 1 IF IDOMEG AND A COMPLETE LISTING OF ALL THE ELEMENTS OF THE OMEGA ARRAY ARE TO BE PRINTED AS OUTPUT.
7. NALPHA.	SET EQUAL TO 1 IF IDALPH AND A COMPLETE LISTING OF ALL THE ELEMENTS OF THE ALPHA ARRAY ARE TO BE PRINTED AS OUTPUT.
8. NRHO.	SET EQUAL TO 1 IF IDRHO AND A COMPLETE LISTING OF THE RHO ARRAY ARE TO BE PRINTED AS OUTPUT.
9. NATRAN.	SET EQUAL TO 1 IF A COMPLETE LISTING OF THE ATRAN ARRAY IS TO BE PRINTED AS OUTPUT.
10. NATROM.	SET EQUAL TO 1 IF A COMPLETE LISTING OF THE ATROM ARRAY IS TO BE PRINTED AS OUTPUT.
11. NATROR.	SET EQUAL TO 1 IF A COMPLETE LISTING OF THE ATROMR ARRAY IS TO BE PRINTED AS OUTPUT.
12. NATROA.	SET EQUAL TO 1 IF A COMPLETE LISTING OF THE ATROMA ARRAY IS TO BE PRINTED AS OUTPUT.
13. NAUX.	SET EQUAL TO 1 IF A COMPLETE LISTING OF THE AUX ARRAY IS TO BE PRINTED AS OUTPUT.
14. NC.	SET EQUAL TO 1 IF A COMPLETE LISTING OF THE C ARRAY IS TO BE PRINTED AS OUTPUT.
15. NUNVRT.	SET EQUAL TO 1 IF A COMPLETE LISTING OF THE UNVERT ARRAY IS TO BE PRINTED AS OUTPUT.
16. NPUNCH.	SET EQUAL TO 1 IF IDALPH, IDOMEG, AND A COMPLETE LISTING OF THE UNVERT ARRAY ARE TO BE PUNCHED AS OUTPUT.

B) ANY NUMBER OF CARDS CONTAINING THE JMAX ELEMENTS OF RHO, SEVEN PER CARD. DATA IS ENTERED AS A LINEAR STRING, FIRST BY ROW, THEN BY COLUMN.

READ STATEMENT 418.

A) ONE CARD CONTAINING.

1. IDOMEG.	AN IDENTIFYING NUMBER FOR THE OMEGA ARRAY. CONSISTING OF NO MORE THAN FIVE DECIMAL DIGITS.

B) ANY NUMBER OF CARDS CONTAINING THE JMAX NONZERO DIAGONAL ELEMENTS OF OMEGA TO BE READ IN WHEN NOMEG1 IS SET EQUAL TO 1. DATA IS ENTERED AS A LINEAR STRING, SEVEN PER CARD, FIRST BY ROW THEN BY COLUMN.

OUTPUT FROM THE PROGRAM CONSISTS OF THE FOLLOWING.

WRITE STATEMENT 1944.

THIS IS AN UNCONDITIONAL OUTPUT STATEMENT WHICH PRINTS THE THREE IDENTIFYING NUMBERS IDALPH, IDRHO, AND IDOMEG, APPROPRIATE TO THE CALCULATION, AND THE KMAX ELEMENTS OF THE FINAL VECTOR BETA.

WRITE STATEMENT 2137.

THIS IS AN UNCONDITIONAL OUTPUT STATEMENT WHICH PRINTS THE THREE IDENTIFYING NUMBERS IDALPH, IDRHO, AND IDOMEG APPROPRIATE TO THE CALCULATION, AND THE KMAX ELEMENTS OF A VECTOR MERIT.

THE ELEMENTS OF MERIT ARE COMPOSED OF THE PRODUCTS OF THE CORRESPONDING ELEMENTS OF BETA AND ATROMR.

WHEN THE CONTROL CONSTANTS HAVE THE APPROPRIATE VALUES. SEE ABOVE.

PUNCH STATEMENT 2251.

```
C       THIS IS A CONDITIONAL PUNCH STATEMENT WHICH IS EXECUTED ONLY
C       WHEN THE CONTROL CONSTANT NPUNCH HAS THE APPROPRIATE VALUE.
C       THE FIRST PUNCHED CARD WILL CONTAIN THE TWO IDENTIFICATION
C       NUMBERS IDALPH AND IDOMEG.  SUBSEQUENT CARDS WILL CONTAIN THE
C       ELEMENTS OF UNVERT, FIVE PER CARD.  RESULTS WILL BE PUNCHED
C       AS A LINEAR STRING, FIRST BY ROW, THEN BY COLUMN.
C
C
C       ADDITIONAL COMMENTS.
C       WHEN OMEGA IS CALCULATED FROM RHO (SEE ABOVE), IDOMEG IS SET
C       EQUAL TO IDRHO.  WHEN OMEGA IS SET EQUAL TO THE UNIT MATRIX,
C       IDOMEG IS ARBITRARILY SET TO 11111.
C       A SPECIAL BLOCK OF EMPTY LOCATIONS CALLED ADD HAS BEEN ADDED
C       TO ALLOW ADDITIONAL INSTRUCTIONS TO BE ASSEMBLED INTO THE
C       PROGRAM WITHOUT RECOMPILING.  UP TO 100 ADDITIONAL INSRUCTIONS
C       CAN BE ACCOMODATED.
C
C
      DIMENSION  ALPHA(100,20),ATRAN(20,100),ATROM(20,100),RHO(100),
     XOMEGA(100), ATROMA(20,20), UNIT(20), C(20,20),AUX(20,20),UNVERT(2
     X,20), ATROMR(20), BETA(20), ADD(100)
      EQUIVALENCE  (ATRAN,ATROM,C), (OMEGA,ATROMR),(OMEGA(21),BETA),
     X(ATRAN(  401), AUX), (ATRAN(  801), UNVERT)
      NONE = 1
    2 READ INPUT TAPE 7,10,IDALPH, JMAX, KMAX, ((ALPHA(J,K),K=1,KMAX),
     XJ=1,JMAX)
   10 FORMAT(I5,2I3/(7F10.6))
    5 READ INPUT TAPE 7,8, IDRHO,NOMEG1,NSYM,NSWTCH,NDUMP,NOMEG2,NALPHA,
     XNRHO,NATRAN,NATROM,NATROR,NATROA,NAUX,NC,NUNVRT,NPUNCH,(RHO(J),J=1
     X,JMAX)
    8 FORMAT (I5,15I1/(7F10.6))
   11 IF (NALPHA-1) 1,16,1
   16 WRITE OUTPUT TAPE 6,18,IDALPH,JMAX,KMAX,((J,K,ALPHA(J,K),K=1,KMAX)
     X,J=1,JMAX)
   18 FORMAT (1H1,16HINPUT DATA SET I5,10H FOR ALPHA   /20HONUMBER OF ROWS
     X =    I5/23H NUMBER OF COLUMNS  =  I5///(7H ALPHA(I2,1H,I2,3H) =,
     XE12.5, 11H     ALPHA(I2,1H,I2,3H) =,E12.5, 11H     ALPHA(I2,1H,I2,
     X3H) =,E12.5, 11H     ALPHA(I2,1H,I2,3H) =,E12.5))
    1 IF (NRHO-1) 7,4,7
    4 WRITE OUTPUT TAPE 6,19,IDRHO,JMAX,NONE,(J,NONE,RHO(J),J=1,JMAX)
   19 FORMAT (1H1,16HINPUT DATA SET I5,10H FOR RHO   /20HONUMBER OF ROWS =
     X   I5/23H NUMBER OF COLUMNS  =  I5///(5H RHO(I2,1H,I2,3H) =E12.5))
    7 IF (NOMEG1-1)  417,418,419
  417 DO 45   J=1,JMAX
  467 OMEGA(J) = 1.0/RHO(J)
      IDOMEG = IDRHO
      GO TO 420
  418 READ INPUT TAPE 7,425,IDOMEG,(OMEGA(J),J=1,JMAX)
  425 FORMAT (I5/(7F10.6))
      GO TO 420
  419 DO 421 J=1,JMAX
  421 OMEGA(J) = 1.0
      IDOMEG = 11111
  420 IF (NOMEG2-1)  17,229,17
  229 WRITE OUTPUT TAPE 6,231,IDOMEG,JMAX,JMAX,(J,J,OMEGA(J),J=1,JMAX)
  231 FORMAT (27H1ELEMENTS OF THE OMEGA SET I5      /20HONUMBER OF ROWS
     X =    I5/23H NUMBER OF COLUMNS  =  I5/35H0ALL NON-DIAGONAL ELEMENT
     XS ARE ZERO///(7H OMEGA(I2,1H,I2,3H) =,E12.5))
   17 DO 517 J=1,KMAX
      DO 517 K=1,JMAX
  517 ATRAN(J,K) = ALPHA(K,J)
      IF ( NATRAN-1)  520,518,520
  518 WRITE OUTPUT TAPE 6,519, KMAX,JMAX,((J,K,ATRAN(J,K),K=1,JMAX),
```

```
     XJ=1,KMAX)
 519 FORMAT (33H1ELEMENTS OF THE ATRAN ARRAY       /20HONUMBER OF ROWS
     X =    I5/23H NUMBER OF COLUMNS  =  I5///(7H ATRAN(I2,1H,I2,3H) =,
     XE12.5, 11H     ATRAN(I2,1H,I2,3H) =,E12.5, 11H     ATRAN(I2,1H,I2,
     X3H) =,E12.5, 11H     ATRAN(I2,1H,I2,3H) =,E12.5))
 520 DO 521 J=1,KMAX
     DO 521 K=1,JMAX
 521 ATROM(J,K)=ATRAN(J,K)*OMEGA(K)
     IF (NATROM-1)  25,522,25
 522 WRITE OUTPUT TAPE 6,524, KMAX, JMAX, ((J,K,ATROM(J,K),K=1,JMAX),
     XJ=1,KMAX)
 524 FORMAT (33H1ELEMENTS OF THE ATROM ARRAY       /20HONUMBER OF ROWS
     X =    I5/23H NUMBER OF COLUMNS  =  I5///(7H ATROM(I2,1H,I2,3H) =,
     XE12.5, 11H     ATROM(I2,1H,I2,3H) =,E12.5, 11H     ATROM(I2,1H,I2,
     X3H) =,E12.5, 11H     ATROM(I2,1H,I2,3H) =,E12.5))
  25 DO 30 J=1,KMAX
  30 ATROMR(J) = 0.0
     DO 35 J=1,KMAX
     DO 35 I=1,JMAX
  35 ATROMR(J) = ATROMR(J) + ATROM(J,I)*RHO(I)
     IF ( NATROR -1) 38,36,38
  36 WRITE OUTPUT TAPE 6,37, KMAX,NONE,(J,NONE,ATROMR(J),J=1,KMAX)
  37 FORMAT (33H1ELEMENTS OF THE ATROMR ARRAY       /20HONUMBER OF ROWS
     X =    I5/23H NUMBER OF COLUMNS  =  I5///(8H ATROMR(I2,1H,I2,3H) =,
     XE14.7))
  38 DO 40 J=1,KMAX
     DO 40 K=1,KMAX
  40 ATROMA(J,K) = 0.0
     DO 41 J=1,KMAX
     DO 41 K=1,KMAX
     DO 41 I=1,JMAX
  41 ATROMA(J,K) = ATROMA(J,K) + ATROM(J,I)*ALPHA(I,K)
     IF ( NATROA - 1 )  45,43,45
  43 WRITE OUTPUT TAPE 6,44, KMAX, KMAX, ((J,K, ATROMA(J,K),K=1,KMAX),
     XJ=1,KMAX)
  44 FORMAT (33H1ELEMENTS OF THE ATROMA ARRAY       /20HONUMBER OF ROWS
     X =    I5/23H NUMBER OF COLUMNS  =  I5///(8H ATROMA(I2,1H,I2,2H)=
     XE12.5, 11H     ATROMA(I2,1H,I2,3H) =,E12.5, 11H     ATROMA(I2,1H,I2,
     X3H) =,E12.5, 11H     ATROMA(I2,1H,I2,3H) =,E12.5))
  45 DO 60 J=1,KMAX
  60 AUX(J,1) = ATROMA(J,1)
     DO 65 K=2,KMAX
  65 AUX(1,K) = ATROMA(1,K)/ATROMA(1,1)
     NDIAG = 2
  69 K = NDIAG
     J = NDIAG
  70 AUX(J,K)= ATROMA(J,K)
     IMAX = K-1
     DO 71 I=1,IMAX
  71 AUX(J,K) = AUX(J,K) - AUX(J,I)*AUX(I,K)
     IF (NSYM-1) 774,771,774
 771 IF (J-K)  773,774,773
 773 AUX(K,J)= AUX(J,K)/AUX(K,K)
 774 J = J + 1
     IF (J-KMAX)  70,70,74
  74 IF (NSYM-1) 75,78,75
  75 J = NDIAG
     IF (NDIAG-KMAX) 750,185,750
```

```
    750 K = NDIAG + 1
     76 AUX(J,K) = ATROMA(J,K)
        IMAX = J-1
        DO 77 I=1,IMAX
     77 AUX(J,K) = AUX(J,K) - AUX(J,I)*AUX(I,K)
        AUX(J,K) = AUX(J,K)/AUX(J,J)
        K =K+1
        IF (K-KMAX)  76,76,78
     78 NDIAG = NDIAG +1
        IF (NDIAG-KMAX) 69,69,185
    185 IF (NAUX-1) 84,181,84
    181 WRITE OUTPUT TAPE 6,182, KMAX,KMAX,((J,K,AUX(J,K),K=1,KMAX),J=1,
       XKMAX)
    182 FORMAT (33H1ELEMENTS OF THE AUX ARRAY          /20HONUMBER OF ROWS
       X =     I5/23H NUMBER OF COLUMNS  =  I5///(7H   AUX(I2,1H,I2,3H) =,
       XE12.5, 11H        AUX(I2,1H,I2,3H) =,E12.5, 11H        AUX(I2,1H,I2,
       X3H) =,E12.5, 11H        AUX(I2,1H,I2,3H) =,E12.5))
     84 DO 85 I=1,KMAX
     85 UNIT(I) = 0.0
        DO 98 K=1,KMAX
        UNIT(K) = 1.0
        C(1,K) = UNIT(1)/AUX(1,1)
        DO 95 J=2,KMAX
        C(J,K) = UNIT(J)
        IMAX = J-1
        DO 90 I=1,IMAX
     90 C(J,K) = C(J,K) - AUX(J,I)*C(I,K)
        C(J,K) = C(J,K) / AUX(J,J)
     95 CONTINUE
        UNIT(K) = 0.0
     98 CONTINUE
        IF ( NC - 1 ) 101,99,101
     99 WRITE OUTPUT TAPE 6,100,KMAX,KMAX,((J,K,C(J,K),K=1,KMAX),J=1,KMAX)
    100 FORMAT (33H1ELEMENTS OF THE C ARRAY            /20HONUMBER OF ROWS
       X =     I5/23H NUMBER OF COLUMNS  =  I5///(7H     C(I2,1H,I2,3H) =,
       XE12.5, 11H          C(I2,1H,I2,3H) =,E12.5, 11H          C(I2,1H,I2,
       X3H) =,E12.5, 11H          C(I2,1H,I2,3H) =,E12.5))
    101 DO 190 K=1,KMAX
        J = KMAX
        UNVERT(J,K) = C(J,K)
    172 J=J-1
        UNVERT(J,K) = C(J,K)
        IMIN = J+1
        DO 175 I=IMIN,KMAX
    175 UNVERT(J,K) = UNVERT(J,K) - AUX(J,I)*UNVERT(I,K)
        IF (J-1)  190,190,172
    190 CONTINUE
        IF ( NUNVRT-1 ) 193,191,193
    191 WRITE OUTPUT TAPE 6,192, KMAX,KMAX,((J,K,UNVERT(J,K),K=1,KMAX),J=
       X1,KMAX)
    192 FORMAT (33H1ELEMENTS OF THE INVERT ARRAY       /20HONUMBER OF ROWS
       X =     I5/23H NUMBER OF COLUMNS  =  I5///(8H INVERT(I2,1H,I2,2H)=
       XE12.5, 11H     INVERT(I2,1H,I2,3H) =,E12.5, 11H     INVERT(I2,1H,I2,
       X3H) =,E12.5, 11H     INVERT(I2,1H,I2,3H) =,E12.5))
    193 IF ( NPUNCH-1) 1193,2251,1193
   2251 PUNCH 2252,IDALPH,IDOMEG,((UNVERT(J,K),K=1,KMAX),J=1,KMAX)
   2252 FORMAT(10HIDALPH =     I5,10HIDOMEG =     I5/(5E14.6))
   1193 DO 293 J=1,KMAX
    293 BETA(J) = 0.0
        DO 194 J =1,KMAX
        DO 194 I =1,KMAX
    194 BETA(J) = BETA(J) + UNVERT(J,I)*ATROMR(I)
   1944 WRITE OUTPUT TAPE 6,195,IDALPH,IDRHO,IDOMEG,(J,BETA(J),J=1,KMAX)
    195 FORMAT(33H1ELEMENTS OF THE BETA VECTOR FOR  /16H ALPHA DATA SET
       XI5/16H RHO DATA SET     I5/16H OMEGA DATA SET  I5///(6H BETA(I2,
       X3H) = E14.7))
        DO 2132 J =1,KMAX
   2132 ADD(J) = BETA(J)*ATROMR(J)
   2137 WRITE OUTPUT TAPE 6,2133, IDALPH,IDRHO,IDOMEG,(J,ADD(J),J=1,KMAX)
   2133 FORMAT (30H1FIGURE OF MERIT CALCULATION    /16H ALPHA DATA SET    I5
       X/16H RHO DATA SET      I5/16H OMEGA DATA SET  I5///(7H MERIT(I2,
       X   3H) = E14.7))
        IF (NDUMP - 1) 196,197,196
    196 IF ( NSWTCH-1)  5,2,5
    197 CALL ERROR
*DATA
```

BIBLIOGRAPHY

1. Jordan, W. H., "Detection of Nuclear Particles", Annual Review of Nuclear Science, I, Annual Reviews, Inc., Stanford, California, 1952.

2. Bell, P. R., "The Scintillation Process", Beta and Gamma-Ray Spectroscopy, ed. Kai Siegbaum, North-Holland Publishing Co., Amsterdam, 1955.

3. Stephenson, R. and Bell, P. R., "Broad Beam Gamma Attenuation", ORNL 1705, July 1954, 19.

4. Miller, W. F., and Snow, W. J., Monte Carlo Calculations of the Energy Loss Spectra for Gamma Rays in Sodium Iodide and Cesium Iodide, ANL 6318, February 1961.

5. Heitler, Walter, The Quantum Theory of Radiation, Oxford, 1944.

6. Einstein, A., "Erzeugung und Verwadlung des Lichtes", Ann. Physik, 17, (1905) 132.

7. Compton, A. H., "A Quantum Theory of the Scattering of X-rays by Light Elements", Phys. Rev., 21, (1923) 482.

8. Anderson, C. D., "The Positive Electron", Phys. Rev., 43, (1933) 494.

9. Kittel, C., Introduction to Solid State Physics, John Wiley and Sons, Inc., New York (1953).

10. Sietz, F., The Modern Theory of Solids, McGraw Hill, New York (1940).

11. Mott, N. F., Elements of Wave Mechanics, Cambridge University Press, 1952.

12. Price, W. J., Nuclear Radiation Detection, McGraw Hill, New York, 1958.

13. Mott, W. E. and Sutton, R. B., "Scintillation and Cerenkov Counters", Handbuch Der Physik, Vol. XLV Nuclear Instrumentation II, ed. S. Flügge, Springer-Verlag, 1958.

14. Bird, L. L., Tracerlog, No. 78, (1956) 12.

15. Wright, G. T., "Low Energy Measurements with the Photomultiplier Scintillation Counter", J. Sci. Instrum., 31, (1954) 462-5.

16. Kelley, G. G., Bell, P. R., Davis, R. C. and Lazar, N. H., "Intrinsic Scintillator Resolution", Nucleonics, 14, No. 4 (1956) 53.

17. Gamble, R. L., "Prompt Fission Gamma Rays from U^{235}", Doctoral Dissertation, University of Texas, June 1955.

18. Swank, R. K. and Buch, W. L., "Observations on Pulse Height Resolution and Photosensitivity", Nucleonics, 10, No. 5, May 1952.

19. Operations Manual for Nuclear Data 256 Pulse Height Analyser, Nuclear Data, Inc., Madison, Wisc., 1960.

20. Bell, P. R., private communication.

21. Vegors, S. H., Marsden, L. L. and Heath, R. L., Calculated Efficiencies of Cylindrical Radiation Detectors, IDO 16370, Sept. 1, 1958.

22. Miller, W. F., Reynolds, J. and Snow, W. J., Efficiencies and Photofractions for Gamma Radiation on NaI(Tl) Activated Crystals, ANL 5902, August 1958.

23. Francis, J. E., Harris, C. C. and Trombka, J. I., "Variation of NaI(Tl) Detection Efficiencies with Crystal Size and Geometry for Medical Research", ORNL 2204, February 12, 1957.

24. Jeffrey, Harold, Theory of Probability, Clarendon Press, Oxford, 1939.

25. Rose, M. E., "The Analysis of Angular Correlation and Angular Distribution Data", Phys. Rev. 91, (1953) 610.

26. Burrus, W. R., "Unscrambling Scintillation Spectrometer Data", IRE Trans. on Nuc. Sci., Vol. INS-7, No. 2-3, February 25-26, 1960.

27. Beale, E. M. L., "On Quadratic Programming", Nav. Res. Logistics Quarterly, 6, September, 1959.

28. Linden, D. A., "Discussion of Sampling Theorems", Proc. IRE. 47, July 1959.

29. Bell, R. E., Graham, R. L. and Petch, H. E., "Disintegration Scheme of I^{131}", Can. J. Phys. 30, (1952) 35.

30. Haskins, J. R. and Kurbatow, J. D., "The Disintegration of I^{131}", Phy. Rev. 88, (1952) 884.

31. Arns, R. G. and Wiedenbeck, M. L., "Energy Levels of Re^{187}", Univ. of Mich. Res. Inst. Report 2863-2-P, August, 1960.

32. Sears, F. W., Principle of Physics, Part III, Optics, Addison Wesley Press, Inc., Cambridge, Mass., 1948.

33. Storm, E., Gilbert, E. and Israel, H., Gamma Ray Absorption Coefficients for Elements 1 through 100 Derived from the Theoretical Values of the National Bureau of Standards, LA 2237, November 18, 1958.

34. Goldstein, H., Fundamental Aspects of Reactor Shielding, Addison-Wesley, Reading, Mass., 1959.

35. Trubey, D. K., "Monte Carlo Calculations of Gamma Ray Penetration of Aluminum Slabs", ORNL 2389, October 18, 1957.

36. Peebles, G. H., Gamma Ray Transmission Through Finite Slabs, Rand R-240, December 1, 1952.

37. Prepared by Brice Carnahan of the University of Michigan Computing Center.